



Fermi National Accelerator Laboratory

FERMILAB-Pub-90/184-A
August 1990

GALAXY CLUSTERING IN A BUBBLY UNIVERSE†

Dongsu Ryu, Joshua A. Frieman, and Angela V. Olinto

*NASA/Fermilab Astrophysics Center
Fermi National Accelerator Laboratory
P. O. Box 500, Batavia, Illinois 60510*

† Submitted to *Astrophysical Journal*



ABSTRACT

Recent redshift surveys suggest that most galaxies are distributed on the surfaces of bubbles surrounding large voids. To investigate the quantitative consistency of this qualitative picture of large-scale structure, we study analytically the clustering properties of galaxies in a universe filled with spherical shells. This phenomenological model comprises three galactic populations: shell galaxies, placed at random on spherical shells distributed randomly in space; cluster galaxies, located at the points where three shells intersect; and a random, unclustered component of background galaxies. We calculate the two-point galaxy correlation function, the galaxy-cluster cross-correlation function, and the void probability function for models with an arbitrary distribution of shell sizes. We also calculate the three-point correlation function and the peculiar velocity correlation tensor for shell galaxies. With $\sim 20\%$ of galaxies in clusters and a power law distribution of shell sizes, $n_{sh}(R) \sim R^{-\alpha}$, $\alpha \simeq 4$, the observed slope and amplitude of the galaxy two-point correlation function $\xi_{gg}(r)$ can be reproduced. (It has recently been shown that the same model parameters reproduce the enhanced *cluster* two-point correlation function, $\xi_{cc}(r)$.) For a Poisson distribution of shells, the galaxy and cluster correlation functions are both positive out to twice the maximum shell radius, and ξ_{gg} does not show a strong break at $r \sim 10h^{-1}$ Mpc. In this model, elliptical galaxies, with a higher percentage of cluster membership, are more strongly correlated than spirals, $\xi_{ee} > \xi_{ss}$, in qualitative agreement with the observed morphological trend; however, the slope of the correlation function for ellipticals is not as steep as the observed value. The scaled three-point correlation function, Q , is moderately flat on scales $r \lesssim 10h^{-1}$ Mpc with amplitude $0.4 \lesssim Q \lesssim 0.8$, in satisfactory agreement with the observed value, $Q_{obs} = 1.0 \pm 0.4$. When measured over larger scales, Q should be found to increase with separation. The model also yields reasonable agreement with the observed slope of the galaxy-cluster cross correlation function, ξ_{cg} , but its correlation length, $r_o^{cg} \simeq 6h^{-1}$ Mpc, is roughly 30% lower than the observed value, $r_o^{cg} \simeq 8.8h^{-1}$ Mpc. Given the uncertainties in the observational determination of r_o^{cg} , this discrepancy is only marginal (about comparable to that between the data and the cold-dark-matter model). Assuming peculiar velocities arise from shell expansion, as expected in some explosion models, the parallel component of the shell galaxy velocity correlation tensor, $\Pi(r)$, is consistent with the observed spiral galaxy velocities on large scales (after subtracting out the bulk motion due to the Great Attractor and Virgo infall). However, the perpendicular velocity component $\Sigma(r)$ is in conflict with the data unless the shell expansion velocity is substantially smaller than the Hubble speed. The void probability function of the model is in reasonable agreement with observations if $\sim 20\%$ of the galaxies are in the unclustered (or weakly clustered) background. We also consider a refined model with ‘self-avoiding’ shells, in which shell interactions are presumed to prevent the centers of shells from lying inside other bubbles, *i.e.*, the bubbles are anticorrelated on small scales. In this case, the two-point correlation function of shell galaxies is steepened, but the amplitude is reduced. When cluster galaxies are included, we expect this model will also provide a good fit to the galaxy two-point function.

Subject headings: cosmology – galaxies: clustering

I. INTRODUCTION

How are galaxies distributed in space on large scales? Although the observational data base in cosmology has improved dramatically in recent years, we still have only a partial understanding of this issue. Beginning in the late seventies (Tift and Gregory 1976; Joeveer and Einasto 1978; Gregory and Thompson 1979; Tarenghi, *et al.* 1980; Gregory, Thompson, and Tift 1981; Kirshner, *et al.* 1981) and especially with the first results of the CfA2 redshift survey extension (de Lapparent, Geller, and Huchra 1986), a picture has emerged in which a large fraction of galaxies appear to be distributed on the surfaces of quasi-spherical shells surrounding large voids, with rich clusters occupying the interstitial regions between shells. The CfA and other recent redshift surveys (Haynes and Giovanelli 1986; Da Costa, *et al.* 1988; Da Costa, *et al.* 1989) suggest that shells with radii up to $30 h^{-1}$ Mpc ($h \equiv H_0/100 \text{ km s}^{-1} \text{ Mpc}^{-1}$) and with a volume filling factor of order unity may be the dominant structures in the Universe.

Such bubbly structure may arise naturally in explosive models of galaxy formation (Ostriker and Cowie 1981; Ikeuchi 1981; Ostriker, Thompson, and Witten 1986; Yoshioka and Ikeuchi 1990), in which positive energy seeds generate shock waves, sweeping the ambient medium onto expanding shells. The shells later cool and, presumably, fragment into galaxies, although this process is not yet well understood (White and Ostriker 1990; Hwang, Vishniac, and Shapiro 1990). In addition, models in which large-scale structure forms via gravitational instability appear to generate voids from *negative* density perturbations (Fillmore and Goldreich 1984; Bertschinger 1985), as well as large two-dimensional sheets and shells (White, *et al.* 1987; Melott and Shandarin 1990; Park 1990) having the same qualitative appearance as the CfA slices.

Although the evidence for the existence of bubbly structure in the redshift surveys is visually compelling, it remains largely qualitative and anecdotal. The interpretation of the data has therefore been a matter of debate. For example, the structures are seen in redshift space rather than physical space, so they are polluted by peculiar velocities (Kaiser 1987; McGill 1990): how coherent does the shell structure remain when such effects are removed? In addition, although at least some of the shells appear to form closed surfaces, it has been suggested that the large-scale topology is sponge-like, with both under- and over-dense regions forming connected, percolating networks (Gott, Melott, and Dickinson 1986). The interpretational problems are compounded by the fact that the largest structures found are comparable to the size of the surveys, so we are not yet dealing with a fair sample to which one can address quantitative, statistical questions (de Lapparent, Geller, and Huchra 1988).

Nevertheless, we would like to know whether the bubble paradigm of large-scale structure is an accurate representation of the galaxy distribution, quantitatively consistent with the observed clustering properties of galaxies. In particular, can a structure dominated by bubbles reproduce the galaxy correlation functions? If so, what does this entail about the properties of the bubble distribution? In this paper, we address these questions by studying galaxy statistics in a class of simple phenomenological models: *most* galaxies (*shell* galaxies) are distributed randomly on thin spherical shells surrounding voids; in addition, some galaxies are placed in clusters located at the intersections of three shells (*cluster* galaxies), and others are distributed in a random, uniform

background (*background* galaxies). For most of the paper, we assume the shells themselves are distributed in a random Poisson process, *i.e.*, they are uncorrelated. We present results for an arbitrary distribution of shell sizes and apply them specifically to the case of a power law distribution of shell radii, $n_{sh}(R) \propto R^{-\alpha}$, truncated at small (R_{min}) and large (R_{maz}) radii. These model parameters are not well constrained by observations: in present redshift surveys, the distribution of void sizes is poorly determined, because the total number of voids is small (de Lapparent, Geller, and Huchra 1988). Determination of the void size distribution will require much larger samples than those currently available (Geller and Huchra 1988).

Previous work on the shell model includes numerical (Weinberg, Ostriker, and Dekel 1989, hereafter WOD; Bahcall, Henriksen, and Smith 1989, hereafter BHS) and analytic (Kulsrud and Cowley 1989) studies of the distribution of galaxy *clusters*, and some numerical work on the galaxy distribution (Saarinen, Dekel, and Carr 1987; Ostriker and Strassler 1989; BHS). In particular, WOD derived the cluster mass function and two-point correlation function for models with equal size shells and a power law distribution of shell radii. In the case of equal size shells, the slope of the cluster two-point correlation function is too flat, and the correlation length is too large compared to the mean separation of clusters. Models with a power law distribution of shell sizes match with cluster observations reasonably well if $\alpha \simeq 3.5 - 4.5$ and the volume filling factor of the shells $f \simeq 0.8 - 1.2$. WOD set $R_{maz} = 30h^{-1}$ Mpc, comparable to the largest voids seen in the redshift surveys, and assumed $R_{min}/R_{maz} = 1/8$. In their best fit models, the cluster correlation length is still somewhat too large, unless shell merging or an unclustered cluster population is taken into account.

We find that the *galaxy* two-point function is a sensitive function of the shell size distribution, and the observed two-point correlation function is reproduced best with shell size index $\alpha \simeq 4$ and with $\sim 20\%$ of galaxies in clusters. It is noteworthy that this choice of shell size index α gives good fits to both the galaxy and cluster correlation functions, since they arise from different geometrical features of the model. Thus, agreement with the galaxy and cluster correlation functions fixes the distribution of shell sizes, a prediction which can be tested when deeper surveys have sufficient data to quantitatively characterize the bubble size distribution. In this sense, we disagree partially with the analysis of BHS, who also included shell galaxies in their numerical simulations. Although their results show large numerical scatter, they find the galaxy two-point function fits well with observations, except that it has a positive tail at large separation, not seen in the data. Moreover, they claim the agreement is insensitive to the model parameters. We show how these statistical features can be derived analytically and that long wavelength tails are artifacts of numerical simulations, and demonstrate the dependence of the results on the parameters of the model. For the above choice of α , we also find that the scaled three-point function, Q , is quite flat over scales $r \lesssim 10 h^{-1}$ Mpc, with an amplitude (for shell galaxies) in reasonable agreement with the observed value.

Although the two- and three-point functions may be reasonably counted as successes of the bubble model, it is well known that a variety of geometrical prescriptions for galaxy clustering can yield satisfactory galaxy two- and three-point functions (Soneira and Peebles 1978). We therefore consider additional statistical tests of the model, in particular, the cluster-galaxy cross-correlation function, the peculiar velocity correlation tensor, and the void probability function. The slope of the cross-correlation function is in good agreement with the observations, based on

the recent reanalysis of the data by Lilje and Efstathiou (1988a,b). The amplitude of ξ_{cg} is lower than the observed value, but is roughly within the observational error bars if uncertainties in the selection function and cosmological correction are taken into account. If we assume that galaxy peculiar velocities arise in part from the expansion velocity of the shells, as would be the case in some versions of the explosion model, we can estimate the peculiar velocity correlation function. We then compare the model with the velocity correlation tensor for a sample of spiral galaxies on scales 1000-3000 km/sec (Górski, *et al.* 1989, hereafter GDSWY; Groth, Juszkiewicz, and Ostriker 1989, hereafter GJO), after the bulk motion due to the Great Attractor and Virgo infall have been subtracted from the data (GJO). Taking the shell expansion velocity expected from explosion models, the parallel component of the velocity correlation is in reasonable agreement with the observations, but the perpendicular component of the model has the wrong sign and too large an amplitude. For consistency, then, we must assume that shell velocities have decayed to small values (*e.g.*, due to shell collisions, or if $\Omega < 1$), and that the residual velocities of the spiral sample arise instead from, *e.g.*, infall into clusters (GJO). Since the shell model is motivated by the observations of large-scale voids, it should be able to reproduce the observed void probability function (VPF). If we include only shell and cluster galaxies, however, the model predicts an excess of voids of radius $r \simeq 3 - 9h^{-1}$ Mpc when compared to the earlier CfA1 redshift data (Maurogordato and Lachieze-Rey 1987). On the other hand, if $\sim 20\%$ of the galaxies are unclustered (or very weakly clustered), they populate a substantial fraction of the voids, and the observed VPF can be reproduced over this range, within the observational uncertainties. Although searches for such unclustered field galaxies suggest that they make up no more than 10% of the galaxy population, the background galaxies in the shell model could be weakly clustered without seriously affecting the VPF. On the other hand, the VPF analysis is based on the relatively shallow CfA1 survey, which was not sensitive to the large $r \simeq 10 - 30h^{-1}$ Mpc voids seen in the CfA2 slices. To accurately constrain the models, we must await statistical analysis of the VPF for the complete CfA2 data, or possibly even larger surveys. (Recently, Ostriker and Strassler (1989) have analyzed the projected two-dimensional void probability for the first CfA2 slice, and find it can be reproduced by a shell distribution.) Furthermore, the void probability for the shell model is sensitive to the spatial distribution of bubbles; if bubble centers are anti-correlated on small scales, *e.g.*, due to shell interactions, the VPF is presumably enhanced.

We note that the bubble model considered here is not in conflict with the possibility that the *topology* of the large-scale galaxy field is sponge-like (Gott, Melott, and Dickinson 1986) rather than ‘bubbly’: if we allowed for clustering within the shells, the bubble surfaces would be patchy, so that both under- and over-dense regions could form connected networks. Here, we are more interested in the *geometrical* aspects of the shell model, which may provide a plausible picture (if not caricature) of the redshift survey data.

In the following sections, we study the galaxy distribution in the shell model by calculating analytically the two- and three-point correlation functions of galaxies, the peculiar velocity correlation function, and the void probability function. In particular, we test whether the values of parameters ($\alpha \simeq 4$ and $f \simeq 1$) used to reproduce the observed distribution of clusters by WOD can also reproduce the observed distribution of galaxies. In §II, we briefly review observations concerning the distribution of galaxies. In §III, a simple version of the bubble model with equal size shells is considered. In §IV, we extend the analysis to an arbitrary distribution of shell sizes, focusing on a model with a power law distribution. In §V, we include the contribution from

cluster galaxies at shell intersections as well as a possible unclustered (randomly distributed) population of background galaxies, focusing on the galaxy two-point correlation function and its morphological dependence, the cluster-galaxy cross correlation function, and the void distribution. In §VI, we take into account the interaction between shells, modifying the bubble distribution so that the centers of shells do not lie inside other bubbles; we show how this anti-correlation of shells on small scales affects the galaxy two-point correlation function. Finally, the results are discussed and avenues for further research are outlined in §VII. In the Appendices, we discuss several mathematical details.

II. OBSERVATIONS

Observationally, the galaxy two-point correlation function $\xi_{gg}(r)$ is well established and fitted by the power law

$$\xi_{gg}(r) = (r/r_o)^{-\gamma_o}. \quad (2.1)$$

From angular correlation studies of the Lick catalog and other samples (Groth and Peebles 1977), the slope was found to be $\gamma_o = 1.77 \pm 0.04$ and the correlation length $r_o \simeq 4.7 h^{-1}$ Mpc, in the range $0.05 h^{-1} \text{ Mpc} \lesssim r \lesssim 9 h^{-1} \text{ Mpc}$. These values are consistent with those obtained from the early CfA1 redshift survey data (Davis and Peebles 1983) and from the Southern Sky and IRAS catalogs (Davis, *et al.* 1988). On the other hand, from the first two slices of the CfA redshift survey extension, de Lapparent, Geller, and Huchra (1988) found $\gamma_o = 1.6 \pm 0.3$ and $r_o = 7.5^{+4.5}_{-2.5} h^{-1}$ Mpc in the range of separation $\sim 3 - 14 h^{-1}$ Mpc, and noted the large uncertainties. At separations larger than about $10 h^{-1}$ Mpc, $\xi_{gg}(r)$ appears to steepen and generally becomes lost in the noise at $r \sim 20 h^{-1}$ Mpc. Recent angular correlation studies with larger samples (Collins, Heydon-Dumbleton, and MacGillivray 1989; Maddox *et al.* 1990) confirm the power law behavior of $\xi_{gg}(r)$. In particular, from the APM survey, Maddox *et al.* (1990) find a best-fit slope parameter $\gamma_o = 1.668$ on scales $r \lesssim 10 h^{-1}$ Mpc; however, on larger scales they find substantially more power than the Lick catalog (the break at $r \simeq 10 h^{-1}$ Mpc is more gentle). In comparing models to the data, we will focus on the range where ξ_{gg} is well approximated by a power law, and will take

$$r_o = 5 \pm 1 h^{-1} \text{ Mpc} \quad ; \quad \gamma_o = 1.8 \pm 0.2 \quad (2.2)$$

as canonical values. We note that clustering due to gravity within shells, not included in the model, will presumably enhance the two-point function on small scales; strictly speaking, then, we should only use the observed correlation function as an upper bound on the shell model value. To compare the model correlation function with the data on larger scales, $r \gtrsim 14 h^{-1}$ Mpc, we are currently investigating the angular two-point function $w(\theta)$ in the shell model. (At present, only the angular surveys yield statistically significant correlations on large scales.)

An important feature of galaxy clustering is the observed morphological segregation of the galaxy population in different environments (see, *e.g.*, Dressler 1980). While some 80% of field galaxies are spirals, as few as 15% of galaxies in compact clusters like Coma display spiral structure. This segregation is reflected in the dependence of the galaxy correlation function on morphological type, first studied by Davis and Geller (1976). (See also Sharp, Jones, and Jones 1978; Sadler and Sharp 1984.) From an angular correlation analysis of the Uppsala catalog,

they found significant variations in the slope and amplitude of the correlation function between different morphological types. For ellipticals, they found $\gamma_o \simeq 2.10$ and $r_o \simeq 6.6 h^{-1}$ Mpc, while $\gamma_o \simeq 1.69$ and $r_o \simeq 4.4 h^{-1}$ Mpc for spiral galaxies. In a recent survey of the Pisces-Perseus supercluster (Giovanelli, Haynes, and Chincarini 1986; Giovanelli *et al.* 1986; Haynes and Giovanelli 1986, 1988), the above trend was confirmed: for ellipticals in Pisces-Perseus $\gamma_o = 2.06$, for Sa and Sab $\gamma_o = 1.81$, for Sb and Sbc $\gamma_o = 1.63$, and for Sc galaxies $\gamma_o = 1.47$. Despite these morphological differences in clustering, it appears that both early- and late-type galaxies trace out the shell structure seen in the first CfA2 slice (Huchra *et al.* 1990).

The three-point galaxy correlation function can be written as a sum of two-point functions plus the reduced three-point function ζ (Peebles 1980). It is conventional to consider the scaled three-point correlation function, defined by

$$Q(r_a, r_b, r_c) \equiv \frac{\zeta(r_a, r_b, r_c)}{\xi_{gg}(r_a)\xi_{gg}(r_b) + \xi_{gg}(r_b)\xi_{gg}(r_c) + \xi_{gg}(r_c)\xi_{gg}(r_a)}. \quad (2.3)$$

The galaxy three-point function has not been as well determined as the two-point correlation function. From the Lick catalog, Groth and Peebles (1977) found that Q is fairly constant on scales $r \lesssim 10 h^{-1}$ Mpc, with an average value $Q = 1.29 \pm 0.21$. Since then, estimates of Q from other surveys have varied: $Q = 0.8 \pm 0.1$ from a subsample of the CfA1 survey (Efstathiou and Jedrejowski 1984); $Q = 0.60 \pm 0.06$ from the Durham-AAT survey and $Q = 1.3 \pm 0.3$ from the Kirshner, Oemler, Schechter (1978) survey (Bean, *et al.* 1983); and $Q \simeq 1$ from the projected bispectrum of the Shane-Wirtanen counts (Fry and Seldner 1982). Recent estimates of Q have been toward the lower end of the spectrum; *e.g.*, Peebles (1988a) quotes $Q \sim 0.7$, while Fry (1990) reports $Q \simeq 0.6$. For comparison with models, we will assume Q is in the range

$$Q = 1.0 \pm 0.4. \quad (2.4)$$

The two-point correlation function of rich clusters has been a subject of intensive study and debate in recent years. The cluster correlation function is apparently consistent with a power law,

$$\xi_{cc}(r) \simeq (r/r_{co})^{-\gamma_{co}}, \quad (2.5)$$

but both the slope and amplitude, in addition to the range over which this form holds, are uncertain. A variety of studies based on the Abell, Zwicky, and Lick catalogs find values in the range

$$14h^{-1}\text{Mpc} < r_{co} < 30h^{-1}\text{Mpc}, \quad \gamma_{co} = 1.6 \pm 0.3 \quad (2.6)$$

(Bahcall and Soneira 1983; Shectman 1985; Postman, Geller, Huchra 1986; for a recent review with more complete references, see Bahcall 1988; see also Geller and Huchra 1988). There is also some question about the largest scale on which ξ_{cc} has been reliably determined to be positive, with estimates ranging from about 40 to over 100 h^{-1} Mpc. These uncertainties are compounded by the issue of projection contamination of cluster catalogs (Sutherland 1988; Dekel, *et al.* 1989; Olivier, *et al.* 1990), which appears to generate spurious clustering on small scales.

In addition to $\xi_{gg}(r)$ and $\xi_{cc}(r)$, the cluster-galaxy cross correlation function $\xi_{cg}(r)$ can be used to test models of the galaxy distribution. From a study of rich Abell clusters and galaxies in the Lick catalog, Seldner and Peebles (1977a,b) found that $\xi_{cg}(r)$ is well described by

$$\xi_{cg}(r) = \left(\frac{r}{7h^{-1}\text{Mpc}}\right)^{-2.5} + \left(\frac{r}{12h^{-1}\text{Mpc}}\right)^{-1.7} \quad (2.7)$$

for $0.5h^{-1}\text{Mpc} \lesssim r \lesssim 40h^{-1}\text{Mpc}$. In a recent reanalysis using redshifts for 204 Abell clusters and modern estimates of the galaxy luminosity function, Lilje and Efstathiou (1988a,b) find that $\xi_{cg}(r)$ is reliably determined only on scales $r \lesssim 20h^{-1}\text{Mpc}$ and is well fitted to a power law,

$$\xi_{cg}(r) = \left(\frac{r}{8.8h^{-1}\text{Mpc}}\right)^{-2.2}. \quad (2.8)$$

The cluster-galaxy cross correlation function is an especially useful probe on these intermediate scales, $10h^{-1}\text{Mpc} \lesssim r \lesssim 20h^{-1}\text{Mpc}$. Although the effects of projection contamination on $\xi_{cg}(r)$ have not yet been studied, it should be more accurately determined than the cluster-cluster two-point function because of the large number of galaxies in the Lick catalog (Lilje and Efstathiou 1988b). Although the quoted statistical errors in the slope and correlation length of ξ_{cg} are small, Lilje and Efstathiou (1988b) note that roughly 25 – 30% errors in the correlation length arise from uncertainties in the observer selection function and the K-correction.

Recently, several groups have analyzed the galaxy peculiar velocity correlation tensor on large scales (GDSWY; GJO; Szalay 1988; Kaiser 1989). The large-scale flows are well modeled by the Great Attractor model, supplemented with Virgo infall; that is, the large-scale velocity field is dominated by gravitational effects. However, when the gravitationally induced bulk flow is subtracted from the data, a statistically significant residual velocity field remains (GJO, Figs. 6 and 7). Splitting the velocity correlation function into parallel (Π) and perpendicular (Σ) components, $\langle \vec{v}(\vec{r}^{\prime}) \cdot \vec{v}(\vec{r}^{\prime} + \vec{r}) \rangle_{\vec{r}} = \Pi(r) + 2\Sigma(r)$, GJO find that the means of the residual components for the spiral galaxy sample are

$$\begin{aligned} \Pi &= (-0.79 \pm 0.16)(100\text{km/sec})^2 \\ \Sigma &= (-0.34 \pm 0.27)(100\text{km/sec})^2 \end{aligned} \quad (2.9)$$

over the range $r = 10 - 30h^{-1}\text{Mpc}$. The parallel component is statistically significant, but the perpendicular component is not. In principle, the residual field could arise from void expansion, in addition to other effects such as infall onto forming clusters (GJO). Barring unlikely cancellations between the different possible sources of the residual field, we can use the values of Π and Σ above as upper bounds on the magnitude of the velocity field generated by shell expansion. (Since a large fraction of spirals lie on the surfaces of shells, it is natural to use the spirals as indicators of shell motion.) Given the observational difficulties, the velocity data should be interpreted with caution: the galaxies are not uniformly sampled, and the presence of bulk flows on scales comparable to the sample size indicates the data do not constitute a fair sample (GJO).

The void probability function (VPF), $\phi_o(r)$, is the probability that a randomly placed sphere of radius r contains no galaxies. The VPF has been analyzed for sub-samples of the CfA1

survey (Hamilton 1985; Panek 1985; Maurogordato and Lachieze-Rey 1987, hereafter ML) and for the Perseus-Pisces survey (Fry, *etal.* 1989), for void radii up to $r \sim 10h^{-1}$ Mpc. We discuss the observations in subsequent sections. Here, we merely note that the ‘raw’ VPF is strongly sensitive to fluctuations in the number density of galaxies in a sample, which are known to be large in present redshift surveys. For example, de Lapparent, Geller, and Huchra (1988) estimate that the uncertainty in the mean density of the CfA1 (14.5) sample is $\delta n_g/n_g \simeq 1$. If galaxies were distributed in a random Poisson process with mean density n_g , the VPF would be $\phi_o(V) = e^{-n_g V}$, so that order unity fluctuations in density propagate into large fluctuations in the void probability. This is displayed dramatically in the randomly diluted samples studied by Einasto, *etal.* (1990). On the other hand, if the galaxy distribution is hierarchical, the modified VPF, $\chi = -\ln(\phi_o)/n_g V$, exhibits a scaling behavior, in which case it is relatively insensitive to the sampling density. An additional problem in using the CfA1 data to test the model is that the depth of the survey is only $D \simeq 60h^{-1}$ Mpc; it therefore does not contain the prominent $r = 25h^{-1}$ Mpc void seen in the first CfA2 slice. As a symptom of this, the VPF is only reliably determined for $r \lesssim 9h^{-1}$ Mpc.

The galaxy statistics above are the observables we will investigate in the shell model. In the context of that model, there are additional features of the large-scale galaxy distribution which, although formally parameters of the model, are what might be called qualitative observables. These include the bubble volume filling factor, $f = \overline{V_{sh} n_{sh}}$, where $\overline{V_{sh}}$ is the mean shell volume and $\overline{n_{sh}}$ the mean number density of shells. Eyeballing the CfA2 slices, the shells appear to have a filling factor of order unity, and a typical radius $\overline{R} \sim 15h^{-1}$ Mpc. These rough estimates are confirmed by the numerical simulations of Ostriker and Strassler (1989), who find that the visual appearance and projected void probability of the first CfA2 slice can be reproduced if $f = 1.0 - 1.5$ and $\overline{R} = (13.5 \pm 1.5)h^{-1}$ Mpc. We will use these numbers as rough guides in studying the shell model below. (We note, however, that Ostriker and Strassler (1989) use a very different shell radius distribution from WOD: their model is closer to the case of equal size shells, discussed in §II below.) The other qualitative feature we note is that the bubbles are not completely empty of galaxies, and are therefore not to be identified one-to-one with voids in the pure sense. For example, the Bootes ‘void’ contains 3 IRAS galaxies where 11 are expected in the mean (Strauss and Huchra 1988), while the CfA2 bubbles seem to have roughly 10% of the mean galaxy number density (Geller and Huchra 1988). On the theoretical side, cold-dark-matter models predict that ‘voids’ comparable to the CfA bubbles have roughly 20 percent of the mean density (White, *etal.* 1987). This qualitatively motivates the inclusion of an unclustered (or very weakly clustered) population of background galaxies in the shell model (see Section V).

III. EQUAL SIZE SHELLS

In the simplest version of the shell model, galaxies are assumed to be placed randomly on the surfaces of equal size shells. In this case, there are only two parameters in the model: the shell radius, R_{sh} , and the volume filling factor, f , defined by

$$f \equiv \frac{4\pi}{3} n_{sh} R_{sh}^3, \quad (3.1)$$

where n_{sh} is the number density of shells. We also assume that shells are randomly distributed in space, and are infinitely thin. Since the typical shell thickness in the CfA slices is $\delta R_{sh} \lesssim 2 -$

$3h^{-1}\text{Mpc}$ (de Lapparent, Geller, and Huchra 1986), our calculations are trustworthy only on scales $r \gtrsim 2 - 3h^{-1}\text{Mpc}$. We verify this in Appendix A by calculating the two-point correlation function of galaxies on shells with finite thickness δR_{sh} and comparing it with the case of infinitely thin shells.

a) Two-Point Correlation Function

The two-point correlation function is defined by

$$\delta P = n_g \delta V [1 + \xi_{gg}(r)]. \quad (3.2)$$

Here, δP is the conditional probability that, starting at a given galaxy, another galaxy is found in the volume element δV at separation r ; n_g is the number density of galaxies, related to the number density of shells by

$$n_g = n_{sh} 4\pi R_{sh}^2 \mathcal{N}_{sh}, \quad (3.3)$$

where \mathcal{N}_{sh} is the surface number density of galaxies on the shells. δP gets contributions from two galaxies on the same shell (δP_s) and from two galaxies on different shells (δP_d); both are easily calculated:

$$\delta P_s = \begin{cases} 2\pi r dr \mathcal{N}_{sh} & \text{if } r < 2R_{sh} \\ 0 & \text{if } r > 2R_{sh}, \end{cases} \quad (3.4)$$

$$\delta P_d = n_g \delta V. \quad (3.5)$$

In writing the expression for δP_d , we assumed the shells have a random Poisson distribution. Using the volume element for a spherical shell,

$$\delta V = 4\pi r^2 dr, \quad (3.6)$$

the two-point correlation function is then

$$\xi_{gg}(r) = \begin{cases} \frac{R_{sh}}{6fr} & \text{if } r < 2R_{sh} \\ 0 & \text{if } r > 2R_{sh} \end{cases} \quad (3.7)$$

(This result was noted independently by Ostriker and Strassler (1989).) Note that the only non-zero component of $\xi_{gg}(r)$ comes from two galaxies on the same shell. We also note the general feature that the correlation function vanishes for $r > 2R_{sh}$.

Figure 1 shows the two-point correlation function for $f = 0.8, 1.0,$ and 1.2 . The two-point function for equal size shells has slope $\gamma_o = 1$, clearly smaller than the observed slope, $\gamma_o = 1.8 \pm 0.2$. The correlation length, $r_o = R_{sh}/(6f)$, is also small: if the typical shell radius is $R_{sh} \approx 15h^{-1}\text{Mpc}$ and $f \approx 1$ (as suggested by the CfA2 survey data), then $r_o \approx 2.5h^{-1}\text{Mpc}$, a factor of 2 below the observed value. The r^{-1} behavior of the two-point correlation function is a reflection of the two-dimensional nature of the galaxy distribution in this model. We suspect this is one of the reasons for the long tails seen in some of the simulations of BHS. However, since the two-point correlation function is cut off at the bubble diameter, a decreasing distribution of larger shell sizes is expected to steepen the slope (see section IV).

b) Three-Point Correlation Function

The three-point correlation function is defined by

$$\delta P = n_g^2 \delta V_2 \delta V_3 [1 + \xi_{gg}(r_a) + \xi_{gg}(r_b) + \xi_{gg}(r_c) + \zeta(r_a, r_b, r_c)]. \quad (3.8)$$

Here, δP is the conditional probability involving two steps that, starting at a given galaxy 1, a second galaxy 2 is found in the volume element δV_2 at separation r_a from galaxy 1 and a third galaxy 3 is found in the volume element δV_3 at separation r_b from galaxy 1 and r_c from galaxy 2. In the shell model, there are three different contributions to δP : 1) that from three galaxies on the same shell (δP_1); 2) that from two galaxies on the same shell and one galaxy on another shell (δP_2); and 3) that from three galaxies on three different shells (δP_3).

δP_1 is given by the product $\delta P_1 = \delta P_{1,1} \cdot \delta P_{1,2}$, where $\delta P_{1,1}$ is the probability of finding galaxy 2, and $\delta P_{1,2}$ is the probability of finding galaxy 3, given galaxies 1 and 2. $\delta P_{1,1}$ is obtained from Eqn.(3.4) by substituting r_a for r . The calculation of $\delta P_{1,2}$, given in Appendix C, involves spherical trigonometry, with the result

$$\delta P_{1,2} = \begin{cases} \frac{4r_b r_c}{\sqrt{F_{abc}}} dr_b dr_c \mathcal{N}_{sh} & \text{if } r_b, r_c < 2R_{sh} \text{ and } F_{abc} > 0 \\ 0 & \text{otherwise} \end{cases}. \quad (3.9a)$$

where

$$F_{abc} \equiv 2r_a^2 r_b^2 + 2r_b^2 r_c^2 + 2r_c^2 r_a^2 - r_a^4 - r_b^4 - r_c^4 - \frac{r_a^2 r_b^2 r_c^2}{R_{sh}^2}. \quad (3.9b)$$

δP_2 is the sum of three components: galaxies 1 and 2 sharing the same shell ($\delta P_{2,1}$), galaxies 2 and 3 sharing the same shell ($\delta P_{2,2}$), and galaxies 3 and 1 sharing the same shell ($\delta P_{2,3}$). Assuming the shells are randomly distributed, we find

$$\delta P_{2,1} = \begin{cases} 2\pi r_a dr_a \mathcal{N}_{sh} \times n_g \delta V_{a,bc} & \text{if } r_a < 2R_{sh} \\ 0 & \text{if } r_a > 2R_{sh} \end{cases} \quad (3.10)$$

where $\delta V_{a,bc}$ is the volume element at separations r_b and r_c from two given points which are separated by r_a . $\delta P_{2,2}$ and $\delta P_{2,3}$ are obtained by permuting indices a , b , and c in Eqn.(3.10). The volume element $\delta V_{a,bc}$, derived in Appendix B, is given by

$$\delta V_{a,bc} = 2\pi \frac{r_b r_c}{r_a} dr_b dr_c. \quad (3.11)$$

Finally,

$$\delta P_3 = n_g^2 \delta V_2 \delta V_3, \quad (3.12)$$

again using the assumption that the shells have a random Poisson distribution. Here, $\delta V_2 = 4\pi r_a^2 dr_a$, and $\delta V_3 = \delta V_{a,bc}$.

Summing $\delta P = \delta P_1 + \delta P_2 + \delta P_3$ and comparing with Eqn.(3.8), after some manipulation we obtain the reduced part of the three-point correlation function,

$$\zeta(r_a, r_b, r_c) = \begin{cases} \frac{R_{sh}^2}{9\pi f^2 \sqrt{F_{abc}}} & \text{if } r_a, r_b, r_c < 2R_{sh} \text{ and } F_{abc} > 0 \\ 0 & \text{otherwise} \end{cases}. \quad (3.13)$$

ζ corresponds to the component δP_1 , *i.e.*, it receives a non-zero contribution only from three galaxies on the same shell. The contribution δP_2 from two galaxies on the same shell and one galaxy on another shell constitutes the terms proportional to $\xi_{gg}(r_a) + \xi_{gg}(r_b) + \xi_{gg}(r_c)$ in Eqn.(3.8), and it is obvious from Eqn.(3.12) that three galaxies on three different shells give rise to the first (Poisson) term in Eqn.(3.8). Using Eqn.(3.7), the scaled three-point correlation function Q , defined in Eqn.(2.3), becomes

$$Q(r_a, r_b, r_c) = \begin{cases} \frac{4}{\pi} \frac{r_a r_b r_c}{(r_a + r_b + r_c) \sqrt{F_{abc}}} & \text{if } r_a, r_b, r_c < 2R_{sh} \text{ and } F_{abc} > 0 \\ 0 & \text{otherwise} \end{cases} \quad (3.14)$$

Note that Q is independent of the shell filling factor f , since $\zeta \propto 1/f^2$ and $\xi_{gg}(r) \propto 1/f$.

Since Q (or ζ) is a symmetric function of its arguments, we can set $r_a < r_b < r_c$ and introduce a new set of variables

$$\begin{aligned} r &= r_a, & u &= r_b/r_a, & v &= (r_c - r_b)/r_a, \\ & & u &> 1, & 0 &< v < 1, \end{aligned} \quad (3.15)$$

following Groth and Peebles (1977). In Figure 2, we plot Q as a function of r : Q was calculated for $0 < r_a, r_b, r_c < R_{sh}$ and averaged over the two variables u, v over this range. The resulting Q is quite flat, but the amplitude ($Q < 0.4$) is somewhat small compared with the observed value ($Q \simeq 1.0 \pm 0.4$). The range of separations, *i.e.*, values of r_a, r_b, r_c , over which Q was calculated and averaged is somewhat arbitrary. However, the resulting Q depends only weakly on the range of values chosen, and we could not reproduce the observed amplitude with any range of values.

c) Peculiar Velocity Correlation Function

So far, we have focused on the purely static, geometric features of the shell model. To calculate the peculiar velocity correlation requires an additional assumption: the dynamics of galaxies. We assume that shells are uniformly expanding or contracting with velocity \mathcal{V}_{sh} and that the peculiar velocities of galaxies arise in part from this radial motion of shells. The velocities of the shells depend on the cosmological model. For example, for an isolated self-similar void in an $\Omega = 1$ universe, the typical expected shell velocity is of order $\mathcal{V}_{sh} = H_0 R_{sh}/5 = 300(R_{sh}/15h^{-1}Mpc)$ km/sec (Bertschinger 1983; Ikeuchi, Tomisaka, and Ostriker 1983). However, in an open universe, peculiar velocities decay, and in a universe dominated by collisionless dark matter, the gravity of the dark matter will slow down the shell expansion for some time. In addition, since the volume filling factor of shells in the CfA2 survey is estimated to be of order unity (Ostriker and Strassler 1989), typical shells have several neighbors with which they have interacted (Yoshioka and Ikeuchi 1990). Presumably, once they collide, the coherent shell motions are damped out. Thus, since the present shell velocities may well be small on the Hubble scale, the estimate of \mathcal{V}_{sh} above should be taken as an upper limit.

The dimensionless peculiar velocity correlation functions are defined by

$$\xi_{vv}^{\parallel}(r) \equiv \frac{\langle \vec{v}_{\parallel}(\vec{r}') \cdot \vec{v}_{\parallel}(\vec{r}' + \vec{r}) \rangle_{\vec{r}'}}{\mathcal{V}_{sh}^2}, \quad (3.16)$$

$$\xi_{vv}^{\perp}(r) \equiv \frac{\langle \vec{v}_{\perp}(\vec{r}') \cdot \vec{v}_{\perp}(\vec{r}' + \vec{r}) \rangle_{\vec{r}}}{\mathcal{V}_{sh}^2}, \quad (3.17)$$

$$\xi_{vv}(r) \equiv \frac{\langle \vec{v}(\vec{r}') \cdot \vec{v}(\vec{r}' + \vec{r}) \rangle_{\vec{r}}}{\mathcal{V}_{sh}^2}, \quad (3.18)$$

and the relative peculiar velocity is defined by

$$v_{12}(r)\hat{r} \equiv \frac{\langle \vec{v}(\vec{r}') - \vec{v}(\vec{r}' + \vec{r}) \rangle_{\vec{r}}}{\mathcal{V}_{sh}}, \quad (3.19)$$

where \vec{v}_{\parallel} and \vec{v}_{\perp} are the parallel and perpendicular components of peculiar velocity with respect to the line joining two galaxies separated by \vec{r} . Here, $\xi_{vv}^{\parallel}(r)$ and $\xi_{vv}^{\perp}(r)$ are the parallel and perpendicular components of $\xi_{vv}(r)$, so $\xi_{vv}(r) = \xi_{vv}^{\parallel}(r) + \xi_{vv}^{\perp}(r)$. Note that $\Pi(r) = \xi_{vv}^{\parallel}(r) \cdot \mathcal{V}_{sh}^2$ is the parallel component of the velocity correlation tensor, and $2\Sigma(r) = \xi_{vv}^{\perp}(r) \cdot \mathcal{V}_{sh}^2$ is twice the perpendicular component. (For discussion of the velocity correlation tensor, see Davis and Peebles 1977; Górski 1988; Szalay 1988; GDSWY; GJO; Kaiser 1989.)

As with the spatial two-point correlation function, the peculiar velocity correlation function and the relative peculiar velocity naturally split into two components: one from two galaxies on the same shell and the other from two galaxies on different shells. For two galaxies on the same shell separated by distance r , elementary trigonometry gives

$$\vec{v}_{\parallel}(\vec{r}') \cdot \vec{v}_{\parallel}(\vec{r}' + \vec{r})|_{same} = -\frac{r^2}{4R_{sh}^2} \mathcal{V}_{sh}^2, \quad (3.20)$$

$$\vec{v}_{\perp}(\vec{r}') \cdot \vec{v}_{\perp}(\vec{r}' + \vec{r})|_{same} = \left(1 - \frac{r^2}{4R_{sh}^2}\right) \mathcal{V}_{sh}^2, \quad (3.21)$$

$$\vec{v}(\vec{r}') \cdot \vec{v}(\vec{r}' + \vec{r})|_{same} = \left(1 - \frac{r^2}{2R_{sh}^2}\right) \mathcal{V}_{sh}^2, \quad (3.22)$$

$$\vec{v}(\vec{r}') - \vec{v}(\vec{r}' + \vec{r})|_{same} = \frac{\vec{r}}{R_{sh}} \mathcal{V}_{sh}. \quad (3.23)$$

Assuming the distribution of shells is random, the contribution from two galaxies on different shells vanishes on average. Hence, the parallel component of the peculiar velocity correlation function becomes

$$\xi_{vv}^{\parallel}(r) = \frac{\vec{v}_{\parallel}(\vec{r}') \cdot \vec{v}_{\parallel}(\vec{r}' + \vec{r})|_{same}}{\mathcal{V}_{sh}^2} \left(\frac{\xi_{gg}(r)}{1 + \xi_{gg}(r)} \right), \quad (3.24)$$

where the last term is the fraction of all galaxy pairs, separated by distance r , which are on the same shell. Using equation (3.7), this becomes

$$\xi_{vv}^{\parallel}(r) = \begin{cases} \frac{-r^2/4R_{sh}^2}{1+6f\tau/R_{sh}} & \text{if } r < 2R_{sh} \\ 0 & \text{if } r > 2R_{sh} \end{cases}. \quad (3.25)$$

Similarly,

$$\xi_{vv}^\perp(r) = \begin{cases} \frac{1-r^2/4R_{sh}^2}{1+6f\tau/R_{sh}} & \text{if } r < 2R_{sh} \\ 0 & \text{if } r > 2R_{sh} \end{cases}, \quad (3.26)$$

$$\xi_{vv}(r) = \begin{cases} \frac{1-r^2/2R_{sh}^2}{1+6f\tau/R_{sh}} & \text{if } r < 2R_{sh} \\ 0 & \text{if } r > 2R_{sh} \end{cases}, \quad (3.27)$$

$$v_{12}(r) = \begin{cases} \frac{\tau/R_{sh}}{1+6f\tau/R_{sh}} & \text{if } r < 2R_{sh} \\ 0 & \text{if } r > 2R_{sh} \end{cases}. \quad (3.28)$$

Figure 3 shows the peculiar velocity correlation function and the relative peculiar velocity for $f = 0.8$. Here, the dot-short dashed curve corresponds to $\xi_{vv}^\parallel(r)$ ($\text{II}/\mathcal{V}_{sh}^2$), the dot-long dashed curve is $\xi_{vv}^\perp(r)$ ($2\Sigma/\mathcal{V}_{sh}^2$), the short dashed curve is $\xi_{vv}(r)$ ($(\text{II} + 2\Sigma)/\mathcal{V}_{sh}^2$), and the solid curve is $v_{12}(r)$. The magnitude of the velocity correlation function and the relative peculiar velocity are smaller if the filling factor f is larger. As expected from the shell geometry, $\xi_{vv}^\parallel(r)$ (II) is always negative and $\xi_{vv}^\perp(r)$ (Σ) is positive.

These results can be compared with recent analyses of large-scale peculiar velocity observations (GDSWY, GJO), in particular, the residual components II and Σ averaged over the range $10h^{-1} - 30h^{-1}$ Mpc, given in Eqn.(2.9). Since the residual field may come from several sources, we use these values as upper limits on the magnitude of the shell velocity. Even qualitatively, the shell model velocities do not accord well with the observations: although the parallel component $\text{II}(r)$ for the spiral sample is negative, it is not a monotonic function of r , in contrast with the shell model. More important, the shell model prediction for the perpendicular component, averaged over the same range in r (assuming $R_{sh} = 15h^{-1}$ Mpc), is $\Sigma \simeq 0.4(100 \text{ km/sec})^2(\mathcal{V}_{sh}/300 \text{ km sec}^{-1})^2$, while $\xi_{vv}^\perp(r)$ ($\Sigma(r)$) for spirals is negative or consistent with zero. For the shell model value of Σ to agree with the observations at the 2σ level, the shell velocity must satisfy $\mathcal{V}_{sh} \lesssim 200 \text{ km/sec} = H_0 R_{sh}/7.5$. In this case, however, the shell model value for II is significantly smaller than the observations, so that shell motions could not dominate the residual velocity field. (Peebles (1988b) has already noted difficulties with the *local* velocity field if one interprets it in terms of the explosion model.)

d) Void Distribution

The most striking feature of the CfA slices is the preponderance of large voids: this is, after all, the motivation of the shell model. Thus, a plausible shell model should accurately reproduce the void distribution. In the shell model, the void probability function (VPF) $\phi_o(r)$ is just the probability that a randomly placed volume $V = (4\pi/3)r^3$ is empty of *bubble walls*. In a more realistic model, galaxies would not be spread uniformly on a shell, but would have a patchy distribution on and within the bubble surface; in this case, the volume V could have bubble walls crossing it which happened to be empty of galaxies in V . We assume this makes a negligible correction to the VPF on scales \gtrsim a few h^{-1} Mpc.

The probability of a void of radius r depends on whether r is larger or smaller than the shell radius R_{sh} . If $r \geq R_{sh}$, then $\phi_o(r)$ is just the probability of having no shell centers within a volume $V' = (4\pi/3)(R_{sh} + r)^3$. On the other hand, if $r \leq R_{sh}$, the VPF is given by the probability of having no shell centers within a volume $V' - V''$, where $V'' = (4\pi/3)(R_{sh} - r)^3$. Since the shell centers have a random Poisson distribution, the probability of finding no shell centers in a volume \tilde{V} is just $\exp(-n_{sh}\tilde{V})$. Thus, the VPF is given by

$$\phi_o(r) = \begin{cases} \exp\left[-f\left(1 + \frac{r}{R_{sh}}\right)^3\right] & \text{if } r \geq R_{sh} \\ \exp\left[-2f\left(3\frac{r}{R_{sh}} + \frac{r^3}{R_{sh}^3}\right)\right] & \text{if } r \leq R_{sh} \end{cases} . \quad (3.29)$$

In Figure 4, the resulting void probability function is plotted for $f = 0.8$ (solid curve) and 1.2 (short dashed curve). For comparison, the VPF for a random Poisson distribution of galaxies is also shown (dot-short dashed curve). To place the latter in the same figure, we have chosen $n_g R_{sh}^3 = 0.01 h^3 \text{Mpc}^{-3} \cdot (15 h^{-1} \text{Mpc})^3 = 33.75$, where n_g is the mean density of galaxies in typical samples.

Care must be taken in comparing the shell model VPF with the data available from redshift surveys. The shell model result for the VPF is apparently inconsistent with the analysis of the CfA1 data by ML: they find the observed VPF approaches the Poisson form at small r , but is enhanced over Poisson for $r > 1 h^{-1}$ Mpc. Unlike the data and most models for large-scale structure formation (Fry, *et al.*, 1989), the VPF for the shell model does not approach a Poisson distribution at small r : the slope of the shell model VPF at zero radius is $-6f/R_{sh}$, while realistic distributions have zero slope at $r = 0$. This difference, however, is an artifact of the assumption of zero-thickness bubbles: clearly Eqn.(3.29) is not valid for $r \lesssim \delta R_{sh} \simeq 2 - 3 h^{-1}$ Mpc. (It is straightforward to show that the slope and curvature of the shell model VPF with finite thickness shells approach zero for $r \ll \delta R_{sh}$.) In Fig. 4, assuming $R_{sh} = 15 h^{-1}$ Mpc, this implies that the shell model curves cannot be extrapolated below $r/2R_{sh} = 0.1$. On the other hand, the plots of ML only extend up to $r = 8.7 h^{-1}$ Mpc, corresponding to $r/2R_{sh} = 0.29$ in Fig. 4. Over the range $3 h^{-1}$ Mpc $< r < 7 h^{-1}$ Mpc where they can be reliably compared, the shell model VPF with $f = 0.8$ and $R_{sh} = 15 h^{-1}$ Mpc agrees with the results of ML to within a factor of 2, although the shell model VPF is flatter, with a tail extending to larger radii. It is difficult to estimate the significance of this, since the figures of ML display no error bars. However, as noted in Section II, the value and slope of the VPF are very sensitive to fluctuations in the mean density of the sample (Einasto, *et al.*, 1990), and for the CfA1 survey, the density fluctuations are estimated to be of order unity (de Lapparent, Geller, and Huchra 1988).

Alternatively, we can consider the scaled void probability (*e.g.*, Fry 1986), $\chi = -\ln(\phi_o)/\overline{N_g}$, where $\overline{N_g} = \overline{n_g}V$ is the mean number of galaxies (in the sample) in a volume $V = (4\pi/3)r^3$. For a hierarchical galaxy distribution, χ is a function only of $\overline{N_g}\xi$, where $\xi = \overline{n_g}^2 \int_V dV_1 dV_2 \xi_{12}/\overline{N_g}^2$. For the case at hand, we have $\overline{N_g}\xi = 4\pi R_{sh} \overline{n_g} r^2 / 15f$, so that

$$\chi = \frac{18}{15} (\overline{N_g}\xi)^{-1} + \frac{2n_{sh}}{\overline{n_g}} . \quad (3.30)$$

The second term here is just twice the inverse number of galaxies per shell; since the VPF data only extends up to $r \simeq 9h^{-1}$ Mpc and we assume $R_{sh} \simeq 15h^{-1}$ Mpc, Eqn.(3.29) shows that we can neglect the second term in Eqn.(3.30) when comparing to the CfA1 data. Thus, over the range that it can be compared to the data, the shell model VPF exhibits the scaling form expected of a hierarchical distribution to excellent approximation. Since $\chi \leq 1$ by definition, Eqn.(3.30) is only valid for $\overline{N_g \xi} > 18/15$. For the CfA1 survey with $\overline{n_g} = 0.01h^{-3}\text{Mpc}^{-3}$, $\overline{N_g \xi} \simeq 1.5(r/h^{-1}\text{Mpc})^{1.23}$ (Fry 1986), so $\overline{N_g \xi} > 18/15$ corresponds to $r > 0.8h^{-1}$ Mpc; clearly this is not an important limitation, since we do not trust the shell model on scales $r \lesssim \delta R_{sh} \simeq 3h^{-1}$ Mpc anyway. On scales $r \gtrsim 3h^{-1}$ Mpc, corresponding to $\overline{N_g \xi} > 5.8$ in the CfA1 survey, the shell model function $\chi(\overline{N_g \xi})$ lies below the data curves for χ from both the CfA1 and Perseus-Pisces surveys (ML; Fry, *etal.*, 1989). That is, the shell model predicts an excess of large voids compared to the data. The shell model function χ does lie above the ‘minimal’ model of Fry (1986), as expected.

IV. DISTRIBUTION OF SHELL SIZES

In this section, we consider models in which shells have a range of radii, generalizing the results of the previous section. The expressions we will derive for the spatial and velocity correlation functions and the void probability function hold for an *arbitrary* distribution of shell radii. As an important application of these general results, in the figures, Tables, and Appendix D, we display results for a power law distribution of shell radii.

Let $n_{sh}(R)dR$ be the number density of shells with radii between R and $R + dR$. The galaxy surface number density, $\mathcal{N}_{sh}(R)$, and the peculiar velocity due to shell expansion or contraction, $\mathcal{V}_{sh}(R)$, are generally functions of the shell radius R as well. Then the number density of galaxies is

$$n_g = \int_0^\infty 4\pi R^2 \mathcal{N}_{sh}(R) n_{sh}(R) dR, \quad (4.1)$$

and the shell volume filling factor is

$$f = \int_0^\infty \frac{4}{3}\pi R^3 n_{sh}(R) dR. \quad (4.2)$$

It is useful to introduce some additional definitions to streamline the notation in this and subsequent sections. The number density of shells with radius $R > r/2$ is given by

$$\overline{n_{sh}}(r/2) = \int_{r/2}^\infty n_{sh}(R) dR. \quad (4.3)$$

The n th moment of the galaxy surface density, averaged over shells with radius $R > r/2$ is defined by

$$\overline{\mathcal{N}_{sh}^n}(r/2) = \frac{1}{\overline{n_{sh}}(r/2)} \int_{r/2}^\infty \mathcal{N}_{sh}^n(R) n_{sh}(R) dR. \quad (4.4)$$

Similarly, we define a shell radius moment,

$$\overline{R_m^n}(r/2) = \frac{1}{\overline{\mathcal{N}_{sh}^m}(r/2) \overline{n_{sh}}(r/2)} \int_{r/2}^\infty R^n \mathcal{N}_{sh}^m(R) n_{sh}(R) dR, \quad (4.5)$$

and a shell velocity moment,

$$\overline{V_m^n}(r/2) = \frac{1}{R_2^m(r/2)\overline{\mathcal{N}_{sh}^2}(r/2)\overline{n_{sh}}(r/2)} \int_{r/2}^{\infty} V_{sh}^n(R) R^m \mathcal{N}_{sh}^2(R) n_{sh}(R) dR. \quad (4.6)$$

Using these definitions, the galaxy number density and shell volume filling factor become

$$n_g = 4\pi \overline{R_1^2}(0) \overline{\mathcal{N}_{sh}^1}(0) \overline{n_{sh}}(0), \quad (4.7)$$

$$f = \frac{4}{3} \pi \overline{R_0^3}(0) \overline{n_{sh}}(0). \quad (4.8)$$

Although we will derive the correlation functions and VPF for an arbitrary distribution of shell radii, it is also useful to focus on a particular class of models (WOD, BHS): a power law distribution of shell radii, with cutoffs at a maximum and minimum radius. Before discussing the general results, we now specify the parameters of the power law model. In this case, the differential shell number density is

$$n_{sh}(R) = \begin{cases} n_{sh,o} (R/R_{max})^{-\alpha} & \text{if } R_{min} \leq R \leq R_{max} \\ 0 & \text{otherwise} \end{cases}. \quad (4.9)$$

We also assume the galaxy surface number density and shell expansion velocity are power law functions of shell radius,

$$\mathcal{N}_{sh}(R) = \mathcal{N}_{sh,o} (R/R_{max})^\beta, \quad (4.10)$$

$$V_{sh}(R) = V_{sh,o} (R/R_{max})^\gamma. \quad (4.11)$$

The various shell density, surface density, shell radius, and shell velocity moments defined in Eqns.(4.3-4.6) are given explicitly in Appendix D for this model.

In the power law model, the spatial distribution of galaxies depends on five independent parameters: f , α , R_{max} , R_{min}/R_{max} , and β . None of these parameters is well determined from observations, although the redshift surveys roughly suggest expected values for several of them. We will use the observations and the theoretical work of WOD as guides to the relevant regions of parameter space to explore. From the first CfA2 slice, the shell volume filling factor is estimated to be $f \simeq 1 - 1.5$ (Ostriker and Strassler 1989), while WOD used $f = 0.8 - 1.2$ to fit the cluster correlation function (the filling factor quoted in WOD is lower than this, because they only included shells with radius in the range $R_{max}/2 < R < R_{max}$ in their definition of f). The largest voids seen in recent redshift surveys have diameters of roughly $50 h^{-1}$ Mpc, suggesting a maximum shell radius of order $R_{max} \simeq 30 h^{-1}$ Mpc. However, since these voids have sizes comparable to the depth of the survey, potentially larger structures could have been missed. For example, the deep pencil-beam surveys suggest the existence of underdense regions with scales up to $130 h^{-1}$ Mpc (Peterson, *et al.* 1986; Koo, Kron, and Szalay 1987; Broadhurst *et al.* 1989). Therefore, this estimate of R_{max} is likely a lower bound to the true value. In the CfA2 data, the shell thickness and mean galaxy separation inside shells appear to be roughly independent of shell diameter (de Lapparent, Geller, and Huchra 1988); this suggests that the galaxy surface density is approximately constant, *i.e.*, $\beta \simeq 0$. On the other hand, if shells are formed by explosions, then the shell mass, and thus the number of galaxies per shell, should be proportional to the bubble volume swept out, which would imply $\beta \simeq 1$. We will therefore consider values of β between 0

and 1. The number of large voids in the redshift surveys is currently too small to determine the shell distribution exponent α (de Lapparent, Geller, and Huchra 1988). On the theoretical side, WOD showed that the observed cluster mass function and cluster two-point correlation function can be fit reasonably well if $\alpha \simeq 4$. In this case, the shell distribution would be approximately scale-invariant, since each logarithmic decade in R makes an equal contribution to the filling factor f . For this choice of α , the number density of galaxies is dominated by the smallest shells if $\beta < 1$. On the other hand, the CfA2 results indicate that the the largest voids lead to significant fluctuations in the galaxy number density across the sample (de Lapparent, Geller, and Huchra 1988), suggesting that perhaps $3 + \beta - \alpha \geq 0$. However, we will see below that this condition does not yield a reasonable galaxy two-point function, so we will not impose it. (The best fit models below violate this condition weakly.) For the reasons cited above, the ratio R_{min}/R_{max} is also poorly determined from observations. In their models, WOD somewhat arbitrarily set $R_{min}/R_{max} = 1/8$, but they argued that the statistics of clusters are insensitive to it. We will see that the statistics of galaxies *are* sensitive to this parameter, and use both $R_{min}/R_{max} = 1/8$ and $1/15$ to span a reasonably broad range of plausible values.

There are two additional parameters which enter into the peculiar velocity correlation function, γ and $\mathcal{V}_{sh,o}$. Following the work on expanding positive energy shells, we will assume the peculiar expansion velocity of each shell is a fixed fraction of its Hubble velocity, *i.e.*, $\gamma = 1$. The parameter $\mathcal{V}_{sh,o}$, which fixes the magnitude of the peculiar velocity of galaxies, only appears as an overall normalization constant in the peculiar velocity correlation function, so it may be scaled out of the problem. Of course, it enters when comparing the model with observations. To summarize, in this and subsequent sections, we will investigate the following ranges of parameter values:

$$\begin{aligned}
0.8 \lesssim f \lesssim 1.2, \\
3.5 \lesssim \alpha \lesssim 4.5, \\
R_{max} = 30h^{-1}\text{Mpc}, \\
R_{min} = 2.0 \text{ and } 3.8h^{-1}\text{Mpc}, \\
0 \leq \beta \leq 1, \\
\gamma = 1.
\end{aligned} \tag{4.12}$$

a) Two-Point Correlation Function

The calculation of the two-point correlation function involves averaging $\xi_{gg}(r)$ for the case of equal size shells [Eqn.(3.7)] over shells with different radii. For randomly distributed shells, the contribution comes from two galaxies on the same shell with radius $R > r/2$. Hence, for $r < 2R_{max}$,

$$\begin{aligned}
\xi_{gg}(r) &= \frac{1}{4\pi r^2 dr n_g \cdot n_g} \int_{r/2}^{\infty} 2\pi r dr \mathcal{N}_{sh}(R) \cdot 4\pi R^2 \mathcal{N}_{sh}(R) n_{sh}(R) dR \\
&= \frac{1}{6fr} \frac{\overline{R_0^3(0)} \overline{R_2^2(r/2)} \overline{\mathcal{N}_{sh}^2(r/2)} \overline{n_{sh}(r/2)}}{\overline{R_1^2(0)} \overline{\mathcal{N}_{sh}^1(0)} \overline{n_{sh}(0)}},
\end{aligned} \tag{4.13}$$

where Eqns. (4.7) and (4.8) have been used. For $r > 2R_{max}$, the correlation function $\xi_{gg}(r)$ vanishes, and it is positive on all smaller scales. This suggests that the galaxy correlations recently found on large scales by Maddox, *et al.*, (1990) may reflect the bubbly structure of the galaxy distribution.

For the power law distribution of shell radii, we find

$$\xi_{gg}(r) \propto \begin{cases} 1/fr & \text{if } r < 2R_{min} \\ \frac{1-(r/2R_{max})^{3+2\beta-\alpha}}{fr(1-(r/2R_{min})^{3+2\beta-\alpha})} & \text{if } 2R_{min} < r < 2R_{max} \\ 0 & \text{if } 2R_{max} < r \end{cases} \quad (4.14)$$

Thus, $\xi_{gg}(r)$ has a simple power law form for $R_{min} \ll R_{max}$ and $2R_{min} \lesssim r \ll 2R_{max}$,

$$\xi_{gg}(r) \propto \begin{cases} r^{2+2\beta-\alpha} & \text{if } \beta \leq (\alpha - 3)/2 \\ r^{-1} & \text{if } \beta > (\alpha - 3)/2. \end{cases} \quad (4.15)$$

For example, if $\alpha = 4$ and $\beta = 0$, the slope of the correlation function is $\gamma_o = 2$, close to the observed value. Figures 5a-d show the two-point correlation function for several values of the free parameters. Noticeable features in the plots are: 1) a sharp break or kink at $r = 2R_{min}$ from $\xi \sim r^{-1}$ to a steeper power law, and 2) the steepening of the slope of ξ_{gg} at large separation r . The first feature is somewhat artificial, since it results from the sharp cutoff in the number density of shells at the minimum radius R_{min} ; a smooth cutoff in the shell distribution would round off the kink into a broad shoulder. The values of the slope γ_o and correlation length r_o for the various models are listed in Table 1. These values were determined by fitting the correlation function between $1/20 \leq r/2R_{max} \leq 1/5$ to the power law form in Eqn.(2.1). For $R_{max} = 30h^{-1}\text{Mpc}$, this range corresponds to $3h^{-1}\text{Mpc} \leq r \leq 12h^{-1}\text{Mpc}$. (Note that the ‘true’ correlation length \tilde{r}_o , defined by $\xi_{gg}(\tilde{r}_o) = 1$, differs slightly from the value of r_o obtained from the power law fit.) The slope γ_o is steeper if more galaxies belong to smaller shells, that is, for larger α , smaller β , and smaller R_{min}/R_{max} , but then the amplitude is smaller, as expected. Although the observed slope ($\gamma_o \simeq 1.8$) can be reproduced by the power law model, Table 1 shows that, for $f = 0.8 - 1.2$, the correlation length $r_o/2R_{max} \simeq 0.03 - 0.04$ is still roughly a factor of two below the observed value, $r_o = 5 \pm 1h^{-1}\text{Mpc}$ or $r_o/2R_{max} = 0.08 \pm 0.02$ for $R_{max} = 30h^{-1}\text{Mpc}$. The observed clustering strength could be reproduced if f were reduced to $f \simeq 0.4$, but this is substantially lower than the filling factor indicated by the redshift data. In the next section, we will see that this problem is alleviated by including cluster galaxies at shell intersections.

b) Three-Point Correlation Function

As with the two-point correlation function, the reduced part of the three-point correlation function, ζ , is found by averaging Eqn. (3.13) over shells with different radii. The only non-zero contribution to ζ comes from three galaxies on the same shell with radius $R > \max(r_a, r_b, r_c)/2$. Thus, for $r_a, r_b, r_c < 2R_{max}$,

$$\begin{aligned} \zeta(r_a, r_b, r_c) &= \frac{\int_{\max(r_a, r_b, r_c)/2}^{\infty} 2\pi r_a dr_a \mathcal{N}_{sh}(R) \cdot \frac{4r_b r_c}{R^2 \sqrt{F_{abc}}} dr_b dr_c \mathcal{N}_{sh}(R) \cdot 4\pi R^2 \mathcal{N}_{sh}(R) n_{sh}(R) dR}{4\pi r_a^2 dr_a n_g \cdot 2\pi \frac{r_b r_c}{r_a} dr_b dr_c n_g \cdot n_g} \\ &= \frac{4}{n_g^3} \int_{\max(r_a, r_b, r_c)/2}^{\infty} \frac{\mathcal{N}_{sh}^3(R) n_{sh}(R) dR}{\sqrt{F_{abc}}} \end{aligned}$$

where

$$F_{abc} = \left[\frac{2r_a^2 r_b^2 + 2r_b^2 r_c^2 + 2r_c^2 r_a^2 - r_a^4 - r_b^4 - r_c^4}{R^4} - \frac{r_a^2 r_b^2 r_c^2}{R^6} \right]. \quad (4.16)$$

Here, $\delta P_{1,2}$ from Eqn.(3.9) and $\delta V_{a,bc}$ from Eqn.(3.11) have been used. In this expression, the integration is only to be carried out over the range where $F_{abc} > 0$. Using Eqns.(4.7) and (4.8), this can be rewritten as

$$\zeta(r_a, r_b, r_c) = \frac{1}{9\pi f^2} \frac{\overline{R_0^3}(0)}{R_1^2(0) \overline{N_{sh}^1}(0) \overline{n_{sh}}(0)} \int_{\max(r_a, r_b, r_c)/2}^{\infty} \frac{\mathcal{N}_{sh}^3(R) n_{sh}(R) dR}{\sqrt{F_{abc}}}. \quad (4.17)$$

In Figures 6a-d, the scaled three-point correlation function Q is shown as a function of r for several values of the power law model parameters (see Eqn.(3.15) for the definition of r). Q was calculated from Eqns.(2.3), (4.13), and (4.17), for $0 < r_a/2R_{max}, r_b/2R_{max}, r_c/2R_{max} < 1/2$, and averaged over the variables u and v . For $r \lesssim 10h^{-1}\text{Mpc}$, corresponding to $r/2R_{max} \lesssim 0.17$ if $R_{max} = 30h^{-1}\text{Mpc}$, Q is fairly flat, with values in the range $0.4 \lesssim Q \lesssim 0.8$. This is in reasonable agreement with the observed value, $Q = 1.0 \pm 0.4$. For most of the parameter range, Q is flat for $r < 2R_{min}$, has an upward break at $r = 2R_{min}$ to an increasing function of r , and eventually falls to zero at $r = 2R_{max}$. (Again, the break would be rounded off in models with a smooth lower cutoff to the shell radius distribution.) Thus, the shell model predicts that Q will show an upward trend when it is measured reliably out to larger separations in the future.

c) Peculiar Velocity Correlation Function

To obtain the velocity correlation functions, we average Eqns.(3.25) to (3.28) over the shell radius distribution. For $r < 2R_{max}$,

$$\xi_{vv}^{\parallel}(r) = \frac{\int_{r/2}^{\infty} \left(-\frac{r^2}{4R^2}\right) \frac{V_{sh}^2(R)}{V_{sh,o}^2} \cdot 2\pi r \mathcal{N}_{sh}(R) \cdot 4\pi R^2 \mathcal{N}_{sh}(R) n_{sh}(R) dR}{4\pi r^2 n_g \cdot n_g \cdot (1 + \xi_{gg}(r))}, \quad (4.18)$$

$$\xi_{vv}^{\perp}(r) = \frac{\int_{r/2}^{\infty} \left(1 - \frac{r^2}{4R^2}\right) \frac{V_{sh}^2(R)}{V_{sh,o}^2} \cdot 2\pi r \mathcal{N}_{sh}(R) \cdot 4\pi R^2 \mathcal{N}_{sh}(R) n_{sh}(R) dR}{4\pi r^2 n_g \cdot n_g \cdot (1 + \xi_{gg}(r))}, \quad (4.19)$$

$$v_{12}(r) = \frac{\int_{r/2}^{\infty} \frac{r}{R} \frac{V_{sh}(R)}{V_{sh,o}} \cdot 2\pi r \mathcal{N}_{sh}(R) \cdot 4\pi R^2 \mathcal{N}_{sh}(R) n_{sh}(R) dR}{4\pi r^2 n_g \cdot n_g \cdot (1 + \xi_{gg}(r))}. \quad (4.20)$$

For $r > 2R_{max}$, the peculiar velocity correlation functions and the relative peculiar velocity are zero. Using Eqns.(4.7) and (4.8), we find

$$\xi_{vv}^{\parallel}(r) = \frac{1}{6fr(1 + \xi_{gg}(r))} \frac{\overline{R_0^3}(0)}{R_1^2(0)} \frac{\overline{\mathcal{N}_{sh}^2}(r/2)}{\overline{\mathcal{N}_{sh}^1}(0)} \frac{\overline{n_{sh}}(r/2)}{\overline{n_{sh}}(0)} \left[-\frac{r^2}{4} \frac{\overline{V_0^2}(r/2)}{V_{sh,o}^2} \right], \quad (4.21)$$

$$\xi_{vv}^{\perp}(r) = \frac{1}{6fr(1 + \xi_{gg}(r))} \frac{\overline{R_0^3(0)}}{\overline{R_1^2(0)}} \frac{\overline{N_{sh}^2(r/2)}}{\overline{N_{sh}^1(0)}} \frac{\overline{n_{sh}(r/2)}}{\overline{n_{sh}(0)}} \left[\frac{\overline{R_2^2(r/2)}}{\overline{V_{sh,o}^2}} \frac{\overline{V_2^2(r/2)}}{\overline{V_0^2(r/2)}} - \frac{r^2}{4} \frac{\overline{V_0^2(r/2)}}{\overline{V_{sh,o}^2}} \right], \quad (4.22)$$

$$\xi_{vv}(r) = \xi_{vv}^{\parallel}(r) + \xi_{vv}^{\perp}(r) \quad (4.23)$$

$$v_{12}(r) = \frac{1}{6f(1 + \xi_{gg}(r))} \frac{\overline{R_0^3(0)}}{\overline{R_1^2(0)}} \frac{\overline{N_{sh}^2(r/2)}}{\overline{N_{sh}^1(0)}} \frac{\overline{n_{sh}(r/2)}}{\overline{n_{sh}(0)}} \left[\frac{\overline{R_2^1(r/2)}}{\overline{V_{sh,o}}} \frac{\overline{V_1^1(r/2)}}{\overline{V_{sh,o}}} \right]. \quad (4.24)$$

Figures 7a-d show the peculiar velocity correlation function and the relative peculiar velocity for several values of power law model parameters. For larger α and smaller β , the velocity functions are smaller, since more of the galaxies belong to smaller shells. The overall features of the velocity functions are similar to those for the case of equal size shells (compare Figure 3), except that here the peculiar velocity functions smoothly approach zero as $r \rightarrow 2R_{max}$. To convert to physical units, the y -axis in Figure 7 should be multiplied by $V_{sh,o}^2$ (for the correlation functions) or $V_{sh,o}$ (for the relative peculiar velocity), where $V_{sh,o}$ is the expansion velocity of the largest shell. For example, in an explosion model with $R_{max} = 30h^{-1}$ Mpc and shell speed 20% of the Hubble velocity, we expect $V_{sh,o} \simeq 600$ km/sec. For this value of R_{max} , the x -axis in Fig. 7 should be multiplied by 6000 km/sec ($60h^{-1}$ Mpc). For these values, the parallel component of the shell velocity tensor is in reasonable accord with the data: for example, for the parameters of Fig. 7b, $\Pi(r = 1000 - 3000 \text{ km/sec}) \simeq -0.56(100\text{km/sec})^2$. However, as for the case of equal size shells, the perpendicular component has the wrong sign and, for the parameters given above, too large an amplitude in comparison with the data. For the model in Fig.7d to agree with the observed Σ to within 2σ , the expansion velocity of the largest shell must satisfy $V_{sh,o} \lesssim 280$ km/sec $\simeq 0.09H_0R_{max}$, substantially less than the value expected for an isolated shell in an $\Omega = 1$ universe. Given this upper bound, the parallel velocity component due to shells would be observationally negligible. For other choices of shell model parameters, the constraint from Σ is not as severe; *e.g.*, for the parameters of Fig. 7a, 2σ agreement with the perpendicular component implies $V_{sh,o} \lesssim 475$ km/sec $\simeq 0.16H_0R_{max}$. However, in all cases in which Σ is consistent at this level, the parallel component Π has insufficient amplitude to explain the residual velocity field.

d) Void Distribution

For a distribution of shell sizes, the void probability becomes

$$\phi_o(r) = \exp \left[- \left\{ \int_0^r V' n_{sh}(R) dR + \int_r^\infty (V' - V'') n_{sh}(R) dR \right\} \right], \quad (4.25)$$

where, as in the case of equal size shells, $V' = (4\pi/3)(R+r)^3$ and $V'' = (4\pi/3)(R-r)^3$. Note that, for a discrete distribution of shell sizes, the VPF is just the *product* of the void probabilities

for each shell radius. Using Eqn.(4.8), we obtain

$$\phi_o(r) = \begin{cases} \exp \left[-\frac{f}{R_0^3(0)} \left(R_0^3(0) + 3\overline{R_0^2}(0)r + 3\overline{R_0^1}(0)r^2 + r^3 \right) \right] & \text{if } r \geq R_{max} \\ \exp \left[-\frac{f}{R_0^3(0)} \left\{ \left(R_0^3(0) + 3\overline{R_0^2}(0)r + 3\overline{R_0^1}(0)r^2 + r^3 \right) - \frac{n_{sh}(r)}{n_{sh}(0)} \left(R_0^3(r) - 3\overline{R_0^2}(r)r + 3\overline{R_0^1}(r)r^2 - r^3 \right) \right\} \right] & \text{if } R_{min} \leq r \leq R_{max} \\ \exp \left[-2\frac{f}{R_0^3(0)} \left(3\overline{R_0^2}(0)r + r^3 \right) \right] & \text{if } r \leq R_{min}. \end{cases} \quad (4.26)$$

In Figure 8, the void probability function is plotted for several values of power law model parameters, keeping $R_{min}/R_{max} = 1/8$ fixed (4 upper curves). The VPF is most sensitive to the volume filling factor f , with additional weak dependence on the size distribution exponent α . For comparison, the void probability function for a random Poisson distribution of galaxies is also shown (dot-short dashed curve). To place the latter in the same figure, we have taken $n_g R_{max}^3 = 0.01 h^3 \text{Mpc}^{-3} (30 h^{-1} \text{Mpc})^3 = 270$, where $n_g = 0.01 h^3 \text{Mpc}^{-3}$ is the mean galaxy density in a typical CfA1 subsample (ML; Hamilton 1985). The VPF for the CfA1 data lies somewhat above the Poisson curve, but well below the shell model curves. For example, at $r = 6 h^{-1} \text{Mpc}$, corresponding to $r/2R_{max} = 0.1$ for our adopted R_{max} , ML find $\phi_o(r = 6 h^{-1} \text{Mpc}) \simeq 0.1$ for their volume-limited CfA1 subsample. For the shell model to yield a VPF this low, the filling factor would need to be $f \gtrsim 5 - 6$, absurdly high. As we show in the next section, this discrepancy may be partially or wholly remedied by allowing for a small fraction of the galaxies to lie off the shells.

V. CLUSTER AND BACKGROUND GALAXIES

The models considered in the previous sections lack two important ingredients of the observed galaxy distribution: clusters of galaxies and field galaxies which do not lie on shells. To make the model more realistic, we now place a fraction of galaxies in clusters at the points where three shells intersect and also allow for a homogeneous population of background galaxies. The number densities of shell, cluster, and background galaxies are n_{sg} (given in Eqn.(4.1)), n_{cg} , and n_{bg} respectively. This modification introduces several additional parameters into the shell model: the number of galaxies in a cluster which forms where three shells with radii R_A , R_B , and R_C meet, $\mathcal{N}_{cl}(R_A, R_B, R_C)$; the fraction of cluster galaxies, $M_c \equiv n_{cg}/(n_{sg} + n_{cg} + n_{bg})$; and the fraction of background galaxies, $M_b \equiv n_{bg}/(n_{sg} + n_{cg} + n_{bg})$. We note that an important limitation of this model is the treatment of clusters, like galaxies, as point-like objects with zero spatial extent; this follows from the assumption of infinitely thin shells. As a consequence, our statistics are not sensitive to the internal density profile of clusters, and our results are not valid on scales smaller than the typical Abell radius, $r_A \simeq 1.5 h^{-1} \text{Mpc}$.

Let $n_{cl}(R_A, R_B, R_C) dR_A dR_B dR_C$ be the number density of clusters formed from three spheres with radii in the intervals dR_A , dR_B , and dR_C . From Kulsrud and Cowley (1989),

$$n_{cl}(R_A, R_B, R_C) = 8\pi^4 n_{sh}(R_A) n_{sh}(R_B) n_{sh}(R_C) R_A^2 R_B^2 R_C^2, \quad (5.1)$$

and the total number density of clusters is

$$n_{cl} = \frac{4\pi^4}{3} \left[\int_0^\infty n_{sh}(R) R^2 dR \right]^3. \quad (5.2)$$

(Here, the factor of 6 is divided because, in integrating over (R_A, R_B, R_C) , the same situation is counted six times.) Therefore, the total number density of cluster galaxies is

$$n_{cg} = \frac{4\pi^4}{3} \int_0^\infty dR_A \int_0^\infty dR_B \int_0^\infty dR_C \mathcal{N}_{cl}(R_A, R_B, R_C) n_{sh}(R_A) n_{sh}(R_B) n_{sh}(R_C) R_A^2 R_B^2 R_C^2. \quad (5.3)$$

We assume that the number of galaxies per cluster has power law dependence on the shell radii R_A , R_B , and R_C ,

$$\mathcal{N}_{cl}(R_A, R_B, R_C) = \mathcal{N}_{cl,o} \left(\frac{R_A}{R_{max}} \right)^\delta \left(\frac{R_B}{R_{max}} \right)^\delta \left(\frac{R_C}{R_{max}} \right)^\delta. \quad (5.4)$$

As noted below, this assumption is physically plausible, and we expect it to hold independently of (and more generally than) the assumption of a power law distribution of shell radii. Using the notation introduced in Eqns.(4.3) to (4.6), n_{cl} and n_{cg} can then be written as

$$n_{cl} = \frac{4\pi^4}{3} \overline{n_{sh}^3(0)} \overline{R_0^2}^3(0), \quad (5.5)$$

$$n_{cg} = \frac{4\pi^4}{3} \frac{\mathcal{N}_{cl,o} \overline{n_{sh}^3(0)} \overline{R_0^{2+\delta}}^3(0)}{R_{max}^{3\delta}}. \quad (5.6)$$

We can choose the three independent additional parameters of the model to be δ , M_c , and M_b (note that $\mathcal{N}_{cl,o}$ is related to n_{cg} and thus M_c , so it is not independent). We will take $\delta = 1$ on the assumptions that (a) the mass of a cluster at the intersection of three shells with radii R_A , R_B , and R_C is proportional to $R_A R_B R_C$, and (b) the number of galaxies in a cluster is proportional to the mass of the cluster. A simple physical argument for assumption (a) is given by WOD. Assumption (b) follows if the galaxy mass function is independent of cluster mass. Observations indicate that the fraction of galaxies belonging to rich clusters and their tails, M_c , is between 5% to 20% (*e.g.*, Bahcall 1986). Searches for a spatially homogeneous (background) field population in galaxy catalogs have proved negative, with resulting quoted upper bounds $M_b < 0.18$ (Soneira and Peebles 1977) and $M_b < 0.05 - 0.1$ (Chincarini 1978; Vettolani, de Souza, and Chincarini 1986). For our purposes, it is not crucial that the background galaxies be completely unclustered (we assume this only for calculational convenience), but it is important that they be allowed to populate regions other than the shell surfaces. Therefore, we do not need to identify background galaxies precisely with the spatially homogeneous field. From the galaxy density in the underdense regions of redshift surveys, we impose the rough upper limit $M_b \lesssim 0.2$. Reiterating, the ranges of the values of the additional parameters considered in this section are

$$\begin{aligned} \delta &= 1, \\ M_c &\lesssim 0.2, \\ M_b &\lesssim 0.2. \end{aligned} \quad (5.7)$$

a) *Two-Point Correlation Function*

Since there are now three galaxy populations, the two-point correlation function can be decomposed into nine components: shell galaxy-shell galaxy, $\xi_{gg}^{ss}(r)$; shell galaxy-cluster galaxy, $\xi_{gg}^{sc}(r)$; shell galaxy-background galaxy, $\xi_{gg}^{sb}(r)$; cluster galaxy-shell galaxy, $\xi_{gg}^{cs}(r)$; cluster galaxy-cluster galaxy, $\xi_{gg}^{cc}(r)$; cluster galaxy-background galaxy, $\xi_{gg}^{cb}(r)$; background-shell, $\xi_{gg}^{bs}(r)$; background-cluster, $\xi_{gg}^{bc}(r)$; and background galaxy-background galaxy, $\xi_{gg}^{bb}(r)$. Since background galaxies are assumed to be randomly distributed, five of these components vanish,

$$\xi_{gg}^{sb}(r) = \xi_{gg}^{cb}(r) = \xi_{gg}^{bs}(r) = \xi_{gg}^{bc}(r) = \xi_{gg}^{bb}(r) = 0. \quad (5.8)$$

Also, since the two-point correlation function is invariant under intercommutation of the galaxies in a pair, $\xi_{gg}^{sc}(r) = \xi_{gg}^{cs}(r)$, etc. Hence, the two-point function is

$$\xi_{gg}(r) = \xi_{gg}^{ss}(r) + 2\xi_{gg}^{cs}(r) + \xi_{gg}^{cc}(r). \quad (5.9)$$

The shell-shell component, $\xi_{gg}^{ss}(r)$, is obtained by multiplying the shell galaxy two-point function, given in Eqn.(4.13), by M_s^2 ,

$$\xi_{gg}^{ss}(r) = M_s^2 \left[\int_{r/2}^{\infty} 2\pi r \mathcal{N}_{sh}(R) \cdot 4\pi R^2 \mathcal{N}_{sh}(R) n_{sh}(R) dR \right] / (4\pi r^2 n_{sg} \cdot n_{sg}). \quad (5.10)$$

Here, M_s is the fraction of shell galaxies ($M_s = 1 - M_c - M_b$). The cluster-shell component $\xi_{gg}^{cs}(r)$ is derived by counting the number of shell galaxies at distance r from a cluster and averaging over clusters with different numbers of galaxies. Using Eqn.(5.1),

$$\begin{aligned} \xi_{gg}^{cs}(r) = & M_c M_s \left[4\pi^4 \int_{r/2}^{\infty} dR_A \int_0^{\infty} dR_B \int_0^{\infty} dR_C 2\pi r \mathcal{N}_{sh}(R_A) \cdot \mathcal{N}_{cl}(R_A, R_B, R_C) \right. \\ & \left. \times n_{sh}(R_A) n_{sh}(R_B) n_{sh}(R_C) R_A^2 R_B^2 R_C^2 \right] / (4\pi r^2 n_{sg} \cdot n_{cg}). \end{aligned} \quad (5.11)$$

Similarly, the cluster galaxy-cluster galaxy component $\xi_{gg}^{cc}(r)$ is derived by counting the number of cluster galaxies at distance r from a cluster and averaging over clusters with different numbers of galaxies. Using the cluster-cluster two-point correlation function given in Kulsrud and Cowley (1989), we have

$$\xi_{gg}^{cc}(r) = \xi_{gg}^{cc,I}(r) + \xi_{gg}^{cc,II}(r) + \xi_{gg}^{cc,III}(r), \quad (5.12)$$

where

$$\begin{aligned} \xi_{gg}^{cc,I}(r) = & \frac{M_c^2 \pi^3}{n_{cg}^2 2r} \int_{r/2}^{\infty} dR_A \int_{r/2}^{\infty} dR_B \int_{r/2}^{\infty} dR_C \mathcal{N}_{cl}^2(R_A, R_B, R_C) \\ & \times n_{sh}(R_A) n_{sh}(R_B) n_{sh}(R_C) \left(R_A^2 - \frac{r^2}{4} \right) \left(R_B^2 - \frac{r^2}{4} \right), \end{aligned} \quad (5.13)$$

$$\begin{aligned} \xi_{gg}^{cc,II}(r) &= \frac{M_c^2 8\pi^4}{n_{cg}^2 r^2} \int_{r/2}^{\infty} dR_A \int_{r/2}^{\infty} dR_B \int_0^{\infty} dR_C \int_0^{\infty} dR_D \mathcal{N}_{cl}(R_A, R_B, R_C) \mathcal{N}_{cl}(R_A, R_B, R_D) \\ &\quad \times n_{sh}(R_A) n_{sh}(R_B) n_{sh}(R_C) n_{sh}(R_D) R_C^2 R_D^2 \left(R_A^2 R_B^2 + R_A^2 \frac{r^2}{4} + R_B^2 \frac{r^2}{4} - \frac{3r^4}{16} \right), \end{aligned} \quad (5.14)$$

$$\begin{aligned} \xi_{gg}^{cc,III}(r) &= \frac{M_c^2 2\pi^7}{n_{cg}^2 r} \int_{r/2}^{\infty} dR_A \int_0^{\infty} dR_B \int_0^{\infty} dR_C \int_0^{\infty} dR_D \int_0^{\infty} dR_E \mathcal{N}_{cl}(R_A, R_B, R_C) \\ &\quad \times \mathcal{N}_{cl}(R_A, R_D, R_E) n_{sh}(R_A) n_{sh}(R_B) n_{sh}(R_C) n_{sh}(R_D) n_{sh}(R_E) R_A^2 R_B^2 R_C^2 R_D^2 R_E^2. \end{aligned} \quad (5.15)$$

Here, $\xi_{gg}^{cc,I}(r)$, $\xi_{gg}^{cc,II}(r)$, and $\xi_{gg}^{cc,III}(r)$ are the contributions from two cluster galaxies sharing three, two, and one common shell, respectively (see Kulsrud and Cowley 1989 for details).

Using Eqns.(4.7) and (4.8), the two-point function components can be written

$$\xi_{gg}^{ss}(r) = \frac{M_s^2 \overline{R_0^3}(0) \overline{R_2^2}(r/2) \overline{\mathcal{N}_{sh}^2}(r/2) \overline{n_{sh}}(r/2)}{6fr \overline{R_1^2}(0) \overline{\mathcal{N}_{sh}^1}(0) \overline{n_{sh}}(0)}, \quad (5.16)$$

$$\xi_{gg}^{cs}(r) = \frac{M_c M_s \overline{R_0^3}(0) \overline{R_1^{2+\delta}}(r/2) \overline{\mathcal{N}_{sh}^1}(r/2) \overline{n_{sh}}(r/2)}{2fr \overline{R_1^2}(0) \overline{R_0^{2+\delta}}(0) \overline{\mathcal{N}_{sh}^1}(0) \overline{n_{sh}}(0)}, \quad (5.17)$$

$$\xi_{gg}^{cc,I}(r) = \frac{2M_c^2 \overline{R_0^3}(0) \overline{R_0^{2\delta}}(r/2) \left(\overline{R_0^{2+2\delta}}(r/2) - \frac{r^2}{4} \overline{R_0^{2\delta}}(r/2) \right)^2 \overline{n_{sh}^3}(r/2)}{3\pi^2 f^3 r \overline{R_0^{2+\delta}}(0) \overline{n_{sh}^3}(0)}, \quad (5.18)$$

$$\begin{aligned} \xi_{gg}^{cc,II}(r) &= \frac{8M_c^2 \overline{R_0^3}(0) \left(\overline{R_0^{2+2\delta}}(r/2) - \frac{r^2}{4} \overline{R_0^{2\delta}}(r/2) \right) \left(\overline{R_0^{2+2\delta}}(r/2) + \frac{3r^2}{4} \overline{R_0^{2\delta}}(r/2) \right)}{\pi^2 f^2 r^2 \overline{R_0^{2+\delta}}(0)} \\ &\quad \times \frac{\overline{n_{sh}^2}(r/2)}{\overline{n_{sh}^2}(0)}, \end{aligned} \quad (5.19)$$

$$\xi_{gg}^{cc,III}(r) = \frac{3M_c^2 \overline{R_0^3}(0) \overline{R_0^{2+2\delta}}(r/2) \overline{n_{sh}}(r/2)}{2fr \overline{R_0^{2+\delta}}(0) \overline{n_{sh}}(0)}. \quad (5.20)$$

Figure 9 shows the two-point correlation function for several values of power law model parameters. Here, the contribution from cluster galaxy-cluster galaxy pairs dominates on small scales, and the kink at $r = 2R_{min}$ is less visible. The slope γ_0 and correlation length r_0 of $\xi_{gg}(r)$ are listed in Table 2. These values were determined by fitting the data between $1/20 \leq r/2R_{max} \leq 1/5$ to the power law form in Eqn.(2.1). The effects of placing $\sim 20\%$ of the galaxies in clusters are to increase the correlation length by a factor of $\sim 1.5 - 2$, and to increase the slope if it is smaller than $\sim 1.4 - 1.5$ but decrease it otherwise. Placing $\sim 20\%$ of the galaxies in a random, uniform background has a less dramatic impact on the two-point function, merely decreasing the correlation length slightly (up to $\sim 20\%$). To reproduce the observed

slope of the correlation function, smaller values of β and R_{min}/R_{max} are preferred (i.e., a higher proportion of galaxies belonging to smaller shells). The results indicate that both the observed slope and correlation length can be reproduced in the shell model with $\alpha \simeq 4$, $R_{max} \simeq 30h^{-1}\text{Mpc}$, $R_{min}/R_{max} \simeq 1/15$, $\beta \simeq 0$, $\delta \simeq 1$, and $M_c \sim 0.2$.

b) Morphological Dependence of the Two-Point Correlation Function

Since the cluster component and the field (shell and background) component of galaxies are identified separately, it is natural to consider the morphological dependence of the two-point correlation function in the shell model. As discussed in §II, there are more spiral galaxies in the field but ellipticals predominate in clusters. Here, we assume that 95% of spirals are shell galaxies and 5% are cluster galaxies and that 67% of ellipticals are shell galaxies and 33% are in clusters. For instance, if $\sim 85\%$ of all galaxies are field galaxies, among which $\sim 65\%$ are spirals and $\sim 20\%$ are ellipticals, and if $\sim 15\%$ of galaxies are in clusters, among which $\sim 20\%$ are spirals and $\sim 60\%$ are ellipticals, then the fractions above are obtained.

Figures 10 and 11 show the resulting two-point correlation functions of spiral-spiral pairs and elliptical-elliptical pairs for several values of power law model parameters. The values of γ_o and r_o for the corresponding two-point functions are listed in Table 3. Again, these values were determined by fitting the data between $1/20 \leq r/2R_{max} \leq 1/5$ to the power law form in Eqn.(2.1). The two-point correlation function of elliptical galaxies, $\xi_{ee}(r)$, has a larger correlation length than that of spiral galaxies, $\xi_{ss}(r)$, indicating that elliptical galaxies are more clustered than spirals; this is in qualitative agreement with the observed morphological trend. However, the slope of $\xi_{ee}(r)$ is lower than the value $\gamma_o \simeq 2.1$ given by observations, and the correlation length for shell model spirals is somewhat smaller than the value $r_o \simeq 4.4h^{-1}\text{Mpc}$ quoted for an observed spiral sample (see §II). On the other hand, this comparison is perhaps a bit premature, since the fractions of spirals and ellipticals in field and cluster components are observationally uncertain.

c) Cluster-Galaxy Cross Correlation Function

The cluster-galaxy cross correlation function, $\xi_{cg}(r)$, is calculated by counting the excess (over the mean) numbers of shell, cluster, and background galaxies at distance r from a cluster. Since the background galaxies are randomly distributed, they make no contribution to the cross correlation. Hence,

$$\xi_{cg}(r) = \xi_{cg}^{cs}(r) + \xi_{cg}^{cc}(r). \quad (5.21)$$

The components $\xi_{cg}^{cs}(r)$ and $\xi_{cg}^{cc}(r)$ can be calculated in a manner analogous to that of the galaxy-galaxy two-point function in Eqns.(5.11) to (5.15):

$$\begin{aligned} \xi_{cg}^{cs}(r) = M_s \left[4\pi^4 \int_{r/2}^{\infty} dR_A \int_0^{\infty} dR_B \int_0^{\infty} dR_C 2\pi r N_{sh}(R_A) \right. \\ \left. \times n_{sh}(R_A)n_{sh}(R_B)n_{sh}(R_C)R_A^2 R_B^2 R_C^2 \right] / (4\pi r^2 n_{sg} \cdot n_{cl}), \end{aligned} \quad (5.22)$$

and

$$\xi_{cg}^{cc}(r) = \xi_{cg}^{cc,I}(r) + \xi_{cg}^{cc,II}(r) + \xi_{cg}^{cc,III}(r), \quad (5.23)$$

where

$$\begin{aligned} \xi_{cg}^{cc,I}(r) = & \frac{M_c}{n_{cg}n_{cl}} \frac{\pi^3}{2r} \int_{r/2}^{\infty} dR_A \int_{r/2}^{\infty} dR_B \int_{r/2}^{\infty} dR_C \mathcal{N}_{cl}(R_A, R_B, R_C) \\ & \times n_{sh}(R_A) n_{sh}(R_B) n_{sh}(R_C) \left(R_A^2 - \frac{r^2}{4} \right) \left(R_B^2 - \frac{r^2}{4} \right), \end{aligned} \quad (5.24)$$

$$\begin{aligned} \xi_{cg}^{cc,II}(r) = & \frac{M_c}{n_{cg}n_{cl}} \frac{8\pi^4}{r^2} \int_{r/2}^{\infty} dR_A \int_{r/2}^{\infty} dR_B \int_0^{\infty} dR_C \int_0^{\infty} dR_D \mathcal{N}_{cl}(R_A, R_B, R_C) \\ & \times n_{sh}(R_A) n_{sh}(R_B) n_{sh}(R_C) n_{sh}(R_D) R_C^2 R_D^2 \left(R_A^2 R_B^2 + R_A^2 \frac{r^2}{4} + R_B^2 \frac{r^2}{4} - \frac{3r^4}{16} \right), \end{aligned} \quad (5.25)$$

$$\begin{aligned} \xi_{cg}^{cc,III}(r) = & \frac{M_c}{n_{cg}n_{cl}} \frac{2\pi^7}{r} \int_{r/2}^{\infty} dR_A \int_0^{\infty} dR_B \int_0^{\infty} dR_C \int_0^{\infty} dR_D \int_0^{\infty} dR_E \mathcal{N}_{cl}(R_A, R_B, R_C) \\ & \times n_{sh}(R_A) n_{sh}(R_B) n_{sh}(R_C) n_{sh}(R_D) n_{sh}(R_E) R_A^2 R_B^2 R_C^2 R_D^2 R_E^2. \end{aligned} \quad (5.26)$$

Using Eqns.(4.7) and (4.8), we have

$$\xi_{cg}^{cs}(r) = \frac{M_s}{2fr} \frac{\overline{R_0^3(0)} \overline{R_1^2(r/2)} \overline{\mathcal{N}_{sh}^1(r/2)} \overline{n_{sh}(r/2)}}{\overline{R_1^2(0)} \overline{R_0^2(0)} \overline{\mathcal{N}_{sh}^1(0)} \overline{n_{sh}(0)}}, \quad (5.27)$$

$$\xi_{cg}^{cc,I}(r) = \frac{2M_c}{3\pi^2 f^3 r} \frac{\overline{R_0^3(0)} \overline{R_0^\delta(r/2)} \left(\overline{R_0^{2+\delta}(r/2)} - \frac{r^2}{4} \overline{R_0^\delta(r/2)} \right)^2 \overline{n_{sh}^3(r/2)}}{\overline{R_0^3(0)} \overline{R_0^{2+\delta}(0)} \overline{n_{sh}^3(0)}}, \quad (5.28)$$

$$\begin{aligned} \xi_{cg}^{cc,II}(r) = & \frac{8M_c}{\pi^2 f^2 r^2} \frac{\overline{R_0^3(0)} \left(\overline{R_0^{2+\delta}(r/2)} - \frac{r^2}{4} \overline{R_0^\delta(r/2)} \right) \left(\overline{R_0^{2+\delta}(r/2)} + \frac{3r^2}{4} \overline{R_0^\delta(r/2)} \right)}{\overline{R_0^2(0)} \overline{R_0^{2+\delta}(0)}} \\ & \times \frac{\overline{n_{sh}^2(r/2)}}{\overline{n_{sh}^2(0)}}, \end{aligned} \quad (5.29)$$

$$\xi_{cg}^{cc,III}(r) = \frac{3M_c}{2fr} \frac{\overline{R_0^3(0)} \overline{R_0^{2+\delta}(r/2)} \overline{n_{sh}(r/2)}}{\overline{R_0^2(0)} \overline{R_0^{2+\delta}(0)} \overline{n_{sh}(0)}}, \quad (5.30)$$

Figure 12 shows the cluster-galaxy cross correlation function for several values of power law model parameters. The values of the slope, γ_o , and the correlation length, r_o , of $\xi_{cg}(r)$ listed in Table 4 were determined by fitting the data between $1/20 \leq r/2R_{max} \leq 1/3$ to a power law. For $R_{max} = 30h^{-1}\text{Mpc}$, this range corresponds to $3h^{-1}\text{Mpc} \leq r \leq 20h^{-1}\text{Mpc}$. The slope and amplitude of the cluster-galaxy correlation function are both larger than those of the galaxy two-point correlation function, in agreement with observations. With the parameter values which best fit the galaxy two-point function, $\alpha \simeq 4$, $R_{max} \simeq 30h^{-1}\text{Mpc}$, $R_{min}/R_{max} \simeq 1/15$, $\beta \simeq 0$,

$\delta \simeq 1$, and $M_c \sim 0.2$, the observed slope of the cluster-galaxy correlation function, $\gamma_o \simeq 2.2$, is also reproduced by the shell model. The shell model prediction for the cross correlation length, $r_o \simeq 6h^{-1}\text{Mpc}$, is 30% below the best fit observed value ($\simeq 8.8h^{-1}\text{Mpc}$). However, when uncertainties in the selection function and K-correction are included, the model value for r_o is only 5 – 10% below the range of the observations (Lilje and Efstathiou 1988b). When projection effects in the Abell catalog are corrected for, this marginal discrepancy may be reduced even further.

d) Void Distribution

It is simple to include the effects of cluster and background galaxies on the void probability function. Since cluster galaxies reside on the shells, they make no change in the VPF given in Eqn.(4.26). The background galaxies are distributed in a random Poisson process, so the probability of finding a void in the background population is just $\phi_{o,bg}(r) = e^{-n_b V(r)}$, where $V(r) = (4\pi/3)r^3$. Since the background component is statistically independent of the shell and cluster components, the total void probability is given by

$$\phi_o(r) = e^{-(4\pi/3)M_b n_g r^3} \phi_{o,sh}(r) , \quad (5.31)$$

where $\phi_{o,sh}(r)$ is the VPF for the shell galaxies given in eqn.(4.26). This is shown as the 4 middle curves in Figure 8 assuming $M_b = 0.2$, $R_{max} = 30h^{-1}\text{Mpc}$, and using the mean density of galaxies in the CfA1 subsample of ML, $n_g = 0.01h^3\text{Mpc}^{-3}$. With this fraction of background galaxies, the shell model agrees with the observed VPF rather well.

VI. SELF-AVOIDING SHELLS

In the CfA2 slices, bubbles do not appear to lie inside each other. Therefore, as another modification to the simple shell models discussed so far, we now consider the case of self-avoiding shells, in which the centers of shells do not lie inside other bubbles; except for this constraint, the distribution of shells is otherwise a random Poisson process. More explicitly, shells centers are assumed to be anticorrelated on separations less than the shell radius: the two-point correlation function of *shells* is given by

$$\xi_{sh}(r) = \begin{cases} -1 & \text{if } r \leq \max(R_1, R_2) \\ 0 & \text{if } r > \max(R_1, R_2). \end{cases} \quad (6.1)$$

Here, R_1 and R_2 are the radii of two shells separated by r . This modification is motivated on physical grounds (WOD; Ostriker and Strassler 1989; Yoshioka and Ikeuchi 1990): if two bubbles have separation less than the shell radius, as they expand they attempt to sweep up mostly the same material, and eventually form one shell rather than two. In this section, we consider the effects of shell self-avoidance on the two-point correlation function of shell galaxies.

This modification of the bubble distribution reduces the amplitude of the galaxy correlation function on separations $r \leq 3R_{max}$. Let

$$\xi_{gg}(r) = \xi_{gg}^o(r) - \xi_{gg}^a(r), \quad (6.2)$$

where $\xi_{gg}^o(r)$ is the two-point correlation function of shell galaxies for a Poisson distribution of shells, Eqn.(4.13), and $\xi_{gg}^a(r)$ is the reduction due to shell anticorrelation. Then, $\xi_{gg}^a(r)$ is calculated by counting all possible contributions from two galaxies belonging to two different shells with the center of one shell lying inside the other shell. The calculation proceeds by the following steps. We set $R_1 > R_2$, since the contribution from the case with $R_1 < R_2$ is the same as that from the case with $R_1 > R_2$. Starting from a galaxy sitting on the surface of the shell with radius R_1 , we draw a sphere with radius r . At a given point on the sphere, we calculate the ratio F of the probability of finding galaxies belonging to the shell with radius R_2 lying inside the shell with radius R_1 to the probability of finding galaxies belonging to the shell with radius R_2 lying everywhere. We then average the ratio over the points on the sphere to obtain \bar{F} :

i) for $R_1 \geq r$:

a) for $R_2 \leq r$,

$$\bar{F}_{1a} = \frac{1}{2} - \frac{R_2^2}{12R_1r} - \frac{r}{4R_1}, \quad (6.3)$$

b) for $r \leq R_2 \leq R_1$,

$$\bar{F}_{1b} = \frac{1}{2} - \frac{R_2}{4R_1} - \frac{r^2}{12R_1R_2}, \quad (6.4)$$

ii) for $r/2 \leq R_1 \leq r$:

a) for $R_2 \leq 2R_1 - r$,

$$\begin{aligned} \bar{F}_{2a} &= \frac{1}{2} - \frac{R_2^2}{12R_1r} - \frac{r}{4R_1} \\ &= \bar{F}_{1a}, \end{aligned} \quad (6.5)$$

b) for $2R_1 - r \leq R_2 \leq R_1$,

$$\bar{F}_{2b} = \frac{1}{4} + \frac{R_2}{8R_1} + \frac{R_1^2}{6R_2r} - \frac{R_2}{8r} - \frac{R_2^2}{24R_1r} - \frac{r}{8R_1} - \frac{r}{8R_2} + \frac{r^2}{24R_1R_2}, \quad (6.6)$$

iii) for $r/3 \leq R_1 \leq r/2$:

a) for $R_2 \leq r - 2R_1$,

$$\bar{F}_{3a} = 0, \quad (6.7)$$

b) for $r - 2R_1 \leq R_2 \leq R_1$,

$$\begin{aligned} \bar{F}_{3b} &= \frac{1}{4} + \frac{R_2}{8R_1} + \frac{R_1^2}{6R_2r} - \frac{R_2}{8r} - \frac{R_2^2}{24R_1r} - \frac{r}{8R_1} - \frac{r}{8R_2} + \frac{r^2}{24R_1R_2} \\ &= \bar{F}_{2b}, \end{aligned} \quad (6.8)$$

iv) for $R_1 \leq r/3$:

$$\bar{F}_4 = 0. \quad (6.9)$$

Finally, we average the ratio over the galaxies on the shell with radius R_1 to get $\xi_{gg}^a(r)$,

$$\xi_{gg}^a(r) = \frac{2}{n_g^2} \int_0^\infty dR_1 \int_0^{R_1} dR_2 \bar{F} \cdot 4\pi R_1^2 \mathcal{N}_{sh}(R_1) n_{sh}(R_1) \cdot 4\pi R_2^2 \mathcal{N}_{sh}(R_2) n_{sh}(R_2). \quad (6.10)$$

Here, the factor of 2 is inserted to include the case with $R_1 < R_2$. Using Eqn.(4.7), we find

$$\begin{aligned} \xi_{gg}^a(r) &= \int_r^\infty dR_1 \int_0^r dR_2 \bar{F}_{1a} G + \int_r^\infty dR_1 \int_r^{R_1} dR_2 \bar{F}_{1b} G \\ &\quad + \int_{r/2}^r dR_1 \int_0^{2R_1-r} dR_2 \bar{F}_{2a} G + \int_{r/2}^r dR_1 \int_{2R_1-r}^{R_1} dR_2 \bar{F}_{2b} G \\ &\quad + \int_{r/3}^{r/2} dR_1 \int_0^{r-2R_1} dR_2 \bar{F}_{3a} G + \int_{r/3}^{r/2} dR_1 \int_{r-2R_1}^{R_1} dR_2 \bar{F}_{3b} G \\ &\quad + \int_0^{r/3} dR_1 \int_0^{R_1} dR_2 \bar{F}_4 G \\ G &= 2 \frac{R_1^2 R_2^2 \mathcal{N}_{sh}(R_1) \mathcal{N}_{sh}(R_2) n_{sh}(R_1) n_{sh}(R_2)}{R_1^2(0) \mathcal{N}_{sh}^1(0) \bar{n}_{sh}^2(0)}, \end{aligned} \quad (6.11)$$

Note that $\xi_{gg}^a(r)$ is independent of f .

For the case of equal size shells, $\xi_{gg}(r)$ has a simple form,

$$\xi_{gg}(r) = \begin{cases} \frac{R_{sh}}{8fr} - \frac{1}{4} + \frac{r^2}{12R_{sh}^2} & \text{if } r < R_{sh} \\ \frac{R_{sh}}{8fr} - \frac{3}{8} + \frac{r}{4R_{sh}} - \frac{r^2}{24R_{sh}^2} & \text{if } R_{sh} < r < 2R_{sh} \\ -\frac{3}{8} + \frac{r}{4R_{sh}} - \frac{r^2}{24R_{sh}^2} & \text{if } 2R_{sh} < r < 3R_{sh} \\ 0 & \text{if } r > 3R_{sh} \end{cases} \quad (6.12)$$

Figure 13 shows the two-point correlation function for equal size shells with $f = 0.8, 1.0$, and 1.2 . The self-avoidance steepens the slope significantly but also reduces the amplitude. Hence, shell self-avoidance *alone* does not improve the match with observations (recall that in the shell models considered in §III and §IV, the amplitude of the two-point function was too small). However, combining shell self-avoidance with cluster (and background) galaxies should provide a quasi-realistic model which reproduces the observations reasonably well. Given the complexity of this combination, analytic calculations appear to be impractical.

VII. DISCUSSION

We have studied analytically the statistical distribution of galaxies in the phenomenological shell model of large-scale structure. Most of the previous studies of this model focused principally on the spatial clustering of galaxy clusters. Yet, the observational motivation for the model comes from the striking bubbly structure seen in the CfA survey extension slices. Since this structure is visibly traced by the shell galaxies discussed here, they are a crucial component of the model.

Including shell galaxies implies that additional observational data can be accounted for, while the number of extra model parameters introduced into the shell model is small.

The model we have studied is admittedly simple: we have assumed spherical geometry, infinitely thin shells with no clustering of shell galaxies within shells, and, for the most part, a random distribution of bubbles. The spherical approximation is probably not a severe limitation (see Borden, Ostriker, and Weinberg 1989), and the assumption of infinitely thin shells does not affect the correlation functions on large scales (see Appendix A). Presumably, gravity will lead to clustering of shell galaxies within shells, but this process is not well understood: how does gravity correlate galaxies on the shells when they go unstable, without destroying the sharp shell structure seen in the redshift surveys (White and Ostriker 1990)? In particular, it is not obvious why the correlation function should be a featureless power law down to scales less than the shell thickness, as is observed, unless gravity dominates on significantly larger scales. The last assumption, of a random bubble distribution, is considered in §VI. In addition, one can imagine other prescriptions for laying down galaxies and clusters in this model: for example, galaxies might be distributed mainly on sheets where two shells meet, and clusters may form at the intersection of four shells, as is the case in the Voronoi tessellation models (Icke and Van de Weygaert 1987, 1990; Van de Weygaert and Icke 1989; Coles 1990).

Despite these idealizations, we find that the shell model fits the observations of the galaxy two-point function rather well, and for the same choice of model parameters which best reproduce the cluster correlation function. Given the different geometrical origins of these functions, we count this a non-trivial success of the shell model. In addition, the galaxy three-point function and the void distribution function (when a substantial fraction of background galaxies are included) appear to be in reasonable agreement with the data. The slope of the cluster-galaxy cross correlation function is in good agreement with the observations, although its amplitude is marginally low. The correlation of clustering strength with morphology is reproduced in the shell model, but the slope of the correlation function of elliptical galaxies is lower than that observed. If we assume that the residual galaxy peculiar velocities (after gravitational effects are subtracted) are dominated by shell expansion, the shell model velocity correlation tensor appears to give a poor fit to the data; in particular, the perpendicular component $\Sigma(r)$ has the wrong sign and too large an amplitude. This argument may be turned around to place an upper limit on the expansion velocity of shells: for 2σ consistency with the spiral velocity data, the shell expansion speed must generally satisfy $V_{sh}(R) \lesssim 0.1 - 0.2 H_0 R$. This is consistent with expectations from several versions of the explosion model. Since the galaxy statistics are sensitive to the assumed spatial distribution of bubbles, we have also investigated the effect of shell anticorrelation on the two-point correlation function. We are currently studying other statistics, in particular the angular correlation function $w(\theta)$, the void probability function, and the expected distribution in a pencil beam survey.

Although the physical understanding of the bubble structure is far from complete, the relative success of the shell model in accounting for a variety of galaxy statistics, in addition to reproducing the qualitative visual structure of the CfA slices, suggests that large-scale galaxy clustering may reflect the geometry of the resulting structure more than the underlying physical processes (gravity vs. explosions) which generate it.

We thank Ed Bertschinger for useful conversations. This work was supported in part by the DOE and by the NASA at Fermilab through grant NAGW-1340.

APPENDIX A

FINITE THICKNESS SHELLS

One of the striking features of the CfA bubbles is their sharp surfaces. The shells in the CfA survey have a typical thickness of 200 – 300km/sec, or $\delta R_{sh} \simeq 2 - 3h^{-1}$ Mpc. Since this is of order the typical peculiar velocity dispersion of galaxies in the field, this is an upper limit to the true physical thickness of the bubbles. Throughout the body of the paper, we follow previous authors in taking the shell thickness δR_{sh} to be zero (or, $\delta R_{sh} \ll R_{sh}$). Thus, we can only meaningfully discuss correlation functions on scales larger than δR_{sh} . We have also taken galaxy clusters to have zero spatial extent, which again limits us to large scales ($\gg R_{Abell} \simeq 1.5h^{-1}$ Mpc). In the context of the shell model, this approximation is also a necessary limitation, for non-linear gravitational effects have presumably steepened the correlation function on scales less than $\sim 3h^{-1}$ Mpc anyway (and may affect the correlation function on even larger scales). Hence, our predictions with the shell model are valid only on scales greater than or of order $\sim 3h^{-1}$ Mpc. However, for completeness, we show here how the two-point correlation function behaves on small scales for shells with finite thickness, in the absence of gravity. The main point is that, if galaxies are randomly distributed within shells, the two-point correlation function will flatten on scales less than the shell thickness. Since this is not observed, we must assume gravity dominates on these scales, correlating the positions of galaxies within a shell (but see White and Ostriker 1990). On the other hand, the fact that the overall shell structure with sharp boundaries is maintained suggests that either gravity does not play an important role on scales larger than $\sim 3h^{-1}$ Mpc or that it is important in building the shell structure itself (as, for instance, in the adhesion model of Kofman, Pogosyan, and Shandarin 1990, and Melott and Shandarin 1990).

Here, we consider the case with equal size shells for simplicity: galaxies are assumed to be randomly distributed on shells with equal size but finite thickness, and the shells are assumed to be randomly distributed in space. Each shell has inner radius, R_{sh} , and outer radius, $R_{sh} + \delta R_{sh}$, and the volume filling factor is defined by

$$f \equiv \frac{4\pi}{3} n_{sh} \left(R_{sh} + \frac{\delta R_{sh}}{2} \right)^3. \quad (\text{A.1})$$

The thickness δR_{sh} is assumed to be smaller than the shell diameter, $2R_{sh}$, so the dominant structures are shells rather than spheres. The two-point correlation function, $\xi_{gg}(r)$, is calculated in the following way: starting from a galaxy, we count the average number of neighbor galaxies at distance r which belong to the same shell, and then we average over galaxies at different radii from the shell center. Then,
for $r \leq \delta R_{sh}$:

$$\xi_{gg}(r) = \frac{(R_{sh} + \delta R_{sh}/2)^3}{f [(R_{sh} + \delta R_{sh})^3 - R_{sh}^3]} \left[1 + \frac{r^3 - 6 \{ (R_{sh} + \delta R_{sh})^2 + R_{sh}^2 \} r}{8 [(R_{sh} + \delta R_{sh})^3 - R_{sh}^3]} \right], \quad (\text{A.1})$$

for $\delta R_{sh} \leq r \leq 2R_{sh}$:

$$\xi_{gg}(r) = \frac{3}{8fr} \frac{(R_{sh} + \delta R_{sh}/2)^3 (2R_{sh} + \delta R_{sh})^2 \delta R_{sh}^2}{[(R_{sh} + \delta R_{sh})^3 - R_{sh}^3]^2}, \quad (\text{A.2})$$

for $2R_{sh} \leq r \leq 2R_{sh} + \delta R_{sh}$:

$$\xi_{gg}(r) = \frac{1}{16f} \frac{(R_{sh} + \delta R_{sh}/2)^3}{[(R_{sh} + \delta R_{sh})^3 - R_{sh}^3]^2} \left[6(2R_{sh} + \delta R_{sh})^2 \delta R_{sh}^2 \frac{1}{r} - 16R_{sh}^3 + 12R_{sh}^2 r - r^3 \right], \quad (\text{A.3})$$

for $2R_{sh} + \delta R_{sh} \leq r \leq 2R_{sh} + 2\delta R_{sh}$:

$$\xi_{gg}(r) = \frac{1}{f} \frac{(R_{sh} + \delta R_{sh}/2)^3}{[(R_{sh} + \delta R_{sh})^3 - R_{sh}^3]^2} \left[(R_{sh} + \delta R_{sh})^3 - \frac{3}{4}(R_{sh} + \delta R_{sh})^2 r + \frac{1}{16} r^3 \right], \quad (\text{A.4})$$

for $r \geq 2R_{sh} + 2\delta R_{sh}$:

$$\xi_{gg}(r) = 0. \quad (\text{A.5})$$

Figure A1 shows the resulting two-point correlation function for $f = 0.8$ and 1.2 and $\delta R_{sh}/2R_{sh} = 1/10$ (or, $\delta R_{sh} = 3h^{-1}\text{Mpc}$ for $R_{sh} = 15h^{-1}\text{Mpc}$). Comparing with the plots for infinitely thin shells in Figure 1, the two-point correlation function becomes flat on scales less than the shell thickness, as expected: at small separation, $r \ll \delta R_{sh}$, the slope $\gamma_0 \simeq 0$. Furthermore, the slope goes to zero smoothly, rather than abruptly, around the separation corresponding to the shell diameter. However, on larger scales, $\delta R_{sh} \lesssim r \lesssim 2R_{sh}$, the behavior of the correlation function is very similar to the case of infinitely thin shells, justifying the neglect of the shell thickness.

APPENDIX B

$\delta V_{a,bc}$

The volume element at separations $r_b \leq r \leq r_b + dr_b$ and $r_c \leq r \leq r_c + dr_c$ from two points separated by $r_a \leq r \leq r_a + dr_a$ is calculated in the following way. Let $r_a < r_b + r_c$, $r_b < r_c + r_a$, and $r_c < r_a + r_b$. If the above conditions are not satisfied, there is no intersection, hence $\delta V_{a,bc} = 0$. From the two points 1 and 2 let us draw two shells with radii r_b and r_c and thicknesses dr_b and dr_c as in Figure B1. Then,

$$\sin \theta_1 = \frac{\sqrt{2r_a^2 r_b^2 + 2r_c^2 r_a^2 + 2r_b^2 r_c^2 - r_a^4 - r_b^4 - r_c^4}}{2r_a r_b}, \quad (\text{B.1})$$

$$\sin \theta_2 = \frac{\sqrt{2r_a^2 r_b^2 + 2r_c^2 r_a^2 + 2r_b^2 r_c^2 - r_a^4 - r_b^4 - r_c^4}}{2r_c r_a}, \quad (\text{B.2})$$

$$\sin \theta_3 = \frac{\sqrt{2r_a^2 r_b^2 + 2r_c^2 r_a^2 + 2r_b^2 r_c^2 - r_a^4 - r_b^4 - r_c^4}}{2r_b r_c}. \quad (\text{B.3})$$

The intersection where the third point 3 is found constitutes a ring with a cross section which is drawn schematically in Figure B2. The length of the circumference of the ring is

$$L = 2\pi r_b \sin \theta_1, \quad (\text{B.4})$$

and the area of the cross section is

$$S = \frac{dr_b dr_c}{\sin \theta_3}. \quad (\text{B.5})$$

Hence, the volume element is

$$\begin{aligned} \delta V_{a,bc} &= L \cdot S \\ &= 2\pi \frac{r_b r_c}{r_a} dr_b dr_c. \end{aligned} \quad (\text{B.6})$$

APPENDIX C

$\delta P_{1,2}$

The probability that, on the surface of a shell with radius R_{sh} , galaxy 2 is found at separation $r_a \leq r \leq r_a + dr_a$ from galaxy 1 and galaxy 3 is found at separations $r_b \leq r \leq r_b + dr_b$ and $r_c \leq r \leq r_c + dr_c$ from galaxies 1 and 2 is the product of the *area* element on the surface at separations $r_b \leq r \leq r_b + dr_b$ and $r_c \leq r \leq r_c + dr_c$ from two points separated by $r_a \leq r \leq r_a + dr_a$, $\delta S_{a,bc}$, and the surface number density of galaxies, \mathcal{N}_{sh} . $\delta S_{a,bc}$ is calculated in a similar way to $\delta V_{a,bc}$ in Appendix B. On the surface of a sphere with radius R_{sh} , let us draw two rings from the two points 1 and 2 with radii r_b and r_c and thicknesses dr_b and dr_c as in Figure C1. Then, the lengths of the arcs on the surface corresponding to the three separations are

$$l_a = R_{sh} \arccos \left(1 - \frac{r_a^2}{2R_{sh}^2} \right), \quad (\text{C.1})$$

$$l_b = R_{sh} \arccos \left(1 - \frac{r_b^2}{2R_{sh}^2} \right), \quad (\text{C.2})$$

$$l_c = R_{sh} \arccos \left(1 - \frac{r_c^2}{2R_{sh}^2} \right), \quad (\text{C.3})$$

and the angles between them are

$$\sin \theta_1 = \frac{\sqrt{1 - x_a^2 - x_b^2 - x_c^2 + 2x_a x_b x_c}}{\sqrt{1 - x_a^2} \sqrt{1 - x_b^2}}, \quad (\text{C.4})$$

$$\sin \theta_2 = \frac{\sqrt{1 - x_a^2 - x_b^2 - x_c^2 + 2x_a x_b x_c}}{\sqrt{1 - x_c^2} \sqrt{1 - x_a^2}}, \quad (\text{C.5})$$

$$\sin \theta_3 = \frac{\sqrt{1 - x_a^2 - x_b^2 - x_c^2 + 2x_a x_b x_c}}{\sqrt{1 - x_b^2} \sqrt{1 - x_c^2}}, \quad (\text{C.6})$$

where $x_a \equiv 1 - (r_a^2/2R_{sh}^2)$ and so on. The derivatives of the arcs are related to the derivatives of the separations by

$$dl_a = \sqrt{\frac{2}{1 + x_a}} dr_a, \quad (\text{C.7})$$

$$dl_b = \sqrt{\frac{2}{1 + x_b}} dr_b, \quad (\text{C.8})$$

$$dl_c = \sqrt{\frac{2}{1 + x_c}} dr_c. \quad (\text{C.9})$$

If $l_a < l_b + l_c$, $l_b < l_c + l_a$, and $l_c < l_a + l_b$, the two rings meet at two intersections where the third point 3 is found. Since the intersections are similar to that in Figure B2, the area element is

$$\begin{aligned} \delta S_{a,bc} &= 2 \frac{dl_b dl_c}{\sin \theta_3} \\ &= \frac{4r_b r_c}{\sqrt{F_{abc}}} dr_b dr_c \end{aligned} \quad (\text{C.10})$$

$$F_{abc} = 2r_a^2 r_b^2 + 2r_b^2 r_c^2 + 2r_c^2 r_a^2 - r_a^4 - r_b^4 - r_c^4 - \frac{r_a^2 r_b^2 r_c^2}{R_{sh}^2}.$$

Note that, here, the conditions $l_a < l_b + l_c$, $l_b < l_c + l_a$, and $l_c < l_a + l_b$ insure $F_{abc} > 0$ and vice versa.

APPENDIX D

$$\overline{n}_{sh}(r/2), \overline{\mathcal{N}}_{sh}^n(r/2), \overline{R}_m^n(r/2), \text{ and } \overline{V}_m^n(r/2)$$

For a power law distribution of shell radii, we define $y \equiv r/2R_{max}$ and $y_{min} \equiv R_{min}/R_{max}$. Then, substituting Eqns.(4.9) to (4.11) into Eqns.(4.3) to (4.6), we find

$$\overline{n}_{sh}(r/2) = \begin{cases} \frac{n_{sh,o} R_{max}}{1-\alpha} (1 - y_{min}^{1-\alpha}) & \text{if } y \leq y_{min} \\ \frac{n_{sh,o} R_{max}}{1-\alpha} (1 - y^{1-\alpha}) & \text{if } y_{min} \leq y \leq 1 \\ 0 & \text{if } y \geq 1, \end{cases} \quad (\text{D.1})$$

$$\overline{\mathcal{N}}_{sh}^n(r/2) = \begin{cases} \mathcal{N}_{sh,o}^n \frac{1-\alpha}{1-\alpha+n\beta} \frac{1-y_{min}^{1-\alpha+n\beta}}{1-y_{min}^{1-\alpha}} & \text{if } y \leq y_{min} \\ \mathcal{N}_{sh,o}^n \frac{1-\alpha}{1-\alpha+n\beta} \frac{1-y^{1-\alpha+n\beta}}{1-y^{1-\alpha}} & \text{if } y_{min} \leq y < 1, \end{cases} \quad (\text{D.2})$$

$$\overline{R}_m^n(r/2) = \begin{cases} R_{max}^n \frac{1-\alpha+m\beta}{n+1-\alpha+m\beta} \frac{1-y_{min}^{n+1-\alpha+m\beta}}{1-y_{min}^{1-\alpha+m\beta}} & \text{if } y \leq y_{min} \\ R_{max}^n \frac{1-\alpha+m\beta}{n+1-\alpha+m\beta} \frac{1-y^{n+1-\alpha+m\beta}}{1-y^{1-\alpha+m\beta}} & \text{if } y_{min} \leq y < 1, \end{cases} \quad (\text{D.3})$$

$$\overline{V}_m^n(r/2) = \begin{cases} \mathcal{V}_{sh,o}^n \frac{m+1-\alpha+2\beta}{m+1-\alpha+2\beta+n\gamma} \frac{1-y_{min}^{m+1-\alpha+2\beta+n\gamma}}{1-y_{min}^{m+1-\alpha+2\beta}} & \text{if } y \leq y_{min} \\ \mathcal{V}_{sh,o}^n \frac{m+1-\alpha+2\beta}{m+1-\alpha+2\beta+n\gamma} \frac{1-y^{m+1-\alpha+2\beta+n\gamma}}{1-y^{m+1-\alpha+2\beta}} & \text{if } y_{min} \leq y < 1. \end{cases} \quad (\text{D.4})$$

TABLES

TABLE 1

Model with Power Law Distribution of Shell Sizes*

$$\alpha = 3.5, R_{min}/R_{max} = 1/8$$

f	$\beta = 0.0$		$\beta = 1.0$	
	γ_0	$r_0/2R_{max}$	γ_0	$r_0/2R_{max}$
0.8	1.22	0.042	1.03	0.052
1.0	1.22	0.035	1.03	0.042
1.2	1.22	0.030	1.03	0.035

$$\alpha = 4.5, R_{min}/R_{max} = 1/8$$

f	$\beta = 0.0$		$\beta = 1.0$	
	γ_0	$r_0/2R_{max}$	γ_0	$r_0/2R_{max}$
0.8	1.43	0.036	1.09	0.039
1.0	1.43	0.031	1.09	0.032
1.2	1.43	0.027	1.09	0.027

$$\alpha = 3.5, R_{min}/R_{max} = 1/15$$

f	$\beta = 0.0$		$\beta = 1.0$	
	γ_0	$r_0/2R_{max}$	γ_0	$r_0/2R_{max}$
0.8	1.66	0.037	1.05	0.047
1.0	1.66	0.033	1.05	0.038
1.2	1.66	0.029	1.05	0.032

$$\alpha = 4.5, R_{min}/R_{max} = 1/15$$

f	$\beta = 0.0$		$\beta = 1.0$	
	γ_0	$r_0/2R_{max}$	γ_0	$r_0/2R_{max}$
0.8	2.37	0.034	1.22	0.031
1.0	2.37	0.031	1.22	0.026
1.2	2.37	0.029	1.22	0.023

*Data between $1/20 \leq r/2R_{max} \leq 1/5$ are used to fit the power law form of the two-point correlation function in Eqn.(2.1).

TABLE 2

Model with Cluster and Background Components*

$$\alpha = 3.5, R_{min}/R_{max} = 1/8, \delta = 1.0, M_s = 0.8, M_c = 0.2, M_b = 0.0$$

f	$\beta = 0.0$		$\beta = 1.0$	
	γ_o	$r_o/2R_{max}$	γ_o	$r_o/2R_{max}$
0.8	1.36	0.108	1.25	0.128
1.0	1.33	0.087	1.22	0.103
1.2	1.30	0.073	1.19	0.085

$$\alpha = 4.5, R_{min}/R_{max} = 1/8, \delta = 1.0, M_s = 0.8, M_c = 0.2, M_b = 0.0$$

f	$\beta = 0.0$		$\beta = 1.0$	
	γ_o	$r_o/2R_{max}$	γ_o	$r_o/2R_{max}$
0.8	1.45	0.079	1.28	0.092
1.0	1.41	0.064	1.24	0.074
1.2	1.39	0.054	1.22	0.062

$$\alpha = 3.5, R_{min}/R_{max} = 1/8, \delta = 1.0, M_s = 0.6, M_c = 0.2, M_b = 0.2$$

f	$\beta = 0.0$		$\beta = 1.0$	
	γ_o	$r_o/2R_{max}$	γ_o	$r_o/2R_{max}$
0.8	1.40	0.095	1.31	0.108
1.0	1.36	0.076	1.27	0.086
1.2	1.33	0.063	1.24	0.071

$$\alpha = 4.5, R_{min}/R_{max} = 1/8, \delta = 1.0, M_s = 0.6, M_c = 0.2, M_b = 0.2$$

f	$\beta = 0.0$		$\beta = 1.0$	
	γ_o	$r_o/2R_{max}$	γ_o	$r_o/2R_{max}$
0.8	1.47	0.069	1.32	0.077
1.0	1.43	0.056	1.29	0.062
1.2	1.41	0.047	1.26	0.051

$$\alpha = 3.5, R_{min}/R_{maz} = 1/15, \delta = 1.0, M_s = 0.8, M_c = 0.2, M_b = 0.0$$

f	$\beta = 0.0$		$\beta = 1.0$	
	γ_o	$r_o/2R_{maz}$	γ_o	$r_o/2R_{maz}$
0.8	1.52	0.087	1.28	0.113
1.0	1.48	0.071	1.24	0.091
1.2	1.46	0.060	1.21	0.076

$$\alpha = 4.5, R_{min}/R_{maz} = 1/15, \delta = 1.0, M_s = 0.8, M_c = 0.2, M_b = 0.0$$

f	$\beta = 0.0$		$\beta = 1.0$	
	γ_o	$r_o/2R_{maz}$	γ_o	$r_o/2R_{maz}$
0.8	1.83	0.056	1.40	0.067
1.0	1.80	0.047	1.37	0.055
1.2	1.78	0.041	1.35	0.047

$$\alpha = 3.5, R_{min}/R_{maz} = 1/15, \delta = 1.0, M_s = 0.6, M_c = 0.2, M_b = 0.2$$

f	$\beta = 0.0$		$\beta = 1.0$	
	γ_o	$r_o/2R_{maz}$	γ_o	$r_o/2R_{maz}$
0.8	1.53	0.079	1.33	0.095
1.0	1.49	0.064	1.29	0.076
1.2	1.46	0.053	1.26	0.063

$$\alpha = 4.5, R_{min}/R_{maz} = 1/15, \delta = 1.0, M_s = 0.6, M_c = 0.2, M_b = 0.2$$

f	$\beta = 0.0$		$\beta = 1.0$	
	γ_o	$r_o/2R_{maz}$	γ_o	$r_o/2R_{maz}$
0.8	1.81	0.051	1.45	0.057
1.0	1.77	0.042	1.41	0.047
1.2	1.74	0.037	1.38	0.039

*Data between $1/20 \leq r/2R_{maz} \leq 1/5$ are used to fit the power law form of the two-point correlation function in Eqn.(2.1).

TABLE 3

Spiral galaxies*

$$\alpha = 3.5, R_{min}/R_{max} = 1/8, \delta = 1.0, M_s = 0.95, M_c = 0.05, M_b = 0.0$$

f	$\beta = 0.0$		$\beta = 1.0$	
	γ_0	$r_0/2R_{max}$	γ_0	$r_0/2R_{max}$
0.8	1.22	0.052	1.06	0.066
1.0	1.21	0.042	1.05	0.052
1.2	1.21	0.036	1.05	0.044

$$\alpha = 4.5, R_{min}/R_{max} = 1/8, \delta = 1.0, M_s = 0.95, M_c = 0.05, M_b = 0.0$$

f	$\beta = 0.0$		$\beta = 1.0$	
	γ_0	$r_0/2R_{max}$	γ_0	$r_0/2R_{max}$
0.8	1.40	0.042	1.11	0.048
1.0	1.39	0.036	1.11	0.039
1.2	1.39	0.031	1.10	0.033

$$\alpha = 3.5, R_{min}/R_{max} = 1/15, \delta = 1.0, M_s = 0.95, M_c = 0.05, M_b = 0.0$$

f	$\beta = 0.0$		$\beta = 1.0$	
	γ_0	$r_0/2R_{max}$	γ_0	$r_0/2R_{max}$
0.8	1.55	0.043	1.08	0.059
1.0	1.54	0.037	1.08	0.047
1.2	1.54	0.033	1.07	0.040

$$\alpha = 4.5, R_{min}/R_{max} = 1/15, \delta = 1.0, M_s = 0.95, M_c = 0.05, M_b = 0.0$$

f	$\beta = 0.0$		$\beta = 1.0$	
	γ_0	$r_0/2R_{max}$	γ_0	$r_0/2R_{max}$
0.8	2.11	0.036	1.24	0.038
1.0	2.11	0.032	1.24	0.031
1.2	2.11	0.030	1.23	0.027

*Data between $1/20 \leq r/2R_{max} \leq 1/5$ are used to fit the power law form of the two-point correlation function in Eqn.(2.1).

Elliptical galaxies*

$$\alpha = 3.5, R_{min}/R_{maz} = 1/8, \delta = 1.0, M_s = 0.67, M_c = 0.33, M_b = 0.0$$

f	$\beta = 0.0$		$\beta = 1.0$	
	γ_0	$r_0/2R_{maz}$	γ_0	$r_0/2R_{maz}$
0.8	1.45	0.168	1.38	0.189
1.0	1.41	0.136	1.33	0.153
1.2	1.37	0.113	1.30	0.128

$$\alpha = 4.5, R_{min}/R_{maz} = 1/8, \delta = 1.0, M_s = 0.67, M_c = 0.33, M_b = 0.0$$

f	$\beta = 0.0$		$\beta = 1.0$	
	γ_0	$r_0/2R_{maz}$	γ_0	$r_0/2R_{maz}$
0.8	1.50	0.120	1.39	0.135
1.0	1.46	0.097	1.35	0.109
1.2	1.43	0.082	1.31	0.092

$$\alpha = 3.5, R_{min}/R_{maz} = 1/15, \delta = 1.0, M_s = 0.67, M_c = 0.33, M_b = 0.0$$

f	$\beta = 0.0$		$\beta = 1.0$	
	γ_0	$r_0/2R_{maz}$	γ_0	$r_0/2R_{maz}$
0.8	1.55	0.137	1.40	0.166
1.0	1.51	0.111	1.36	0.135
1.2	1.47	0.094	1.32	0.113

$$\alpha = 4.5, R_{min}/R_{maz} = 1/15, \delta = 1.0, M_s = 0.67, M_c = 0.33, M_b = 0.0$$

f	$\beta = 0.0$		$\beta = 1.0$	
	γ_0	$r_0/2R_{maz}$	γ_0	$r_0/2R_{maz}$
0.8	1.79	0.081	1.52	0.095
1.0	1.74	0.067	1.47	0.079
1.2	1.71	0.058	1.44	0.067

*Data between $1/20 \leq r/2R_{maz} \leq 1/5$ are used to fit the power law form of the two-point correlation function in Eqn.(2.1).

TABLE 4

Cluster-Galaxy Cross correlation function*

$$\alpha = 3.5, R_{min}/R_{max} = 1/8, \delta = 1.0, M_s = 0.8, M_c = 0.2, M_b = 0.0$$

f	$\beta = 0.0$		$\beta = 1.0$	
	γ_0	$r_0/2R_{max}$	γ_0	$r_0/2R_{max}$
0.8	1.63	0.170	1.52	0.180
1.0	1.59	0.142	1.47	0.149
1.2	1.55	0.123	1.44	0.127

$$\alpha = 4.5, R_{min}/R_{max} = 1/8, \delta = 1.0, M_s = 0.8, M_c = 0.2, M_b = 0.0$$

f	$\beta = 0.0$		$\beta = 1.0$	
	γ_0	$r_0/2R_{max}$	γ_0	$r_0/2R_{max}$
0.8	1.93	0.120	1.75	0.125
1.0	1.88	0.103	1.70	0.106
1.2	1.85	0.091	1.67	0.092

$$\alpha = 3.5, R_{min}/R_{max} = 1/15, \delta = 1.0, M_s = 0.8, M_c = 0.2, M_b = 0.0$$

f	$\beta = 0.0$		$\beta = 1.0$	
	γ_0	$r_0/2R_{max}$	γ_0	$r_0/2R_{max}$
0.8	1.79	0.119	1.59	0.129
1.0	1.74	0.101	1.54	0.107
1.2	1.71	0.088	1.50	0.092

$$\alpha = 4.5, R_{min}/R_{max} = 1/15, \delta = 1.0, M_s = 0.8, M_c = 0.2, M_b = 0.0$$

f	$\beta = 0.0$		$\beta = 1.0$	
	γ_0	$r_0/2R_{max}$	γ_0	$r_0/2R_{max}$
0.8	2.30	0.075	1.99	0.077
1.0	2.26	0.066	1.95	0.067
1.2	2.23	0.060	1.92	0.060

*Data between $1/20 \leq r/2R_{max} \leq 1/3$ are used to fit the power law form of the cross correlation function.

REFERENCES

- Bahcall, N. A. 1986, *Ap.J. (Letters)*, **302**, L41.
- Bahcall, N. A. 1988, *Ann. Rev. Astron. Astrophys.*, **26**, 631.
- Bahcall, N. A., Henriksen, M. J., and Smith, T. E. 1989, *Ap.J. (Letters)*, **346**, L45 (BHS).
- Bahcall, N. A., and Soneira, R. M. 1983, *Ap.J.*, **270**, 20.
- Bean, A. J., Efstathiou, G., Ellis, R. S., Peterson, B. A., and Shanks, T. 1983, *M.N.R.A.S.*, **205**, 605.
- Bertschinger, E. W. 1983, *Ap.J.*, **268**, 17.
- Bertschinger, E. W. 1985, *Ap.J. Suppl.*, **58**, 1.
- Borden, D., Ostriker, J. P., and Weinberg, D. H. 1989, *Ap.J.*, **345**, 607.
- Broadhurst, T. J., Ellis, R. S., Koo, D. C., and Szalay, A. S. 1990, *Nature*, **343**, 726.
- Chincarini, G. 1978, *Nature*, **272**, 515.
- Coles, P. 1990, preprint.
- Collins, C. A., Heydon-Dumbleton, N. H., and MacGillivray, H. T. 1989, *M.N.R.A.S.*, **236**, 7p.
- Da Costa, L. N., Pellegrini, P. S., Sargent, W. L. W., Tonry, J., Davis, M., Meiksin, A., Latham, D. W., Menzies, J. W., and Coulson, I. A. 1988, *Ap.J.*, **327**, 544.
- Da Costa, L. N., Pellegrini, P. S., Willmer, C., and Latham, D. W. 1989, *Ap.J.*, **344**, 20.
- Davis, M., and Geller, M. J. 1976, *Ap.J.*, **208**, 13.
- Davis, M., Meiksin, A., Strauss, M. A., Da Costa, L. N., and Yahil, A. 1988, *Ap.J. (Letters)*, **333**, L9.
- Davis, M., and Peebles, P. J. E. 1977, *Ap.J. Suppl.*, **34**, 425.
- Davis, M., and Peebles, P. J. E. 1983, *Ap.J.*, **267**, 465.
- Dekel, A., Blumenthal, G. R., Primack, J. R., and Olivier, S. 1989, *Ap.J. (Letters)*, **338**, L5.
- de Lapparent, V., Geller, M. J., and Huchra, J. P. 1986, *Ap.J. (Letters)*, **302**, L1.

- de Lapparent, V., Geller, M. J., and Huchra, J. P. 1988, *Ap.J.*, **332**, 44.
- Dressler, A. 1980, *Ap.J.*, **236**, 351.
- Efstathiou, G., and Jedredjewski, R. I. 1984, *Adv. Space Res.*, **3**, 379.
- Einasto, J., Einasto, M., Gramann, M., and Saar, E. 1990, preprint.
- Fillmore, J. A., and Goldreich, P. 1984, *Ap.J.*, **281**, 9.
- Fry, J. 1986, *Ap.J.*, **306**, 358.
- Fry, J. 1990, preprint.
- Fry, J., Giovanelli, R., Haynes, M., Melott, A., Scherrer, R. 1989, *Ap.J.*, **340**, 11.
- Fry, J., and Seldner, M. 1982, *Ap.J.*, **259**, 474.
- Geller, M. J., and Huchra, J. P. 1988, in *Large-Scale Motions in the Universe: A Vatican Study Week*, ed. V. C. Rubin and G. V. Coyne (Princeton: Princeton University Press), p.3.
- Giovanelli, R., Haynes, M. P., and Chincarini, G. L. 1986, *Ap.J.*, **300**, 77.
- Giovanelli, R., Haynes, M. P., Myers, S. T., and Roth, J. 1986, *A.J.*, **92**, 250.
- Górski, K. M. 1988, *Ap.J. (Letters)*, **332**, L7.
- Górski, K. M., Davis, M., Strauss, M. A., White, S. D. M., and Yahil, A. 1989, *Ap.J.*, **344**, 1 (GDSWY).
- Gott, J. R., III, Melott, A., and Dickinson, M. 1986, *Ap.J.*, **306**, 341.
- Gregory, S. A., and Thompson, L. A. 1979, *Ap.J.*, **222**, 784.
- Gregory, S. A., Thompson, L. A., and Tifft, W. 1981, *Ap.J.*, **243**, 411.
- Groth, E. J., Juskiewicz, R., and Ostriker, J. P. 1989, *Ap.J.*, **346**, 558 (GJO).
- Groth, E. J., and Peebles, P. J. E. 1977, *Ap.J.*, **217**, 385.
- Haynes, M. P. and Giovanelli, R. 1986, *Ap.J. (Letters)*, **306**, L55.
- Haynes, M. P. and Giovanelli, R. 1988, in *Large-Scale Motions in the Universe: A Vatican Study Week*, ed. V. C. Rubin and G. V. Coyne (Princeton: Princeton University Press), p.31.
- Huchra, J. P., Geller, M. J., de Lapparent, V., and Corwin, H. G., Jr. 1990, *Ap.J. Suppl.*, **72**, 433.

- Hwang, J., Vishniac, E. T., and Shapiro, P. R. 1990, *Ap.J.*, **353**, 1.
- Icke, V., and Van de Weygaert, R. 1987, *Astron. Astrophys.*, **184**, 16.
- Icke, V., and van de Weygaert, R. 1990, preprint.
- Ikeuchi, S. 1981, *Pub. Astr. Soc. Japan*, **33**, 211.
- Ikeuchi, S., Tomisaka, K., and Ostriker, J. P. 1983, *Ap.J.*, **265**, 583.
- Joeveer, M., and Einasto, J. 1978, in *IAU Symposium 79: The Large Scale Structure of the Universe*, ed. M. S. Longair and J. Einasto (Dordrecht: Reidel), p.241.
- Kaiser, N. 1987, *M.N.R.A.S.*, **227**, 1.
- Kaiser, N. 1989, in *Large-Scale Structure and Motions in the Universe*, ed. G. Giuricin, F. Mardirossian, M. Mezzotti, and M. Ramella (Trieste: Kluwer Academic), p.198.
- Kirshner, R. P., Oemler, A., Schechter, P. L., and Shectman, S. A. 1981, *Ap.J. (Letters)*, **248**, L57.
- Kofman, L., Pogosyan, D., and Shandarin, S. 1990, *M.N.R.A.S.*, **242**, 200.
- Koo, D., Kron, R., and Szalay, A. 1987, in *Thirteenth Texas Symposium on Relativistic Astrophysics*, ed. M. Ulmer (Singapore: World Scientific), p.284.
- Kulsrud, R. M., and Cowley, S. C. 1989, *Ap.J.*, **346**, 546.
- Lilje, P. B., and Efstathiou, G. 1988a, in *The Post-Recombination Universe*, ed. N. Kaiser and A. N. Lasenby (Dordrecht: Kluwer Academic Publishers), p.277.
- Lilje, P. B., and Efstathiou, G. 1988b, *M.N.R.A.S.*, **231**, 635.
- Maddox, S. J., Efstathiou, G., Sutherland, W. J., and Loveday, J. 1990, *M.N.R.A.S.*, **242**, 43p.
- Maurogordato, S., and Lachieze-Rey, M. 1987, *Ap.J.*, **320**, 13 (ML).
- McGill, C. 1990, *M.N.R.A.S.*, **242**, 428.
- Melott, A., and Shandarin, S. 1990, preprint.
- Olivier, S., Blumenthal, G. R., Dekel, A., Primack, J. R., and Stanhill, D. 1989, preprint.
- Ostriker, J. P., and Cowie, L. L. 1981, *Ap.J. (Letters)*, **243**, L127.
- Ostriker, J. P., and Strassler, M. 1989, *Ap.J.*, **338**, 579.

- Ostriker, J. P., Thompson, C., and Witten, E. 1986, *Phys. Letters B*, **180**, 231.
- Panek, M. 1985, *M.N.R.A.S.*, **216**, 85.
- Park, C. 1990, *M.N.R.A.S.*, **242**, 59p.
- Peebles, P. J. E. 1980, *The Large-Scale Structure of the Universe* (Princeton: Princeton University Press).
- Peebles, P. J. E. 1988a, in *Large-Scale Motions in the Universe: A Vatican Study Week*, ed. V. C. Rubin and G. V. Coyne (Princeton: Princeton University Press), p.457.
- Peebles, P. J. E. 1988b, *Ap.J.*, **332**, 17.
- Peterson, B. A., Ellis, R. S., Efstathiou, G., Shanks, T., Bean, A. J., Fong, R., and Zen-Long, Z. 1986, *M.N.R.A.S.*, **221**, 233.
- Postman, M., Geller, M. J., and Huchra, J. P. 1986, *A.J.*, **91**, 1267.
- Saarinen, S., Dekel, A., and Carr, B. 1987, *Nature*, **325**, 598.
- Sadler, E. M., and Sharp, N. A. 1984, *Ap.J.*, **287**, 80.
- Seldner, M., and Peebles, P. J. E. 1977a, *Ap.J. (Letters)*, **214**, L1.
- Seldner, M., and Peebles, P. J. E. 1977b, *Ap.J.*, **215**, 703.
- Sharp, N. A., Jones, B., and Jones, J. 1978, *M.N.R.A.S.*, **185**, 456.
- Shectman, S. A. 1985, *Ap.J. Suppl.*, **57**, 77.
- Soneira, R. M., and Peebles, P. J. E. 1977, *Ap.J.*, **211**, 1.
- Soneira, R. M., and Peebles, P. J. E. 1978, *A.J.*, **83**, 845.
- Strauss, M. and Huchra, J. 1988, *A.J.*, **95**, 1602.
- Sutherland, W. 1988, *M.N.R.A.S.*, **234**, 159.
- Szalay, A. 1988, in *Large-Scale Motions in the Universe: A Vatican Study Week*, ed. V. C. Rubin and G. V. Coyne (Princeton: Princeton University Press), p.323.
- Tarengi, M., Chincarini, G., Rood, H. J., and Thompson, L. A. 1980, *Ap.J.*, **235**, 724.
- Tift, W. G., and Gregory, S. A. 1976, *Ap.J.*, **205**, 696.

- Van de Weygaert, R. and Icke, V. 1989, *Astron. Astrophys.*, **213**, 1.
- Vettolani, G, de Souza, R., and Chincarini, G. 1986, *Astron. Astrophys.*, **154**, 343.
- Weinberg, D. H., Ostriker, J. P., and Dekel, A. 1989, *Ap.J.*, **336**, 9 (WOD).
- White, S. D. M., Frenk, C. S., Davis, M., and Efstathiou, G. 1987, *Ap.J.*, **313**, 505.
- White, S. D. M., and Ostriker, J. P. 1990, *Ap.J.*, **349**, 22.
- Yoshioka, S., and Ikeuchi, S. 1990, *Ap.J.*, **360**, 352.

FIGURE CAPTIONS

- Fig. 1.— The galaxy two-point correlation function for the equal size shell model with $f = 0.8, 1.0,$ and 1.2 . Dashed line at lower left shows $r^{-1.8}$ slope for comparison.
- Fig. 2.— The scaled three-point correlation function Q for the equal size shell model plotted against r . Q was calculated for $0 < r_a/2R_{sh}, r_b/2R_{sh}, r_c/2R_{sh} < 1/2$ and averaged over u and v .
- Fig. 3.— The peculiar velocity correlation function and the relative peculiar velocity of the equal size shell model for $f = 0.8$, normalized to the shell velocity V_{sh} . The dot-short dashed curve is $\xi_{vv}^{\parallel}(r)$, dot-long dashed curve $\xi_{vv}^{\perp}(r)$, short dashed curve $\xi_{vv}(r)$, and the solid curve is $v_{12}(r)$.
- Fig. 4.— The void probability function of the equal size shell model for $f = 0.8$ (solid curve) and 1.2 (short dashed curve). The void probability function for a random Poisson distribution of galaxies with $n_g = 0.01h^3\text{Mpc}^{-3}$ (assuming $R_{sh} = 15h^{-1}\text{Mpc}$) is also shown (dot-short dashed curve) for comparison.
- Fig. 5.— The galaxy two-point correlation function for the power law model. (a) $R_{min}/R_{max} = 1/8$, $\alpha = 3.5$, $\beta = 0.0$, and $f = 0.8, 1.0,$ and 1.2 ; (b) same as (a) except $\alpha = 4.5$; (c) same as (a) except $R_{min}/R_{max} = 1/15$; (d) same as (a) except $R_{min}/R_{max} = 1/15$ and $\alpha = 4.5$. Dashed line corresponding to $r^{-1.8}$ is shown at lower left for comparison.
- Fig. 6.— The scaled three-point correlation function Q for the power law model plotted against r . Q was calculated for $0 < r_a/2R_{max}, r_b/2R_{max}, r_c/2R_{max} < 1/2$ and averaged over u and v . (a) $R_{min}/R_{max} = 1/8$, $\alpha = 3.5$, $\beta = 0.0$; (b) same as (a) except $\beta = 1.0$; (c) same as (a) except $\alpha = 4.5$; (d) same as (a) except $\alpha = 4.5$ and $\beta = 1.0$.
- Fig. 7.— The peculiar velocity correlation function and the relative peculiar velocity of the power law model. (a) $R_{min}/R_{max} = 1/8$, $\alpha = 3.5$, $\beta = 0.0$, $\gamma = 1.0$, and $f = 0.8$; (b) same as (a) except $\beta = 1.0$; (c) same as (a) except $\alpha = 4.5$; (d) same as (a) except $\alpha = 4.5$ and $\beta = 1.0$. The dot-short dashed curve is $\xi_{vv}^{\parallel}(r)$, dot-long dashed curve $\xi_{vv}^{\perp}(r)$, short dashed curve $\xi_{vv}(r)$, and the solid curve is $v_{12}(r)$.
- Fig. 8.— The void probability function of the power law model (4 upper curves) and the power law model with cluster and background galaxies (4 middle curves). Here, $R_{min}/R_{max} = 1/8$. The solid curve corresponds to $f = 0.8$ and $\alpha = 3.5$, dotted curve $f = 0.8$ and $\alpha = 4.5$, short-dashed curve $f = 1.2$ and $\alpha = 3.5$, and long dashed curve $f = 1.2$ and $\alpha = 4.5$. In addition, the middle curves assume $M_b = 0.2$, $n_g = 0.01h^3\text{Mpc}^{-3}$, and $R_{max} = 30h^{-1}\text{Mpc}$ (see §V). The void probability function for a random Poisson distribution of galaxies with $n_g = 0.01h^3\text{Mpc}^{-3}$ (assuming $R_{max} = 30h^{-1}\text{Mpc}$) is also plotted (lower dot-short dashed curve) for comparison.

- Fig. 9.— The galaxy two-point correlation function for the the power law model including cluster and background galaxies. (a) $R_{min}/R_{max} = 1/8$, $\alpha = 3.5$, $\beta = 0.0$, $\delta = 1.0$, $M_c = 0.2$, $M_b = 0.0$ and $f = 0.8, 1.0$, and 1.2 ; (b) same as (a) except $\alpha = 4.5$; (c) same as (a) except $M_b = 0.2$; (d) same as (a) except $M_b = 0.2$ and $\alpha = 4.5$. Dashed line corresponding to $r^{-1.8}$ is plotted at lower left for comparison.
- Fig. 10.— The spiral galaxy two-point correlation function. Here, spiral galaxies are assumed to comprise 95% shell (field) galaxies and 5% cluster galaxies. (a) $R_{min}/R_{max} = 1/8$, $\alpha = 3.5$, $\beta = 0.0$, $\delta = 1.0$, and $f = 0.8, 1.0$, and 1.2 ; (b) same as (a) except $\alpha = 4.5$. Dashed line corresponding to $r^{-1.8}$ is plotted at lower left for comparison.
- Fig. 11.— The elliptical galaxy two-point correlation function. Here, elliptical galaxies are assumed to comprise 67% shell (field) galaxies and 33% cluster galaxies. (a) $R_{min}/R_{max} = 1/8$, $\alpha = 3.5$, $\beta = 0.0$, $\delta = 1.0$, and $f = 0.8, 1.0$, and 1.2 ; (b) same as (a) except $\alpha = 4.5$. Dashed line corresponding to $r^{-1.8}$ is plotted at lower left for comparison.
- Fig. 12.— The cluster-galaxy cross correlation function. (a) $R_{min}/R_{max} = 1/8$, $\alpha = 3.5$, $\beta = 0.0$, $\delta = 1.0$, $M_c = 0.2$, $M_b = 0.0$ and $f = 0.8, 1.0$, and 1.2 ; (b) same as (a) except $\alpha = 4.5$. Dashed line corresponding to $r^{-1.8}$ is plotted at lower left for comparison.
- Fig. 13.— The galaxy two-point correlation function with equal size, self-avoiding shells for $f = 0.8, 1.0$, and 1.2 . Dashed line corresponding to $r^{-1.8}$ is plotted at lower left for comparison.
- Fig. A1.— The galaxy two-point correlation function with equal size, finite thickness shells for $f = 0.8$ and 1.2 and $\delta R_{sh}/2R_{sh} = 1/10$. Dashed line corresponding to $r^{-1.8}$ is plotted at lower left for comparison.
- Fig. B1.— Schematic diagram for the volume element at the point 3, separated by $r_b \leq r \leq r_b + dr_b$ and $r_c \leq r \leq r_c + dr_c$ from the two points, 1 and 2, which are separated by $r_a \leq r \leq r_a + dr_a$.
- Fig. B2.— The cross section of the ring at the intersection of two shells in Figure B1.
- Fig. C1.— Schematic diagram to find, on the surface of a shell, the area element at the point 3, separated by $l_b \leq l \leq l_b + dl_b$ and $l_c \leq l \leq l_c + dl_c$ from two points, 1 and 2, which are separated by $l_a \leq l \leq l_a + dl_a$.

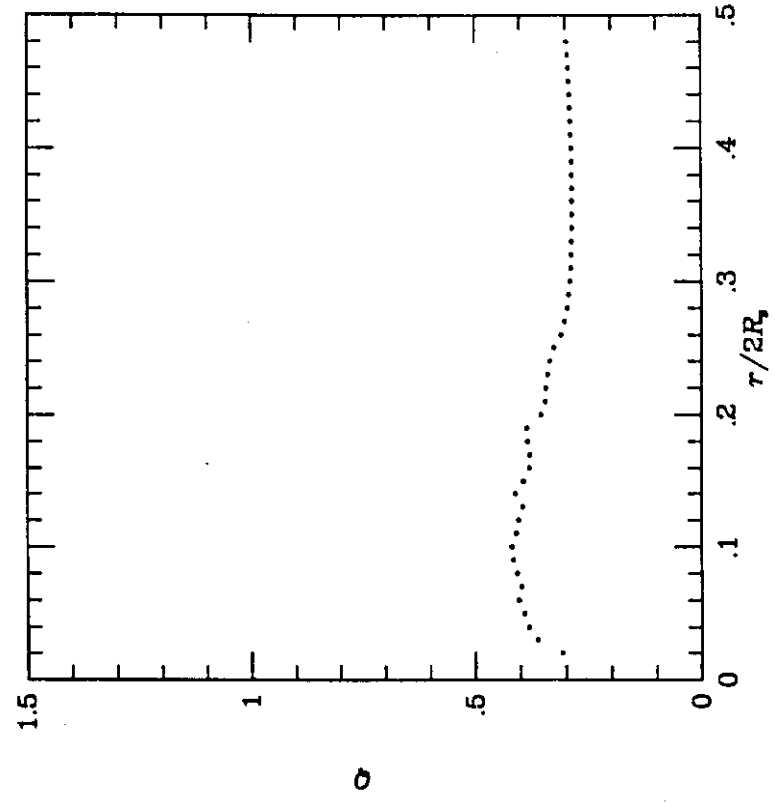


Fig 2

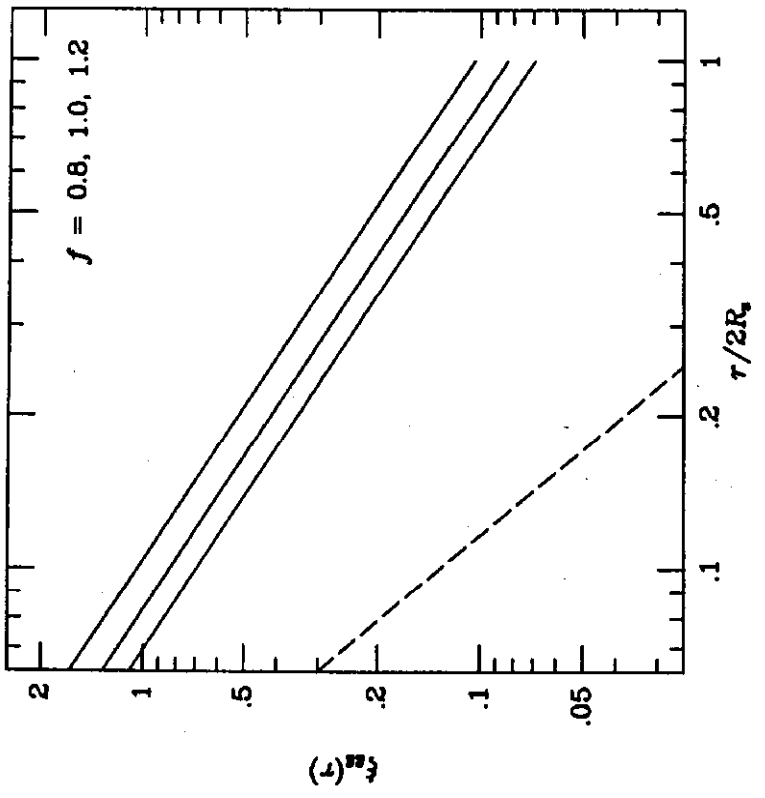


Fig 1

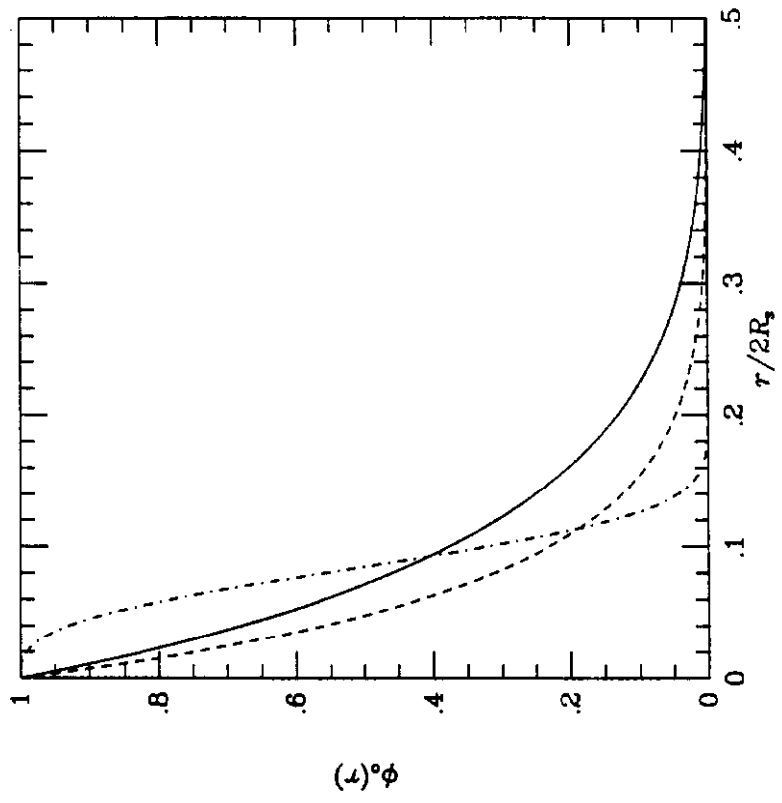


Fig 1

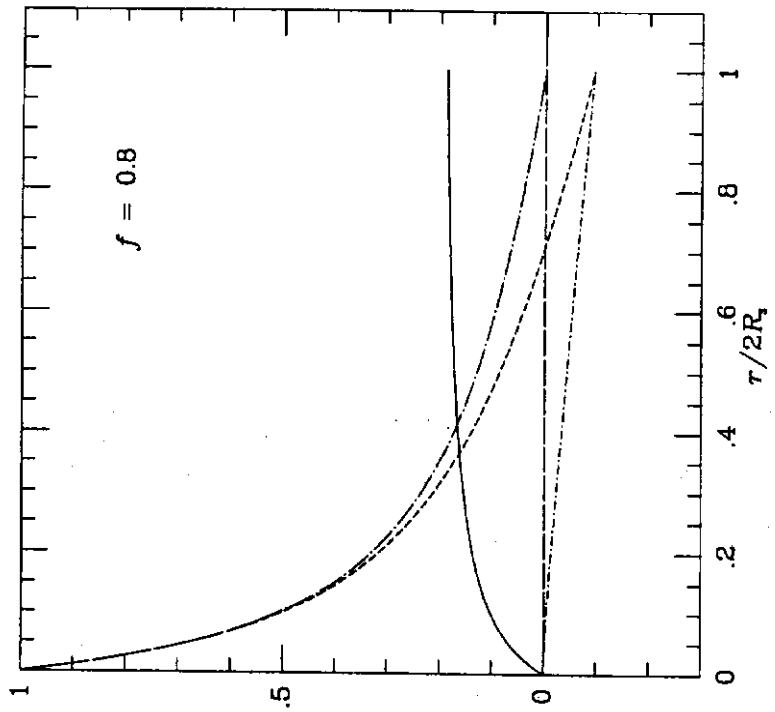


Fig 3

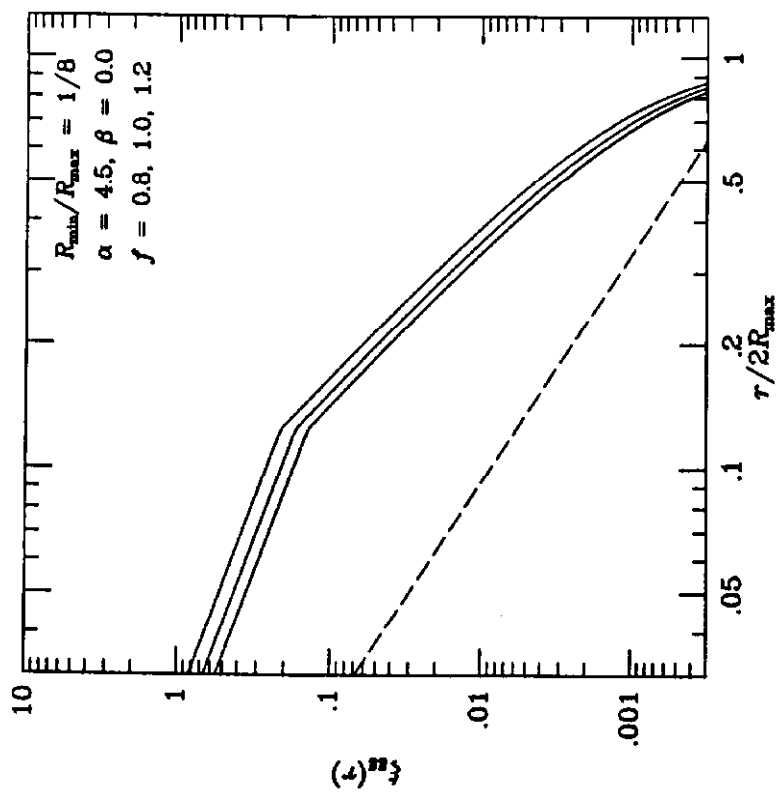


Fig. 5b

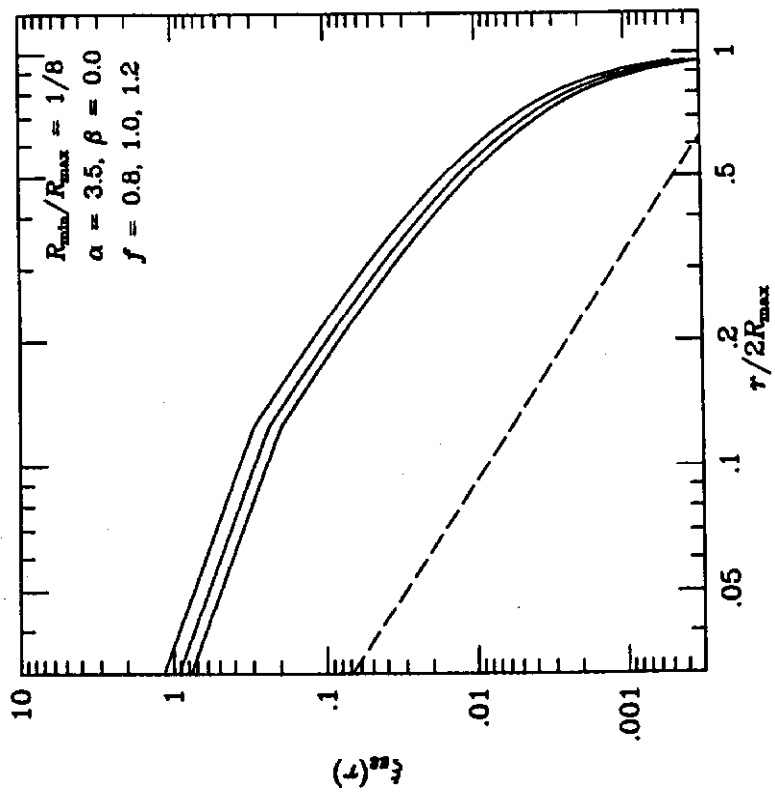


Fig. 5a

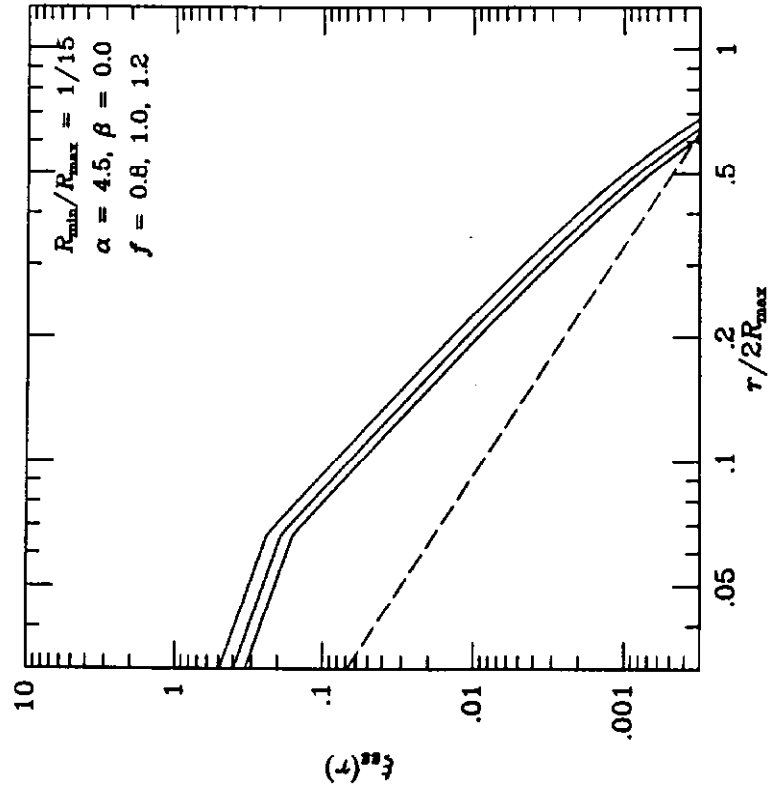


Fig 5d

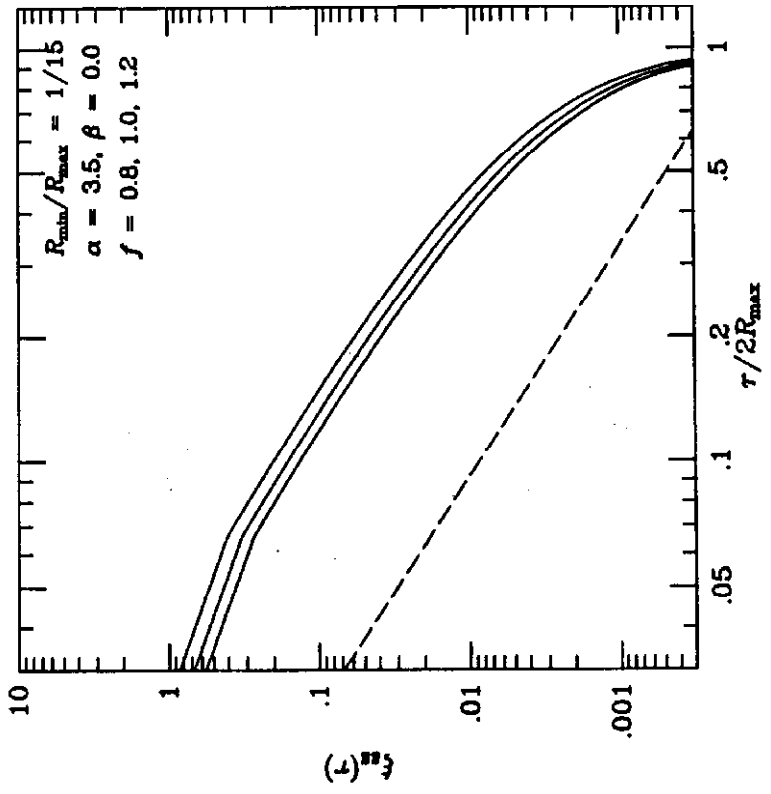


Fig 5c

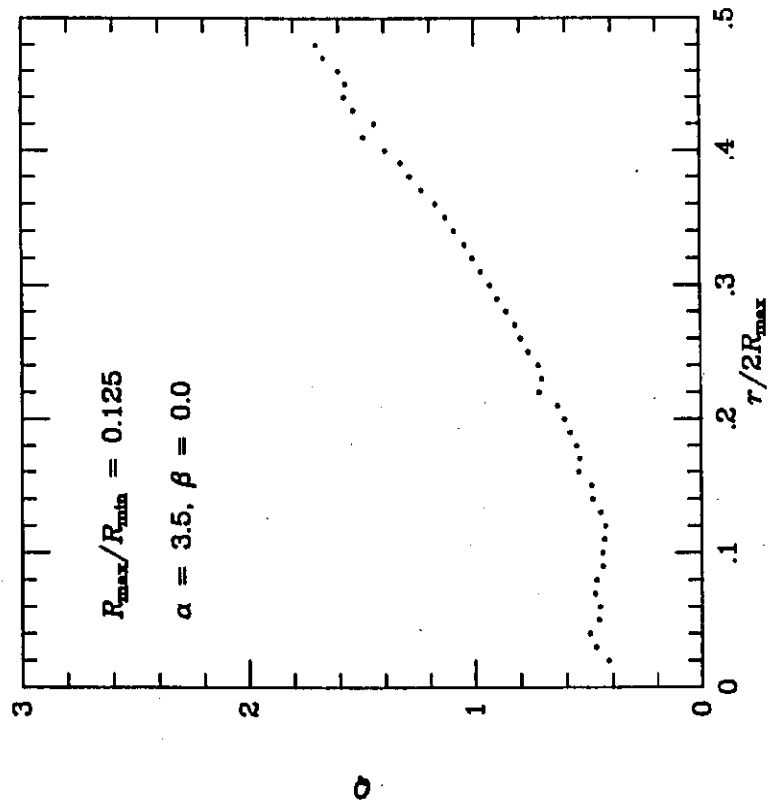


Fig 6a

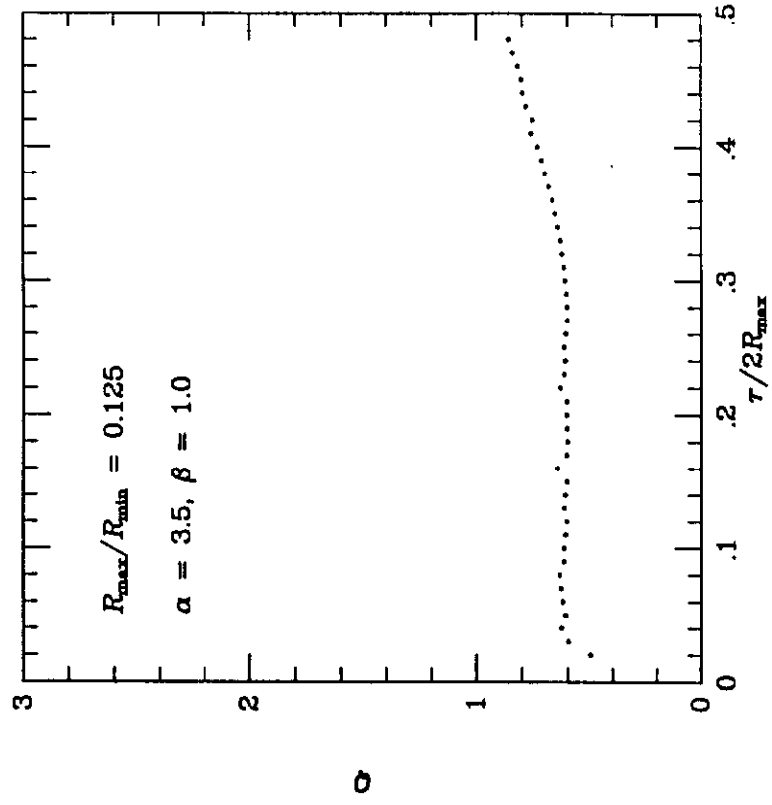


Fig 6b

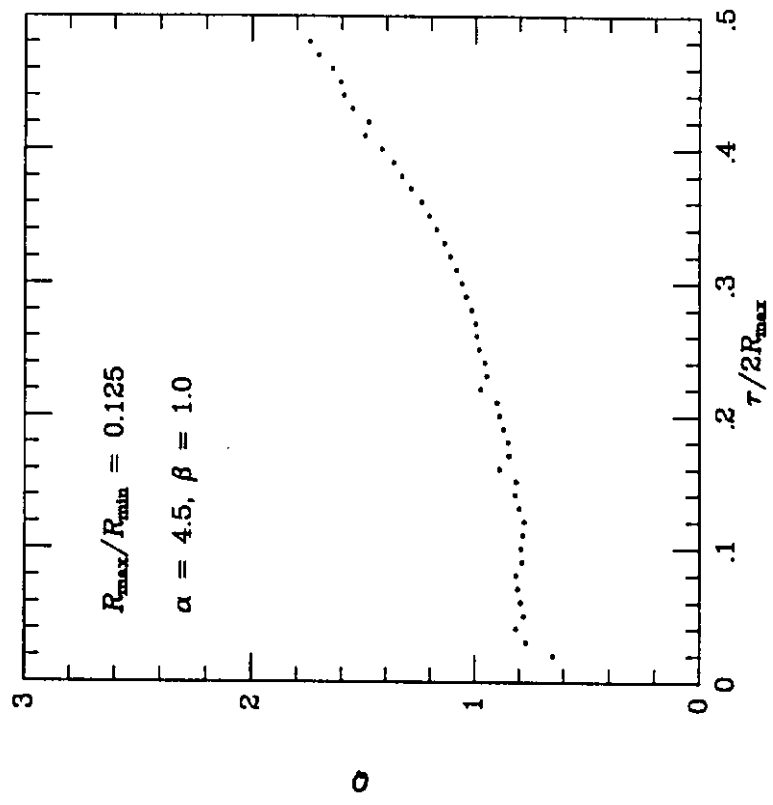


Fig 6d

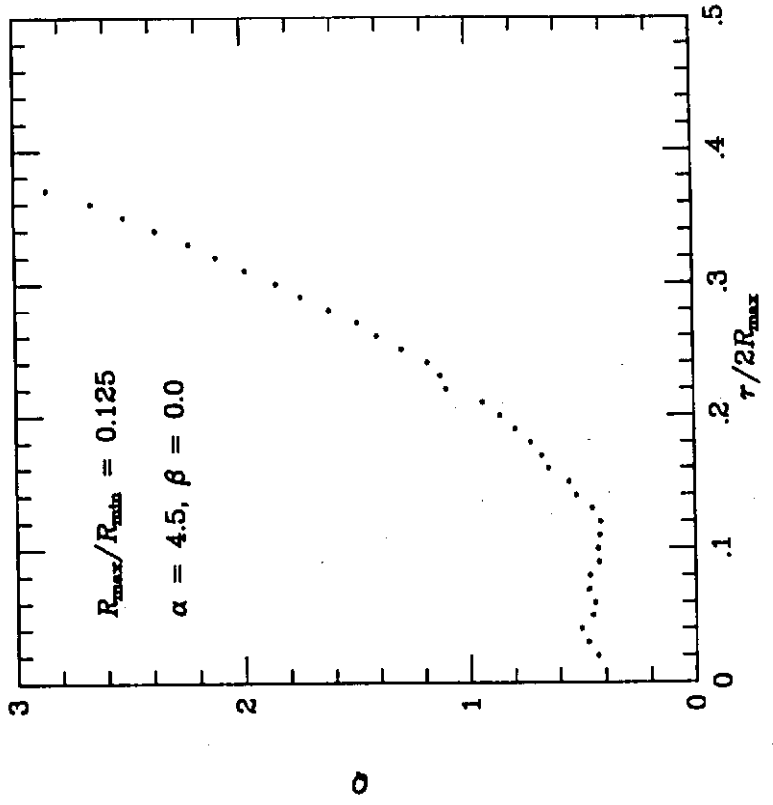


Fig 6c

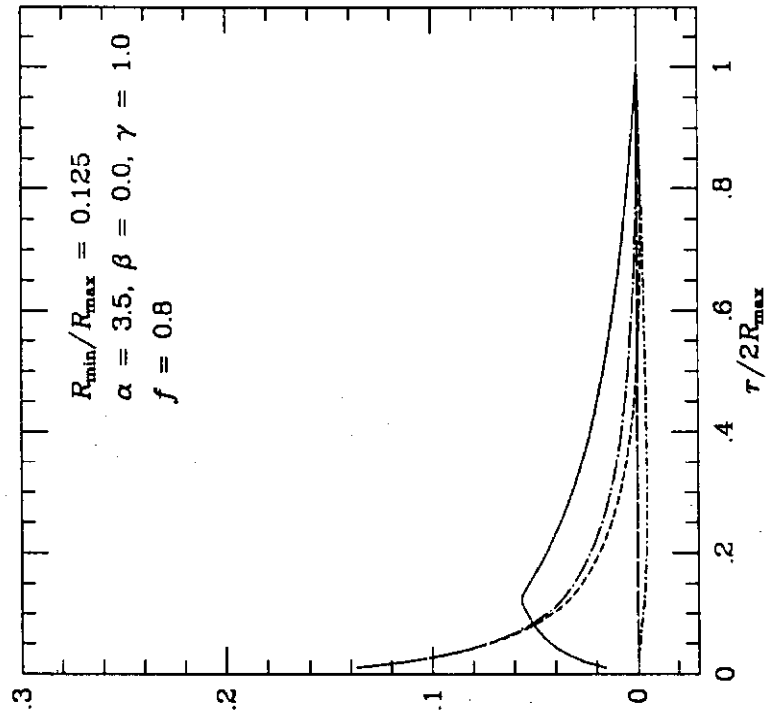


Fig 7a

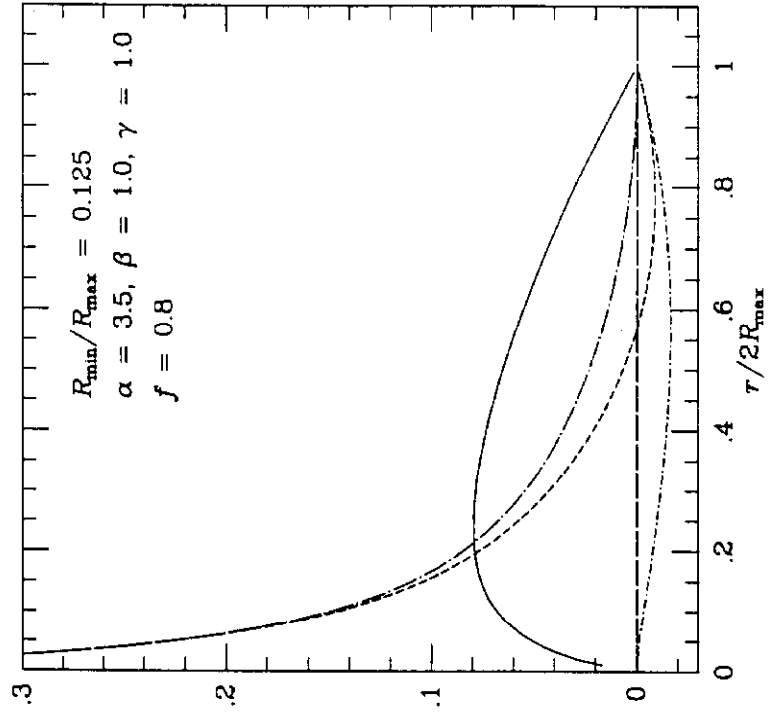


Fig 7b

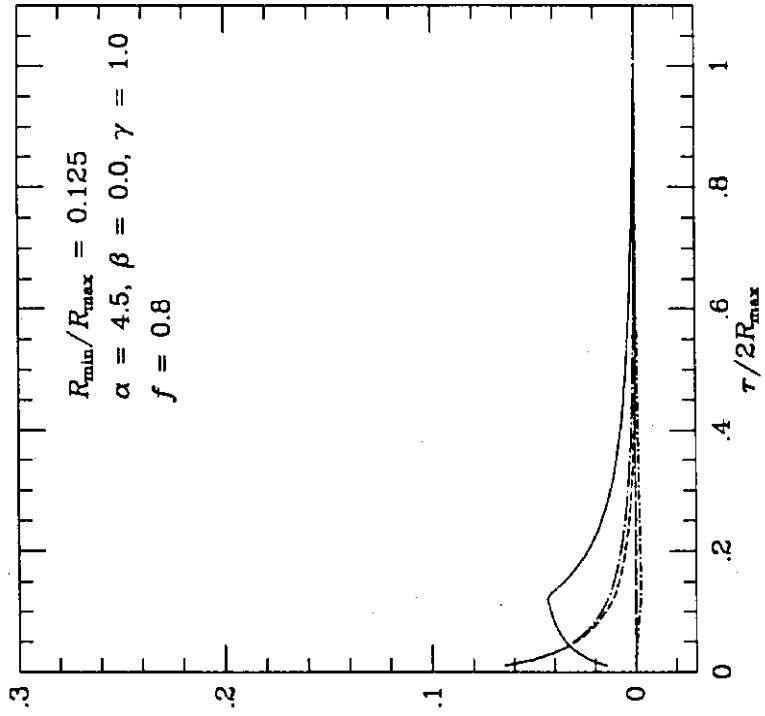


Fig 7c

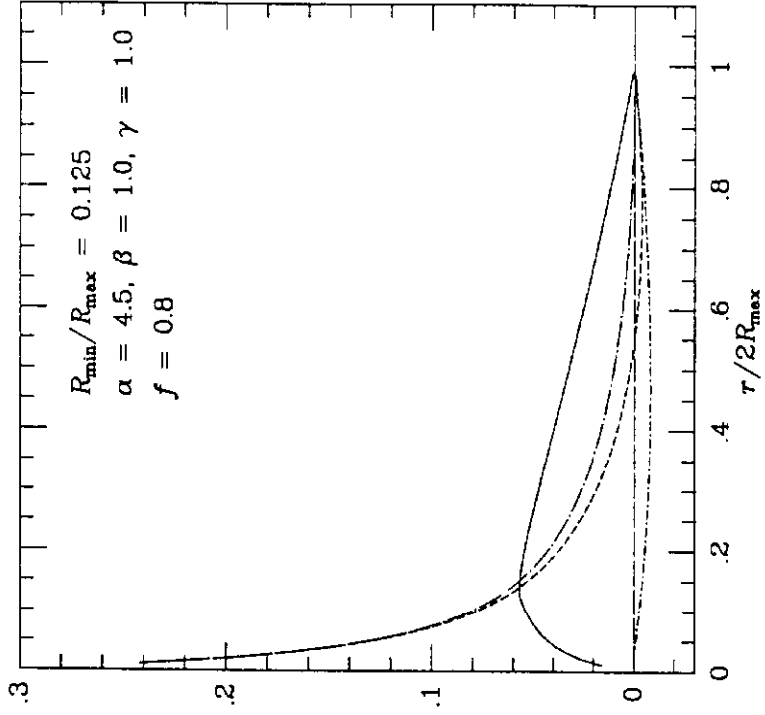


Fig 7d

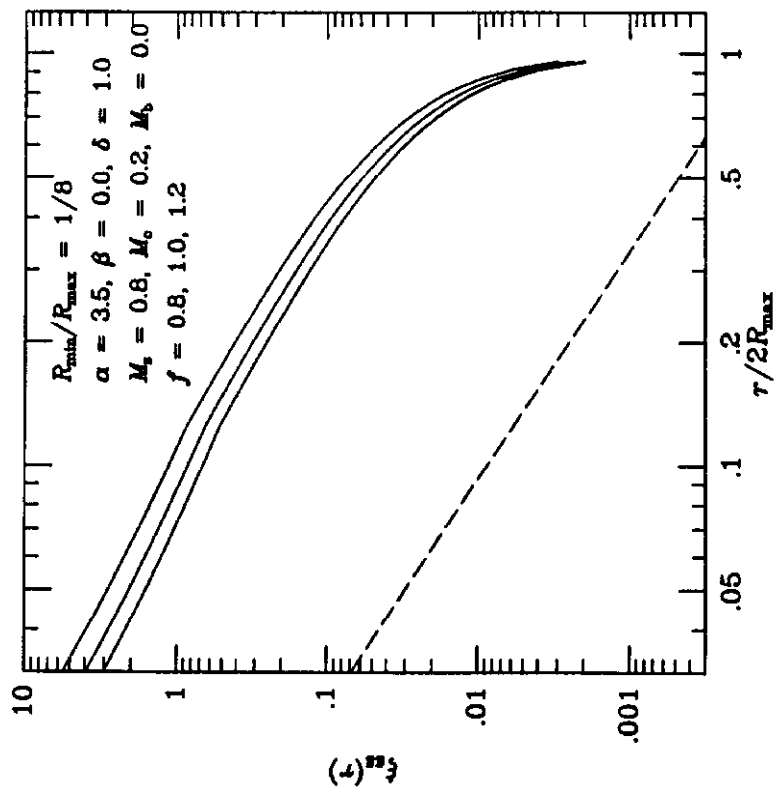
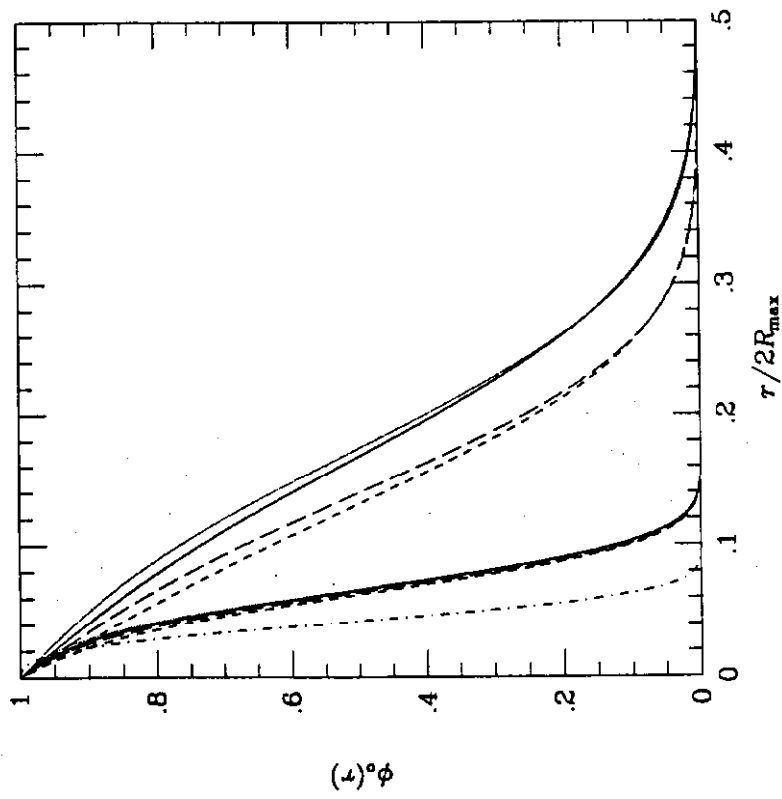


Fig 8

Fig 9a

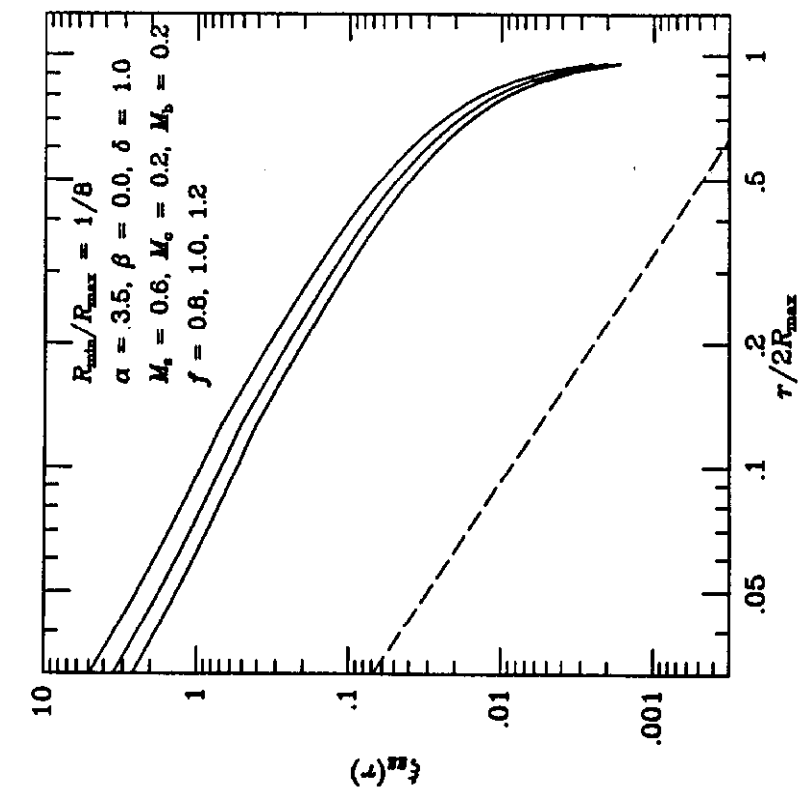


Fig 9c

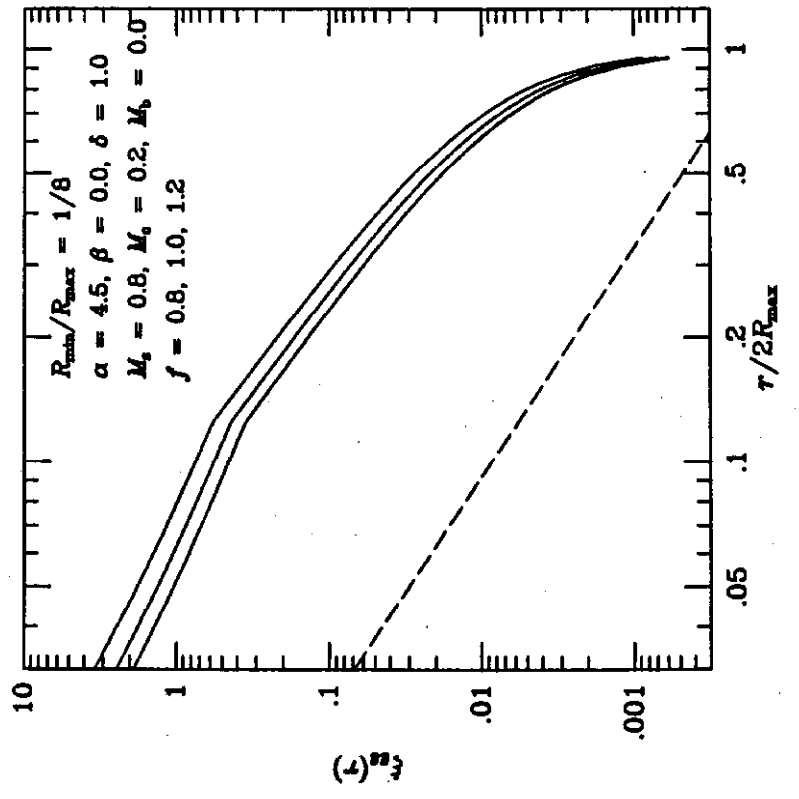


Fig 9b

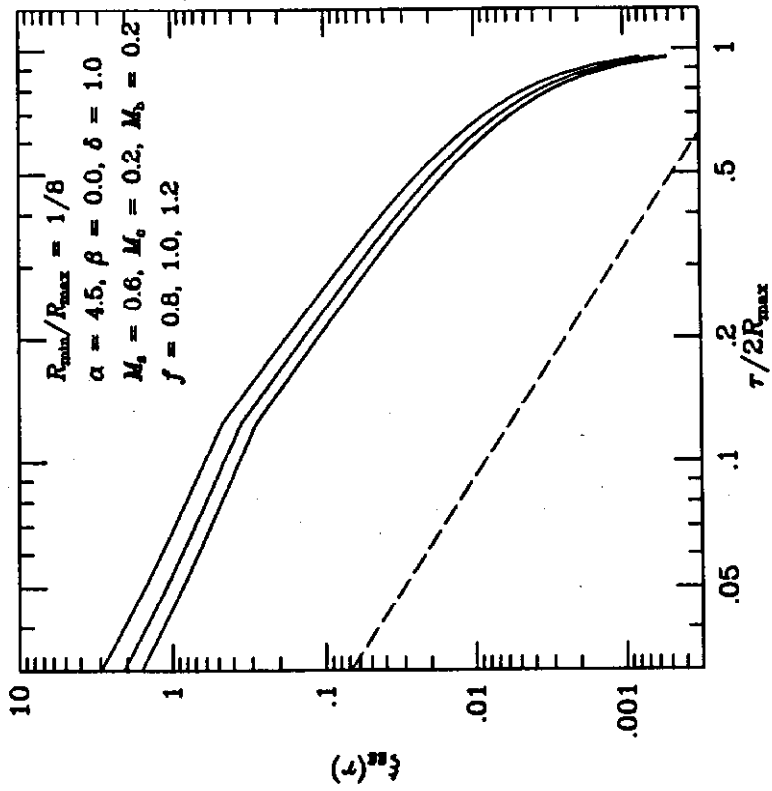


Fig 9d

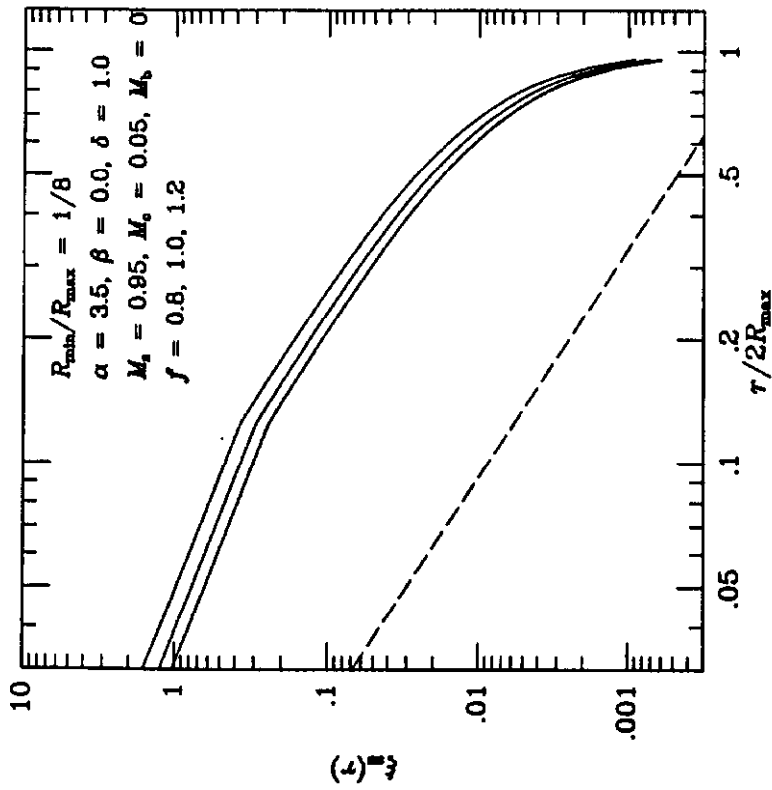


Fig 10a

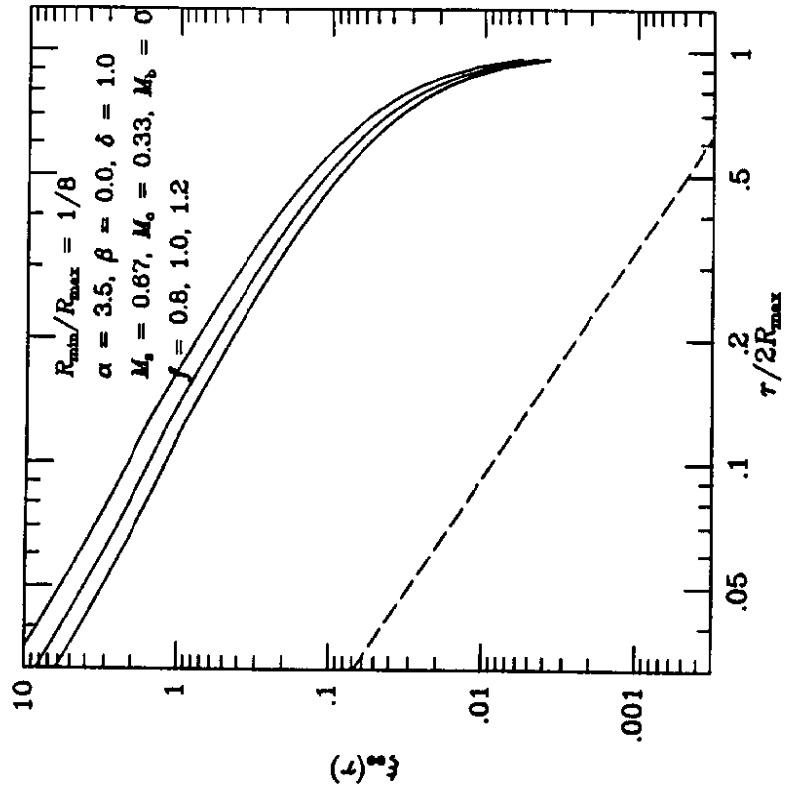


Fig 11a

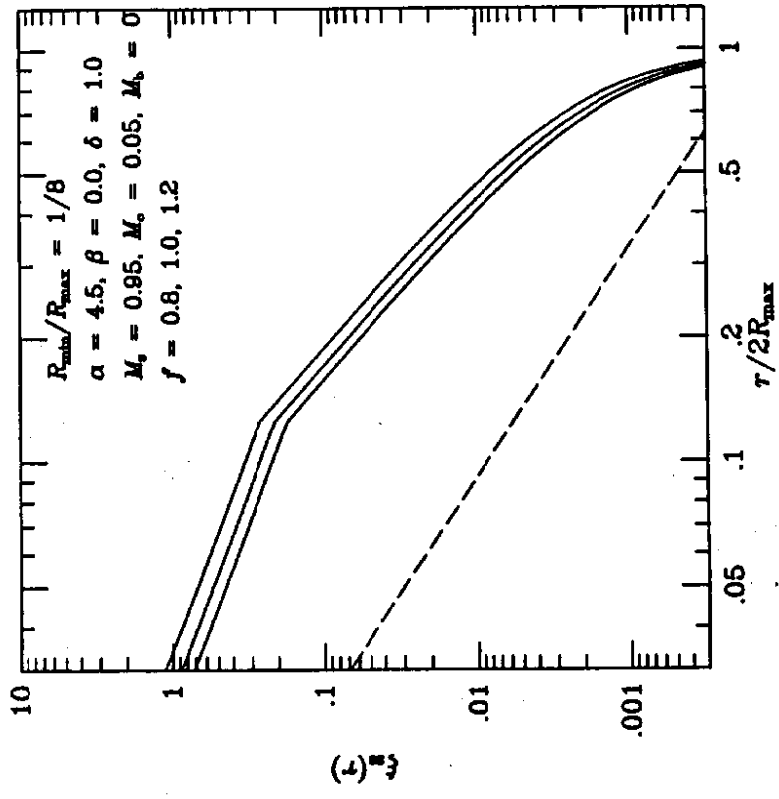


Fig 11b

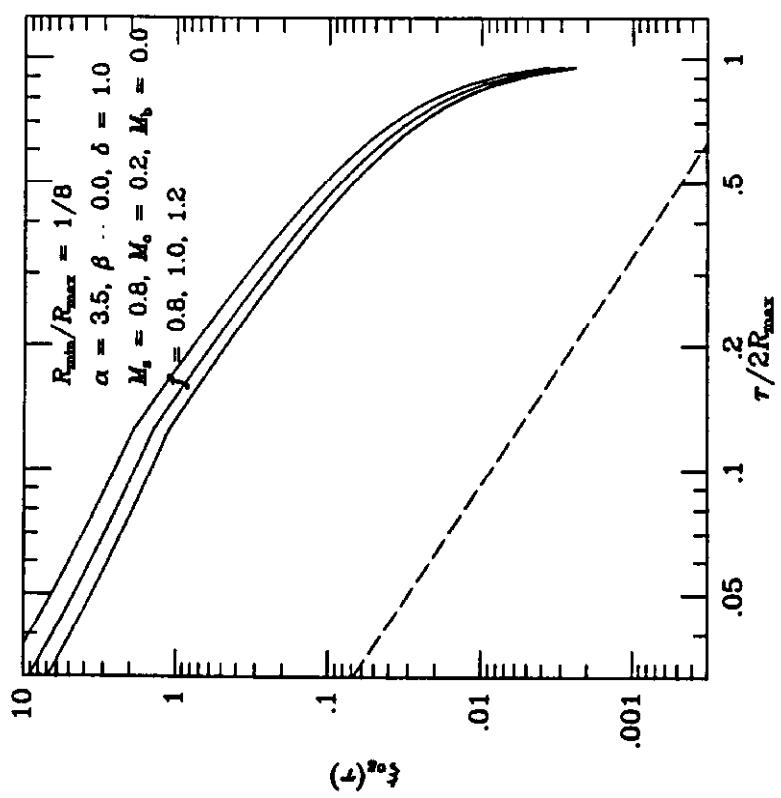


Fig 10a

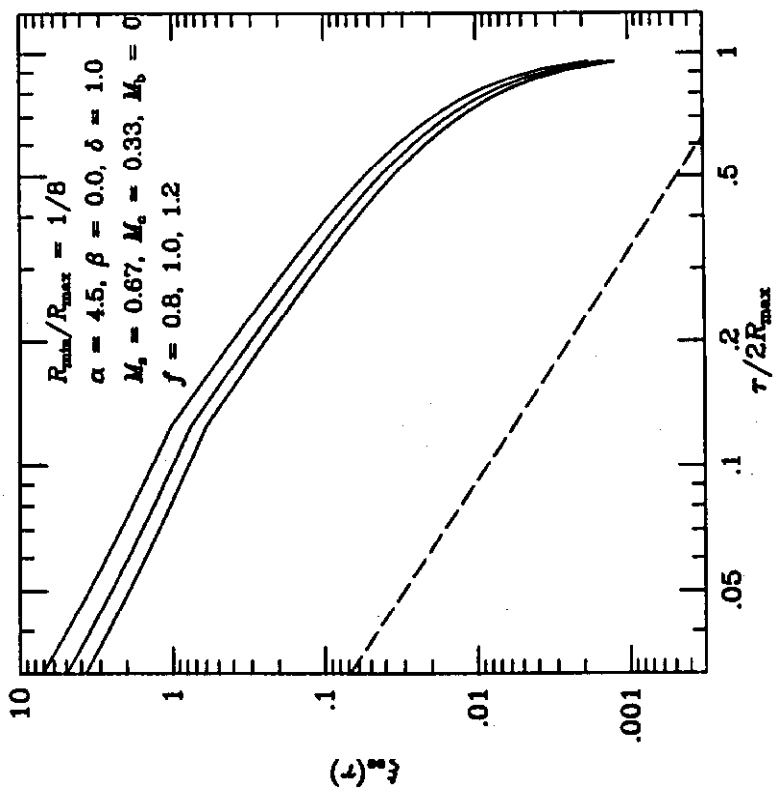


Fig 10b

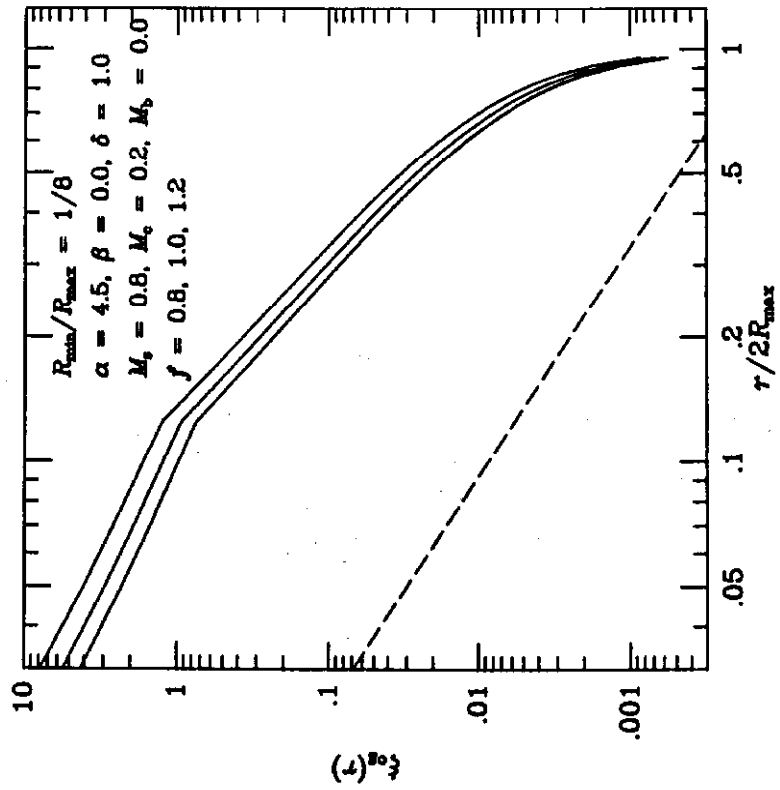


Fig 12b

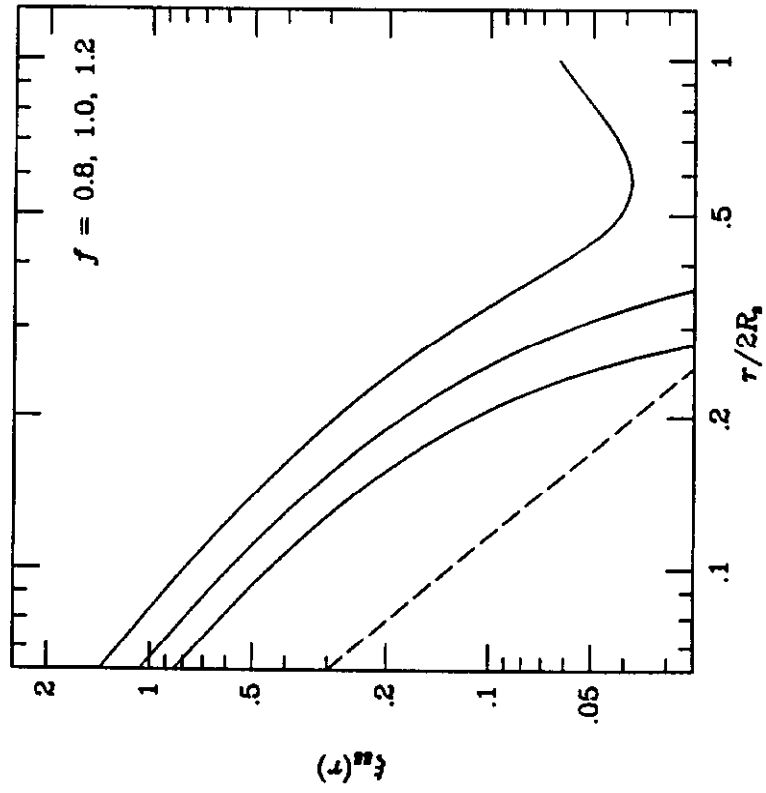


Fig 12c

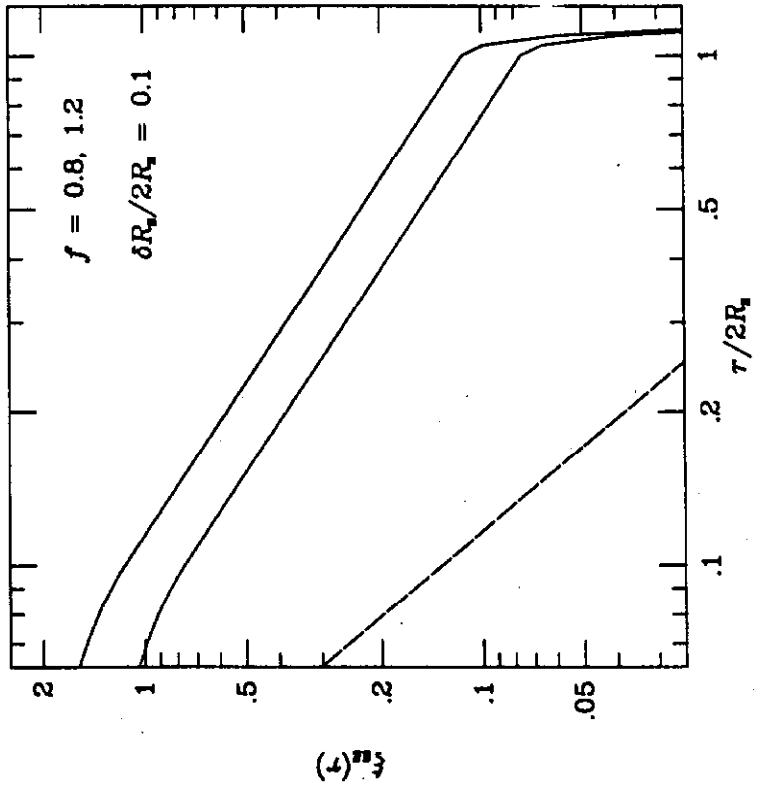


Fig A1

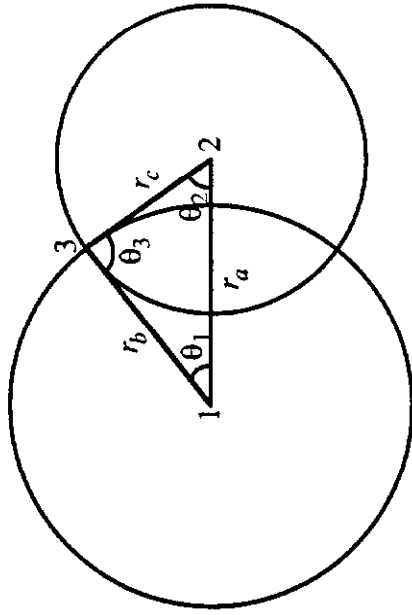


Fig. 01

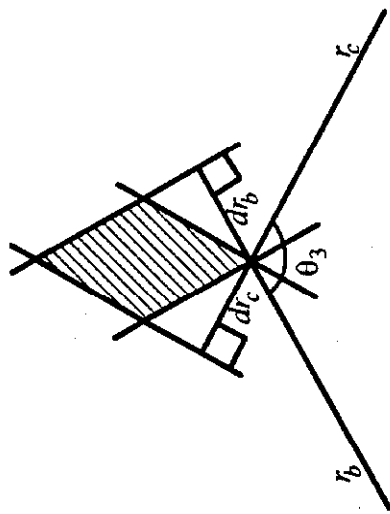
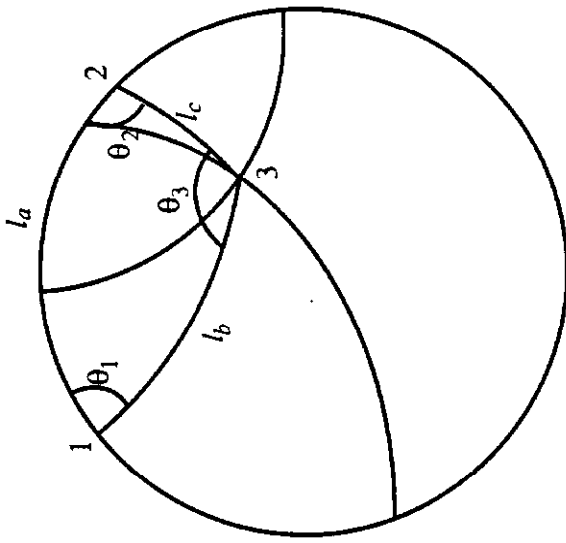


Fig. 01

Fig. 02

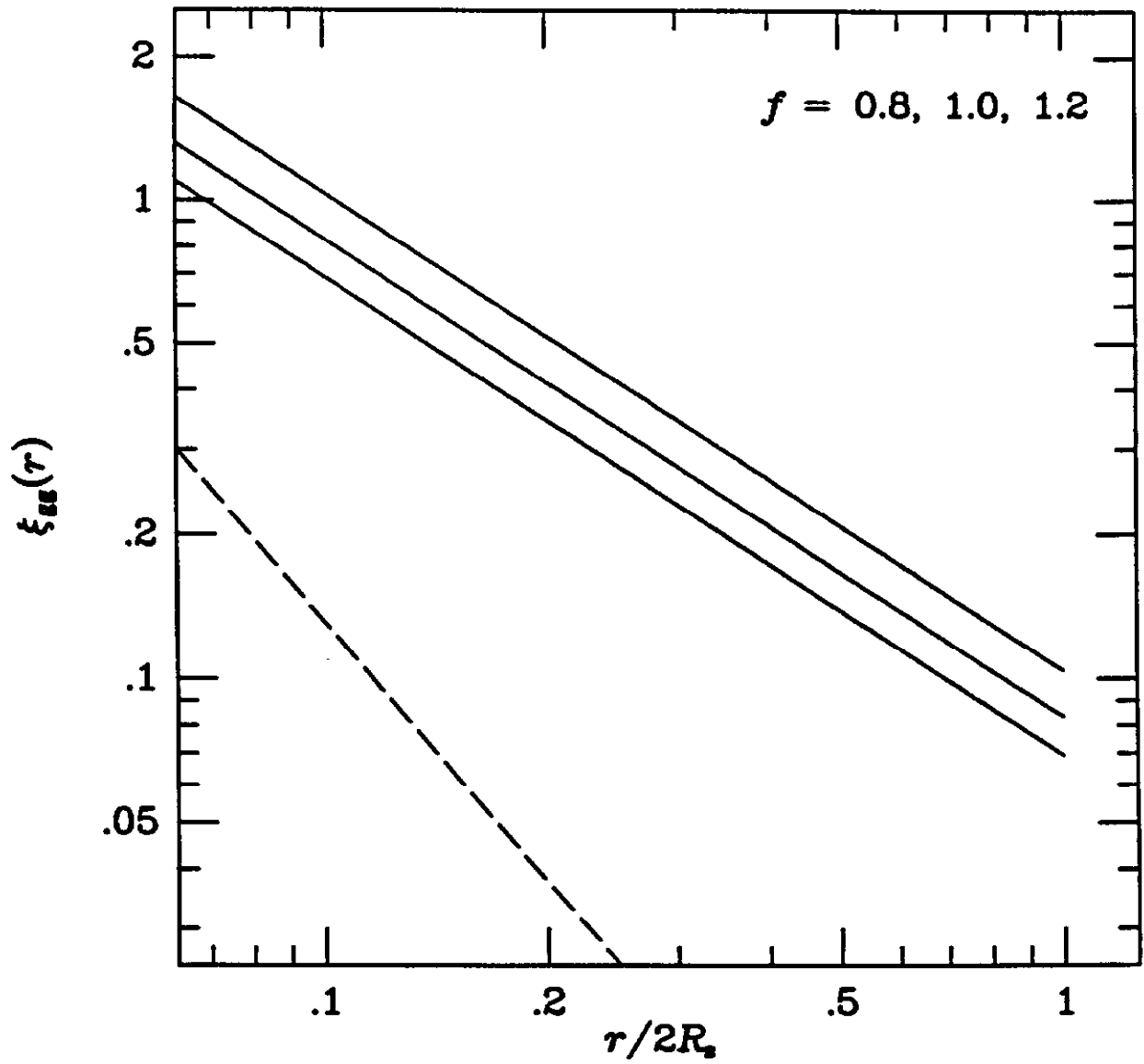


Fig 1

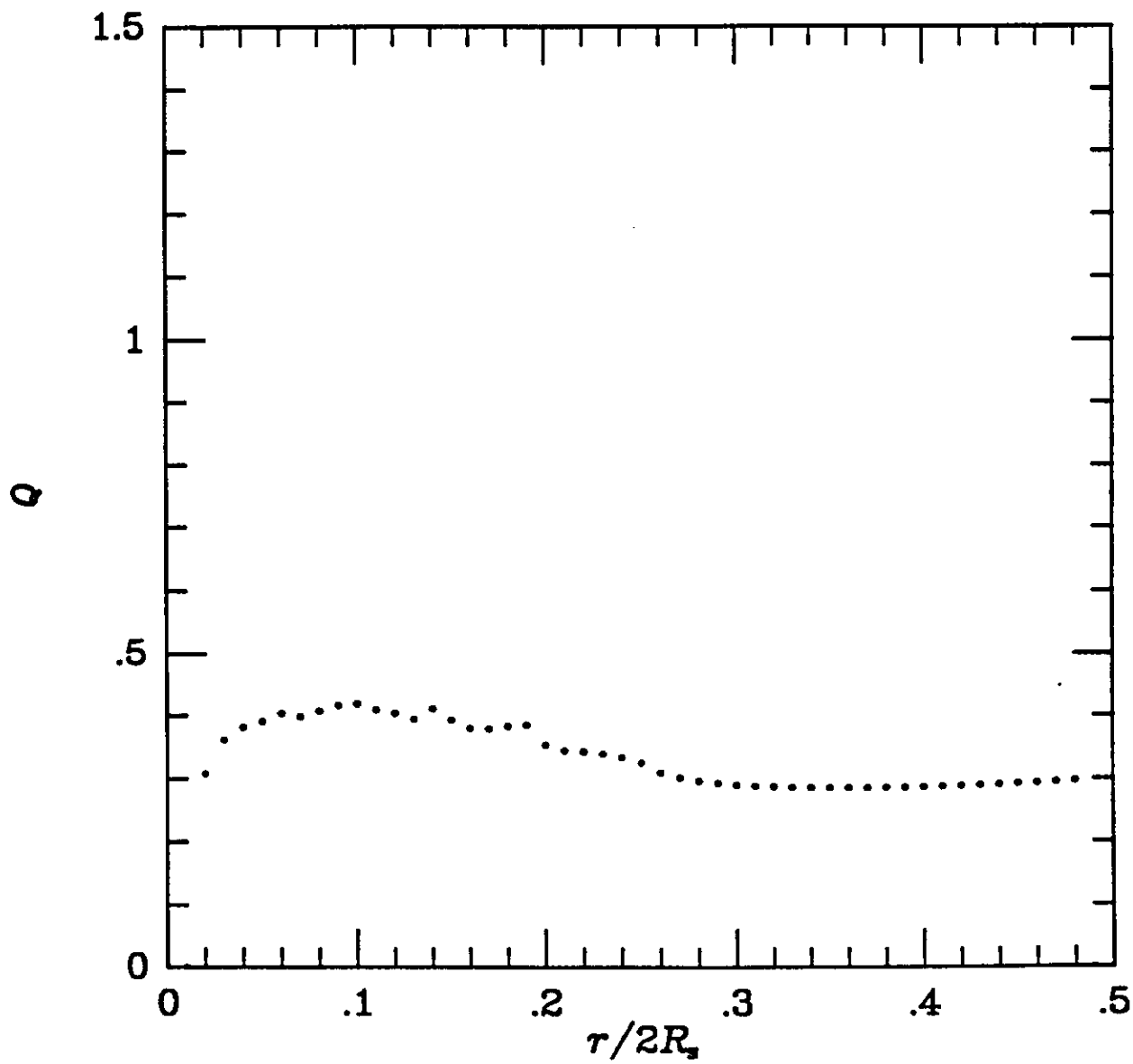


Fig 2

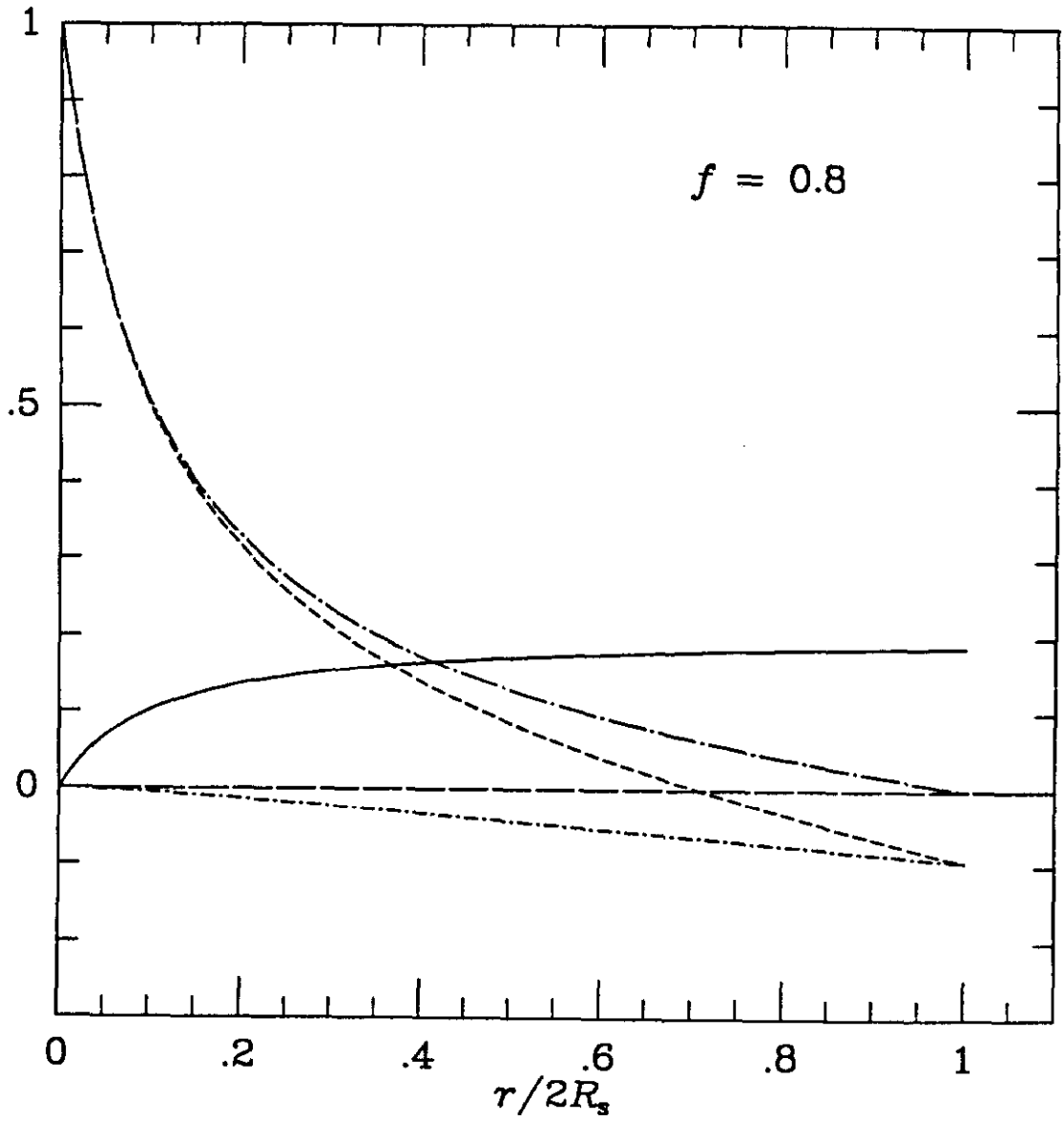


Fig 3

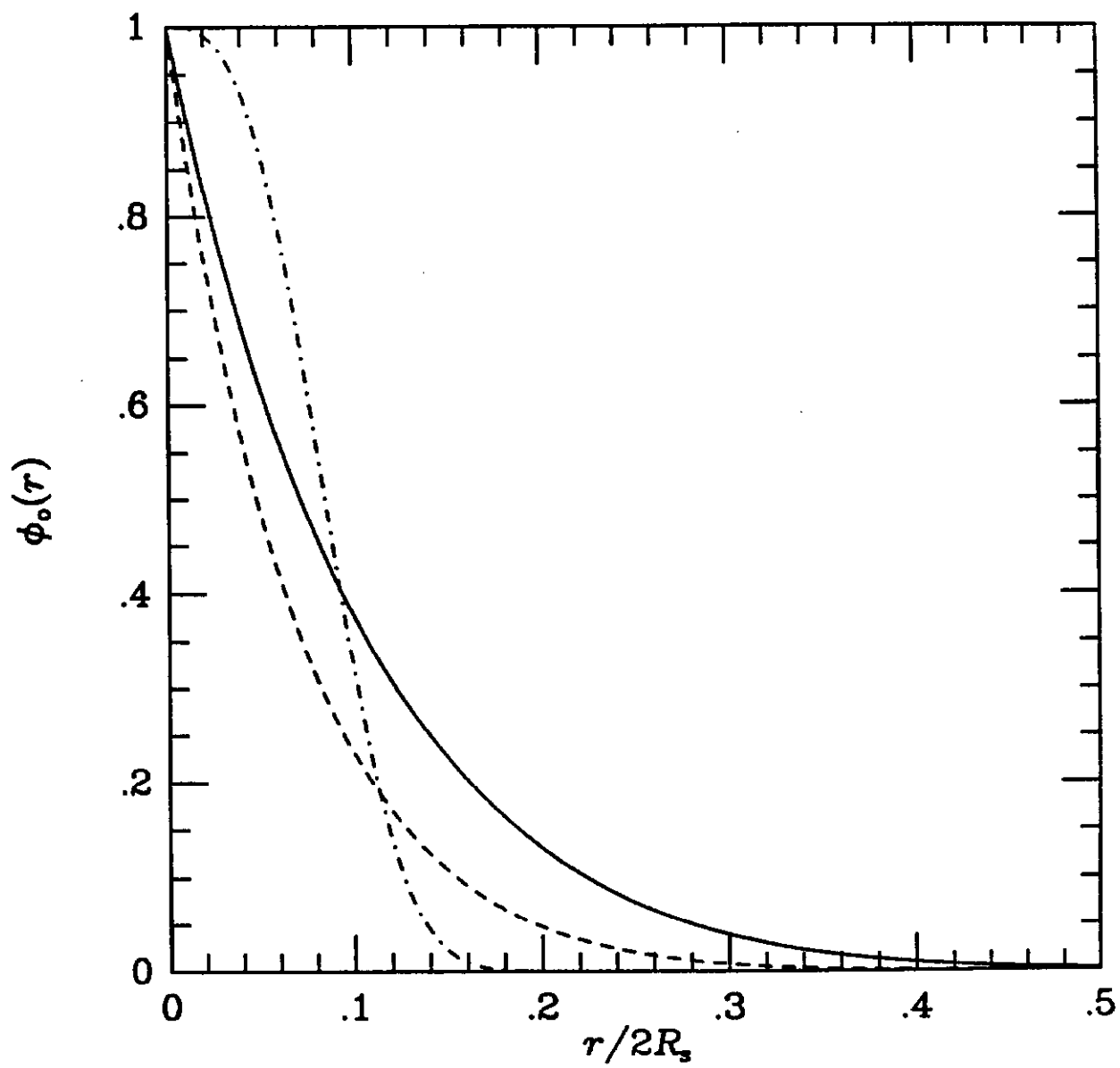


Fig 1

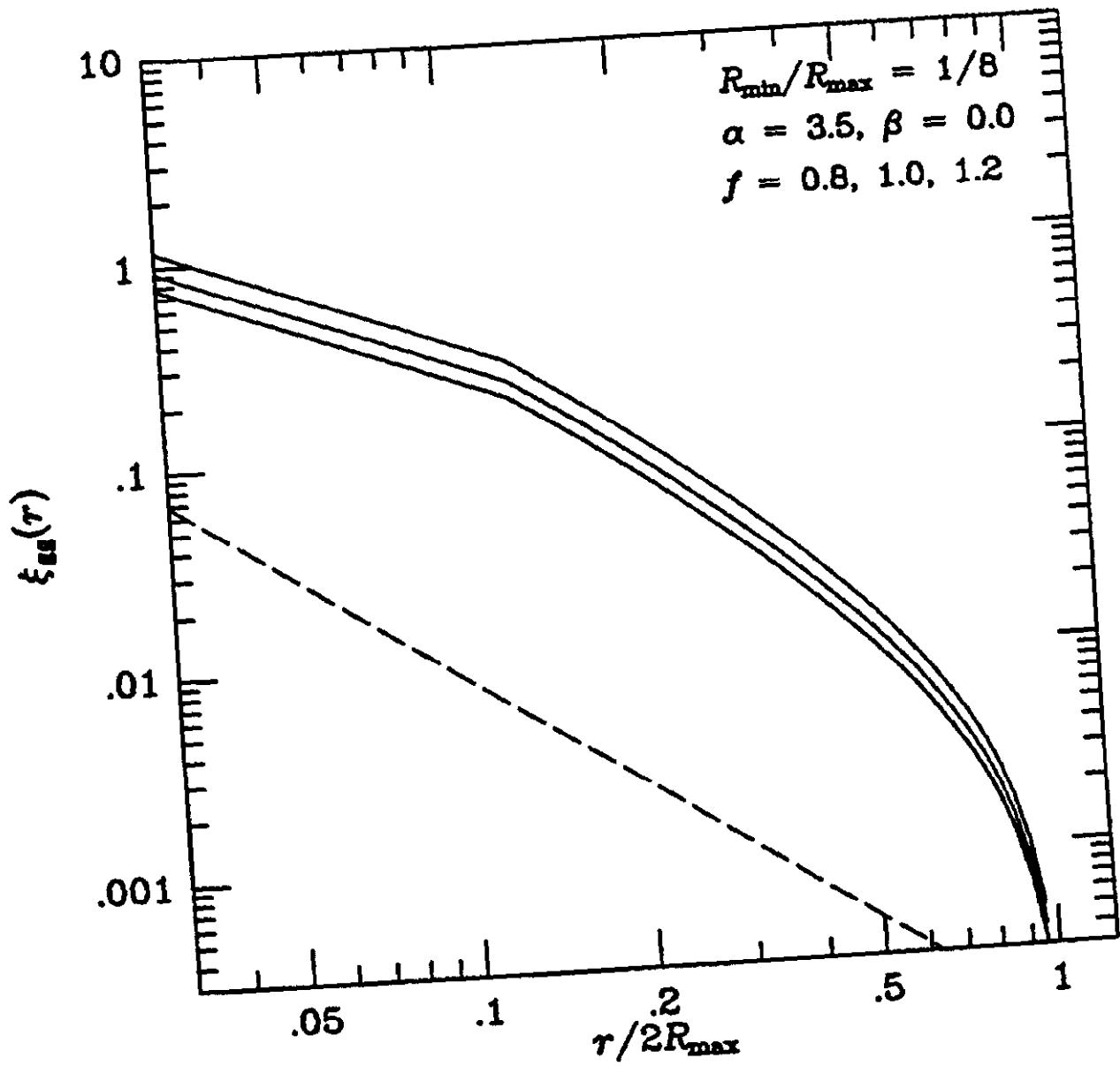


Fig 5a

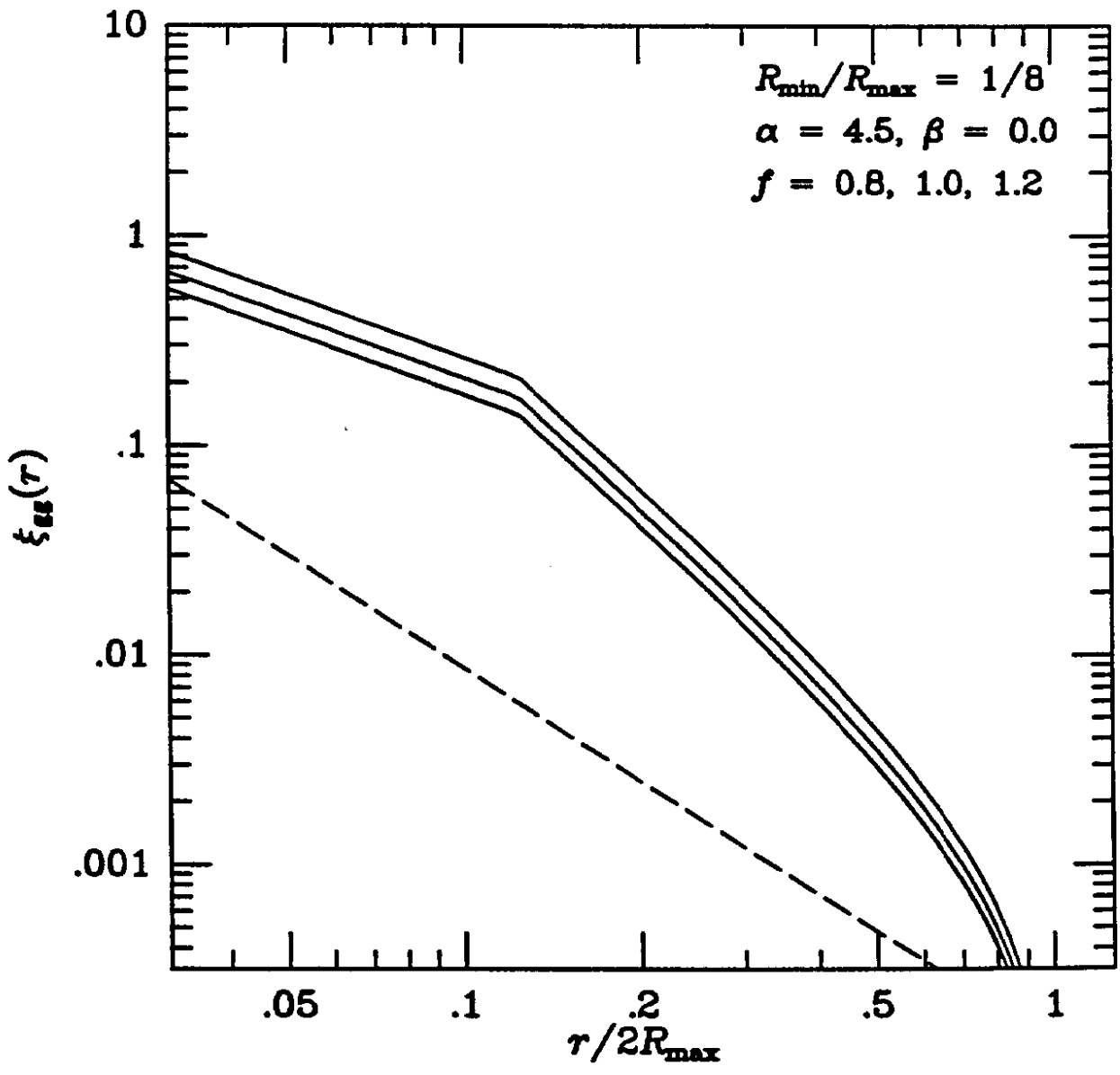


Fig 5b

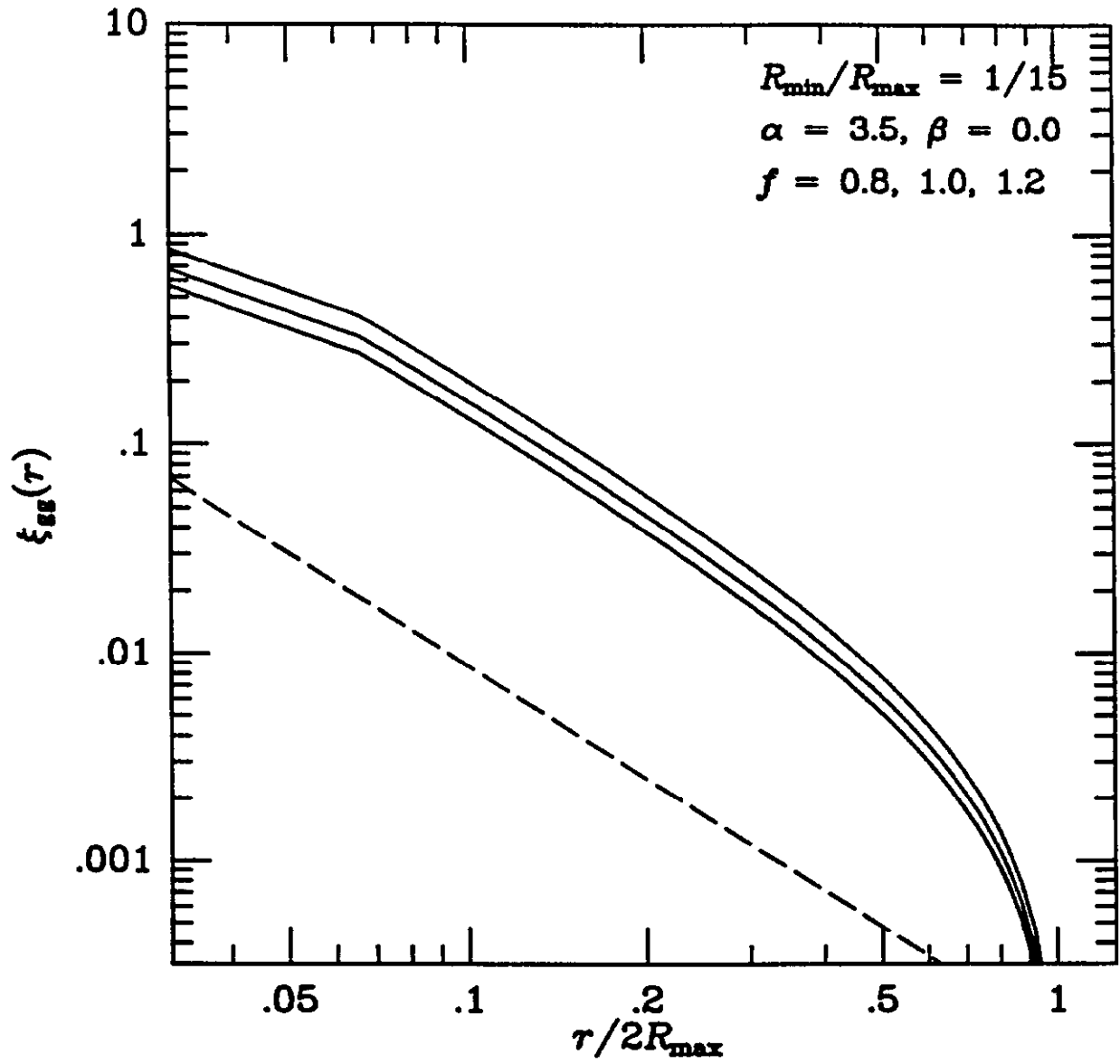


Fig 5c

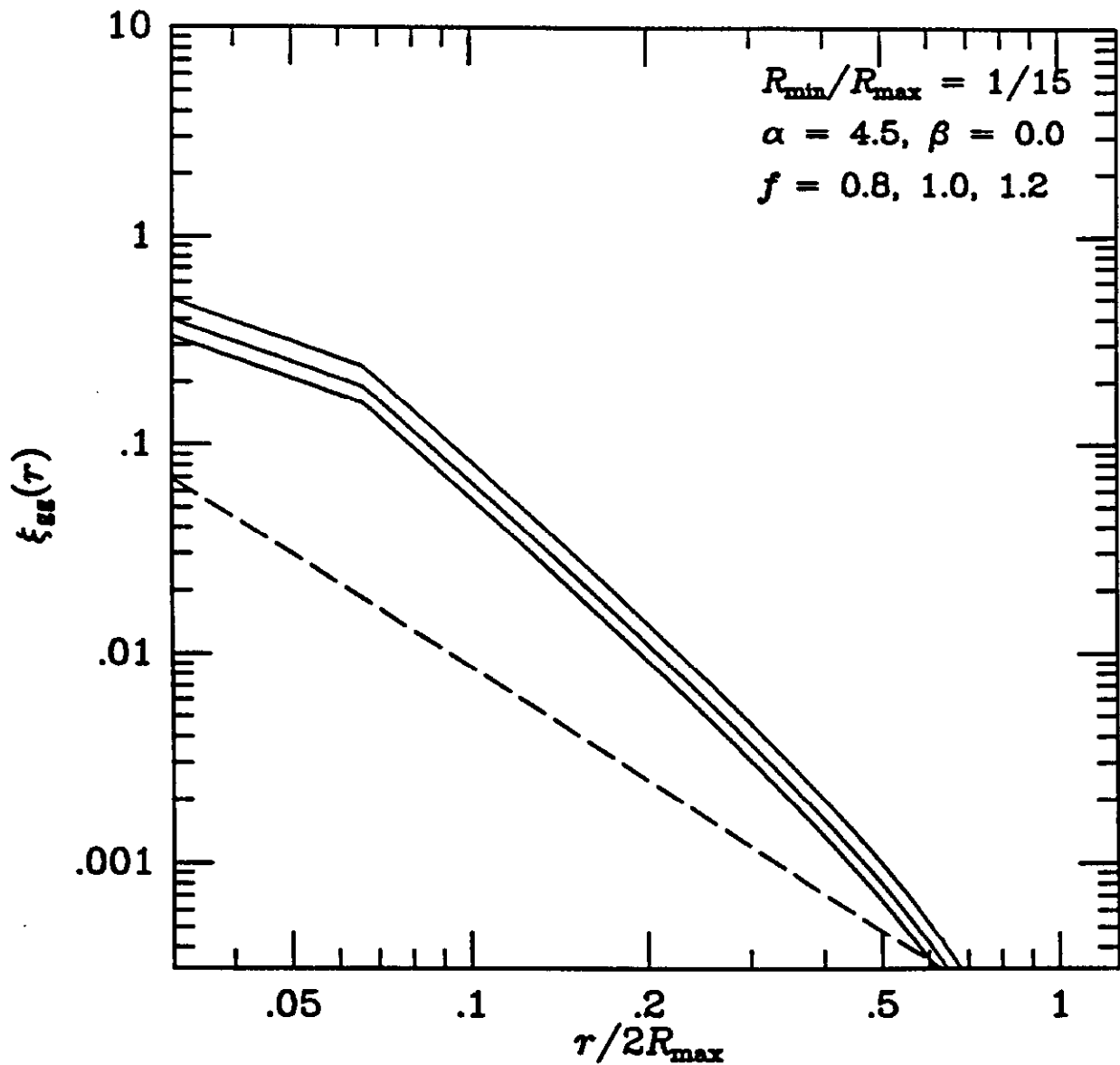


Fig 5d

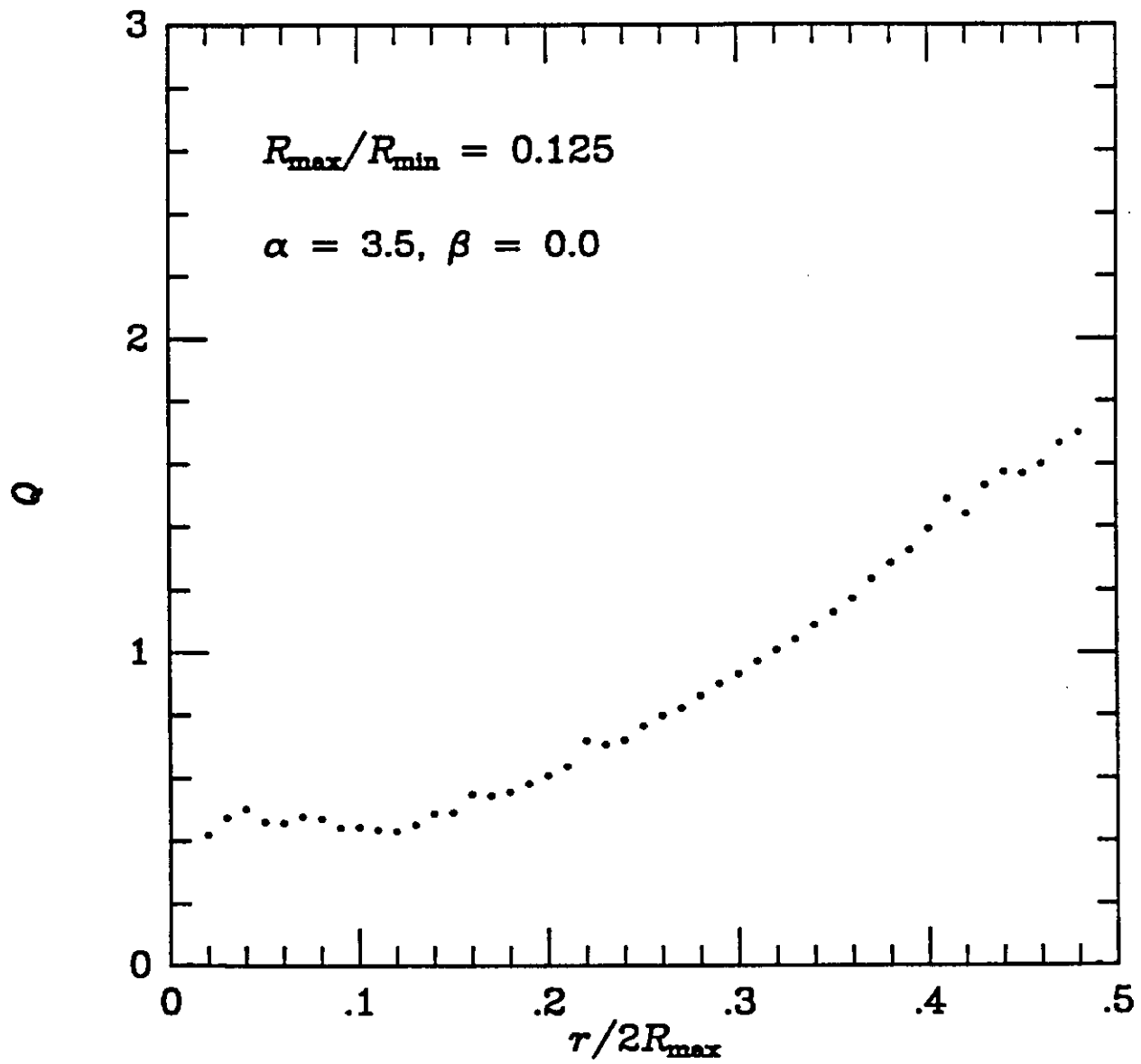


Fig 6a

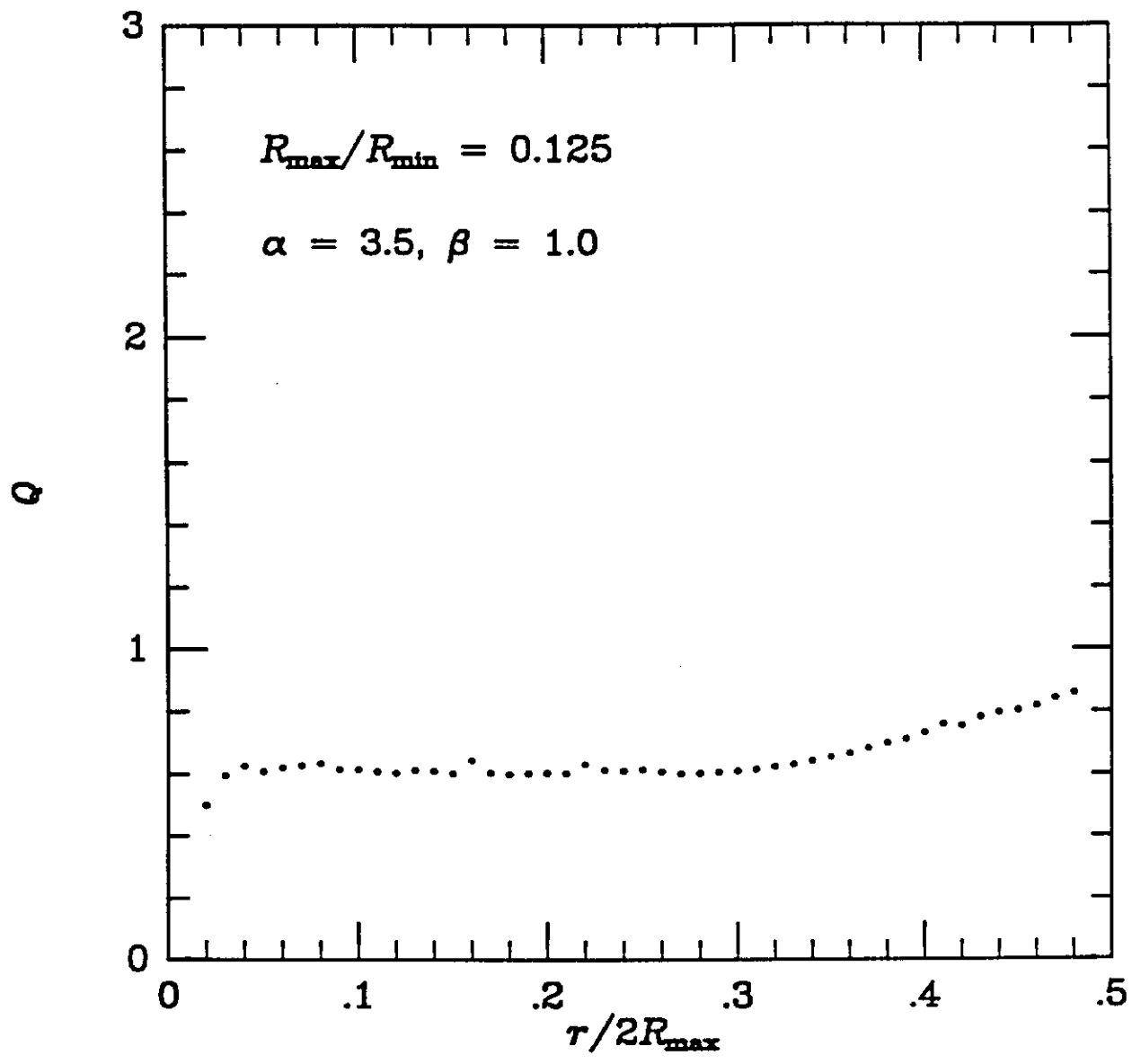


Fig 6b

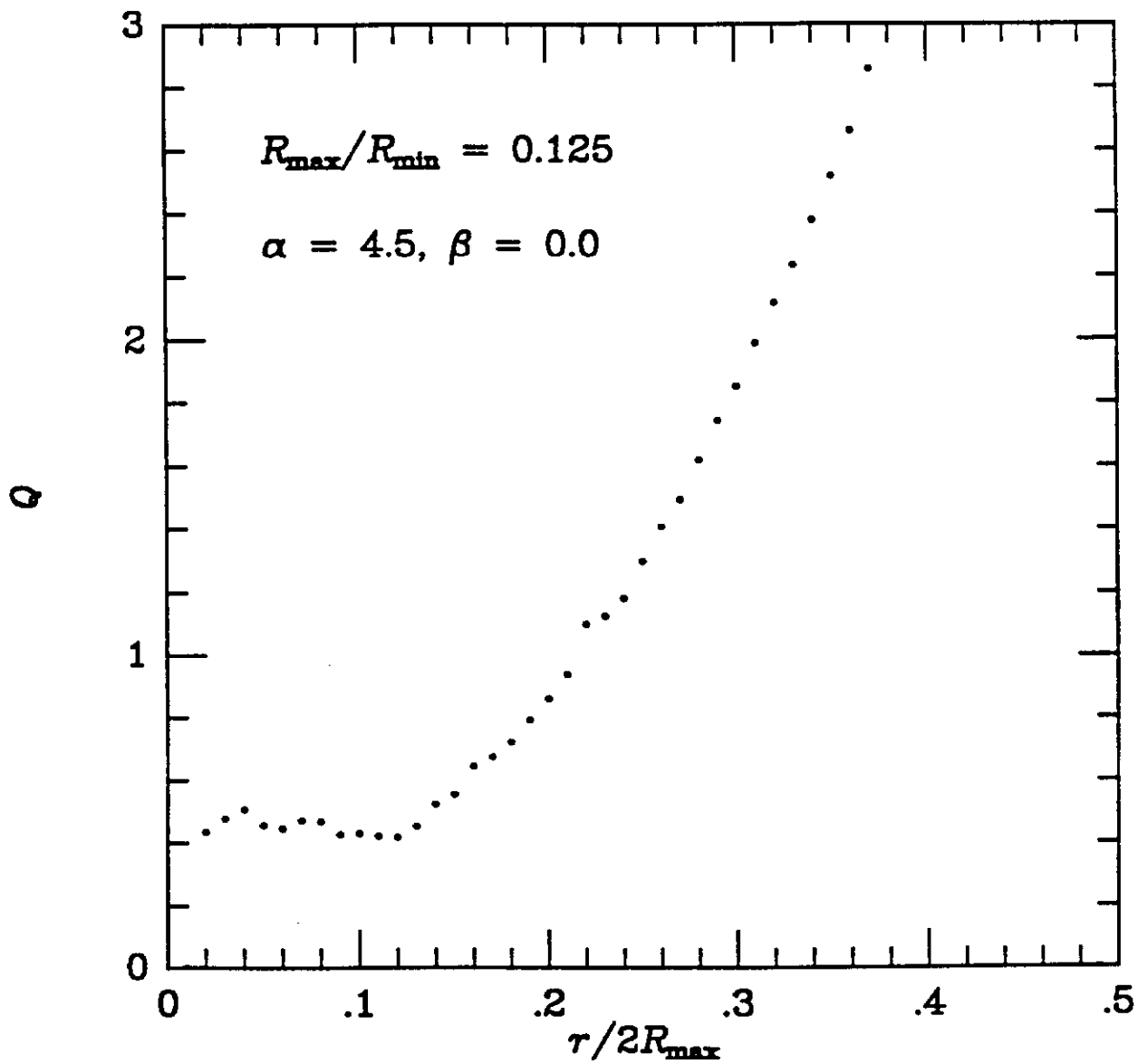


Fig 6c

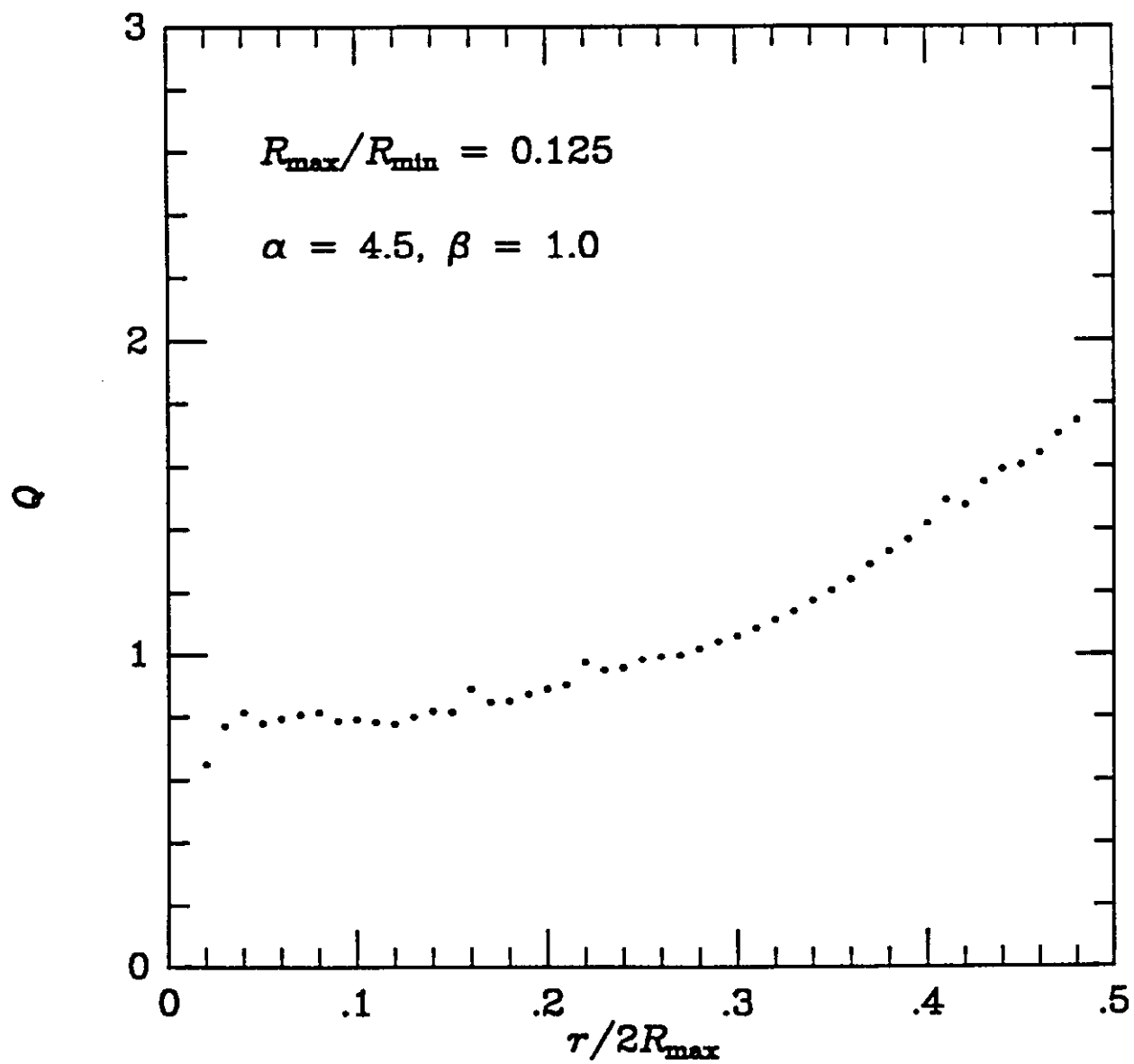


Fig 6d

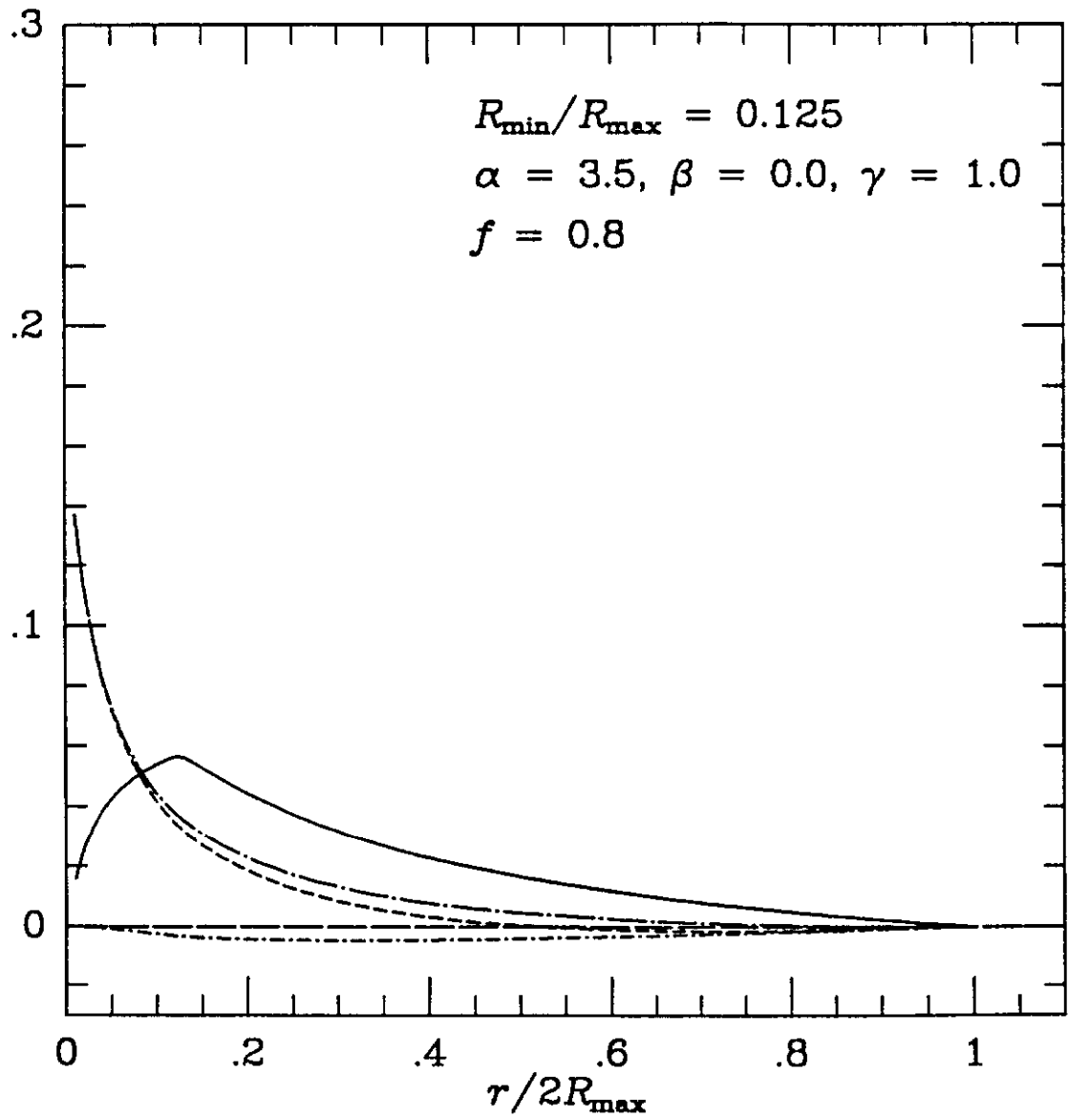


Fig 7a

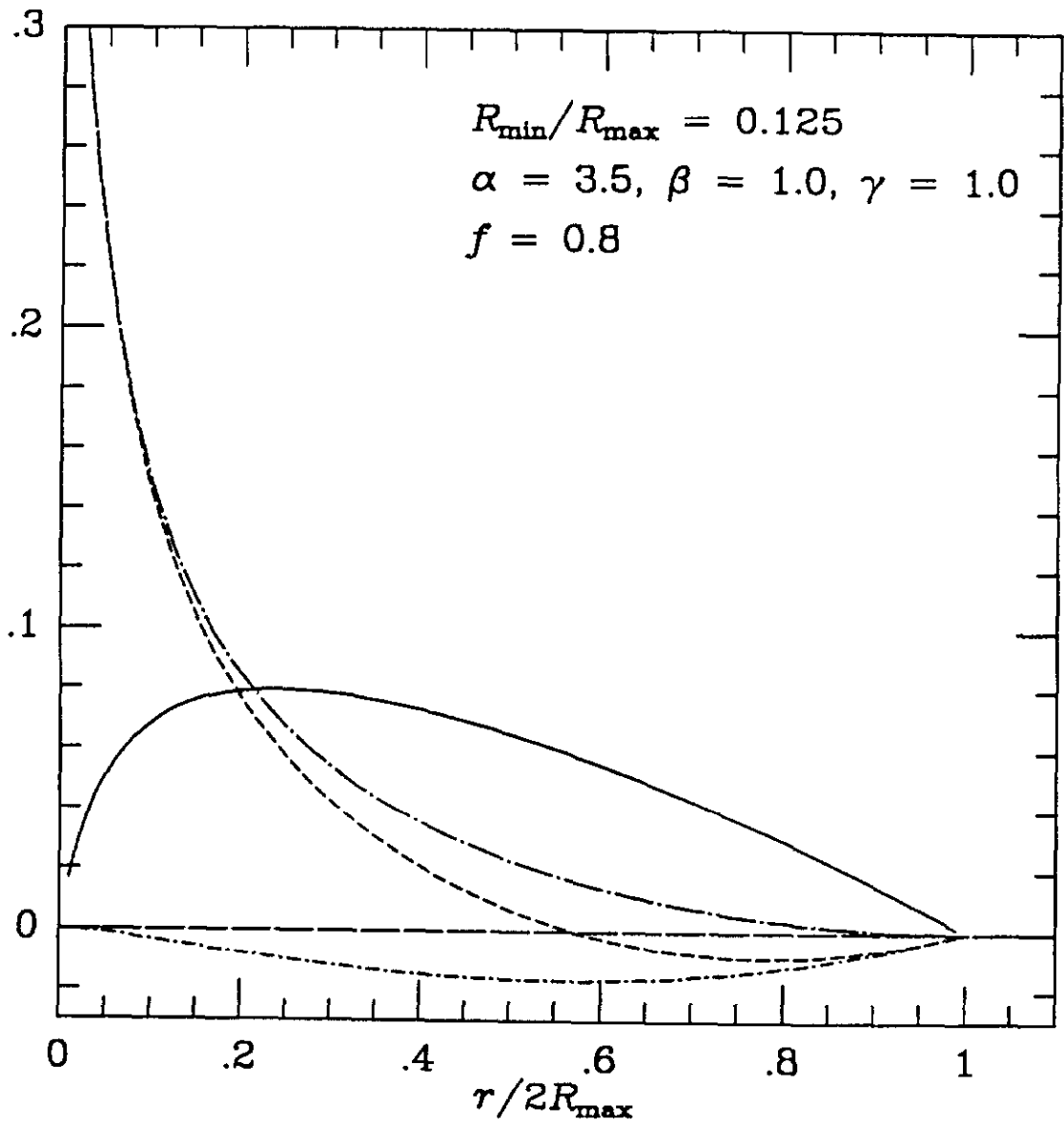


Fig 76

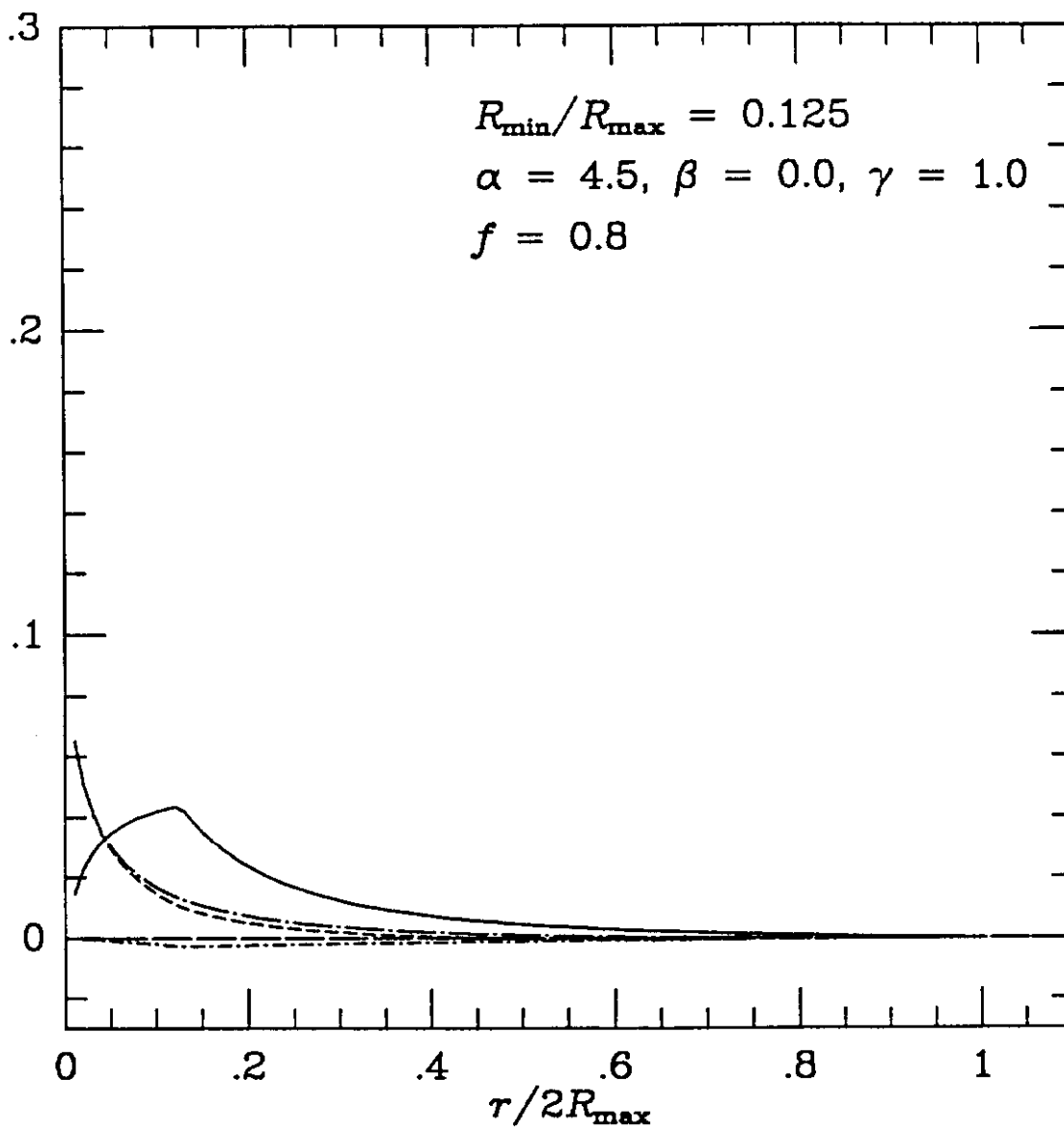


Fig 7c

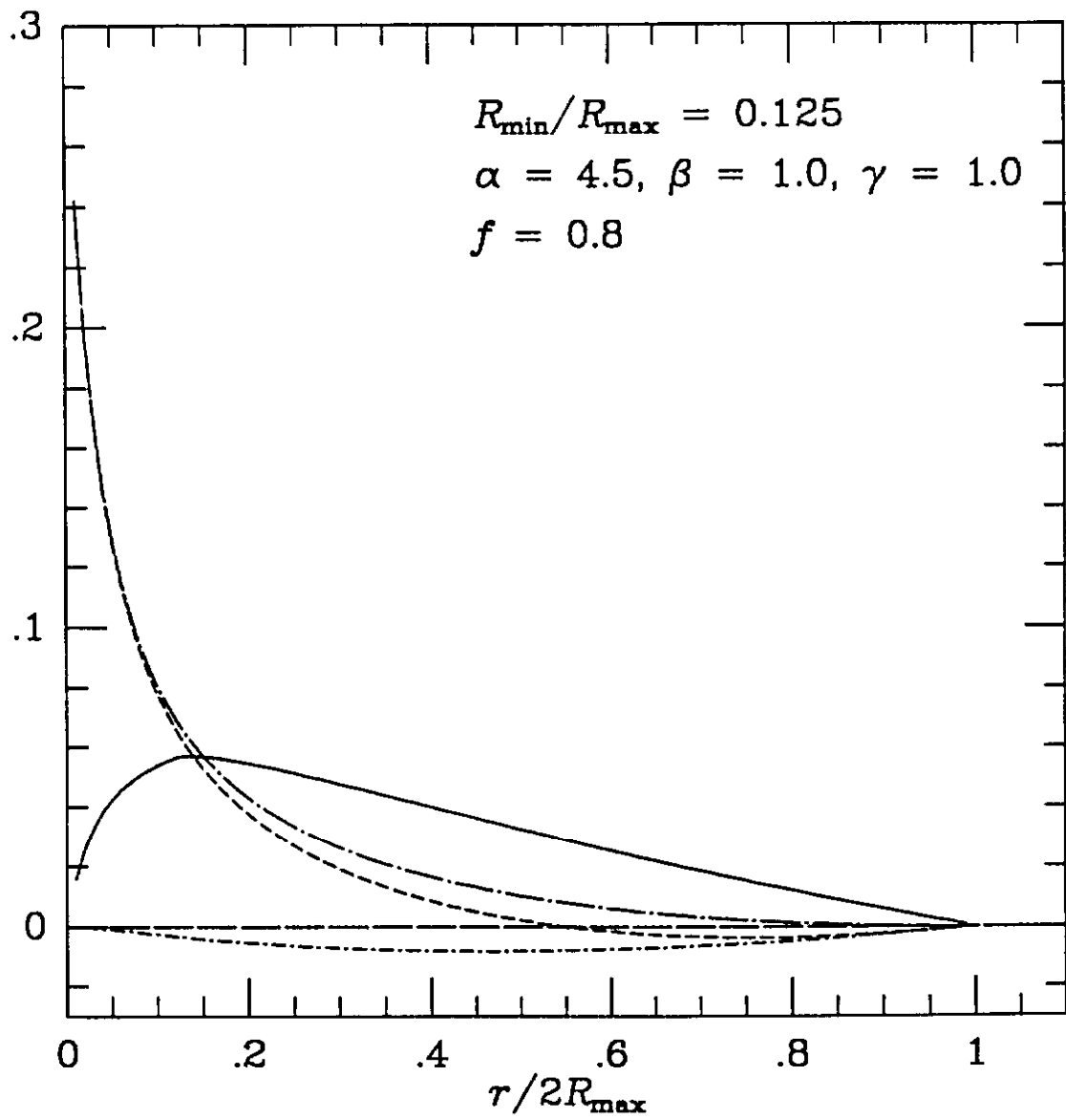


Fig 7d

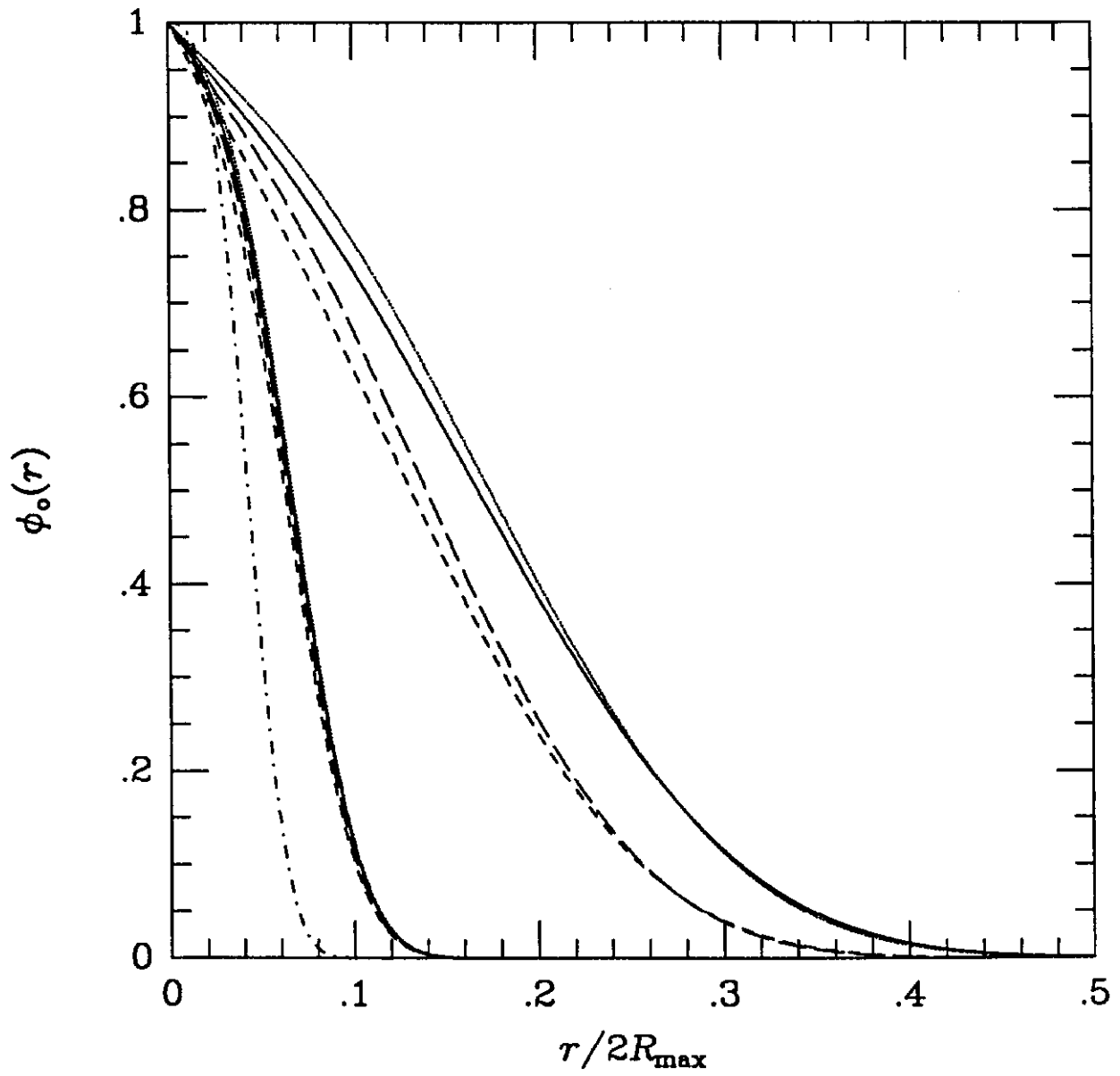


Fig 8

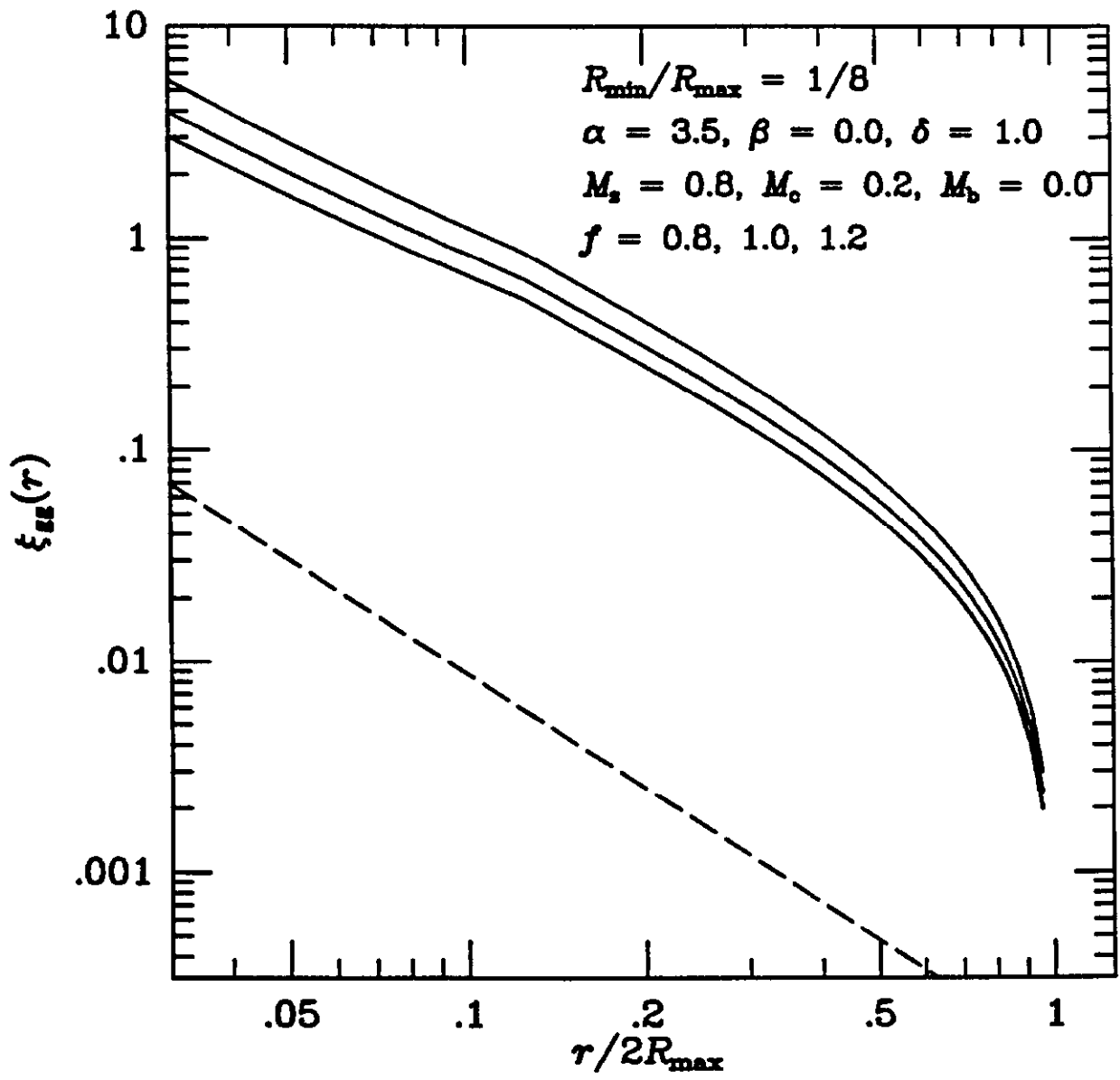


Fig 9a

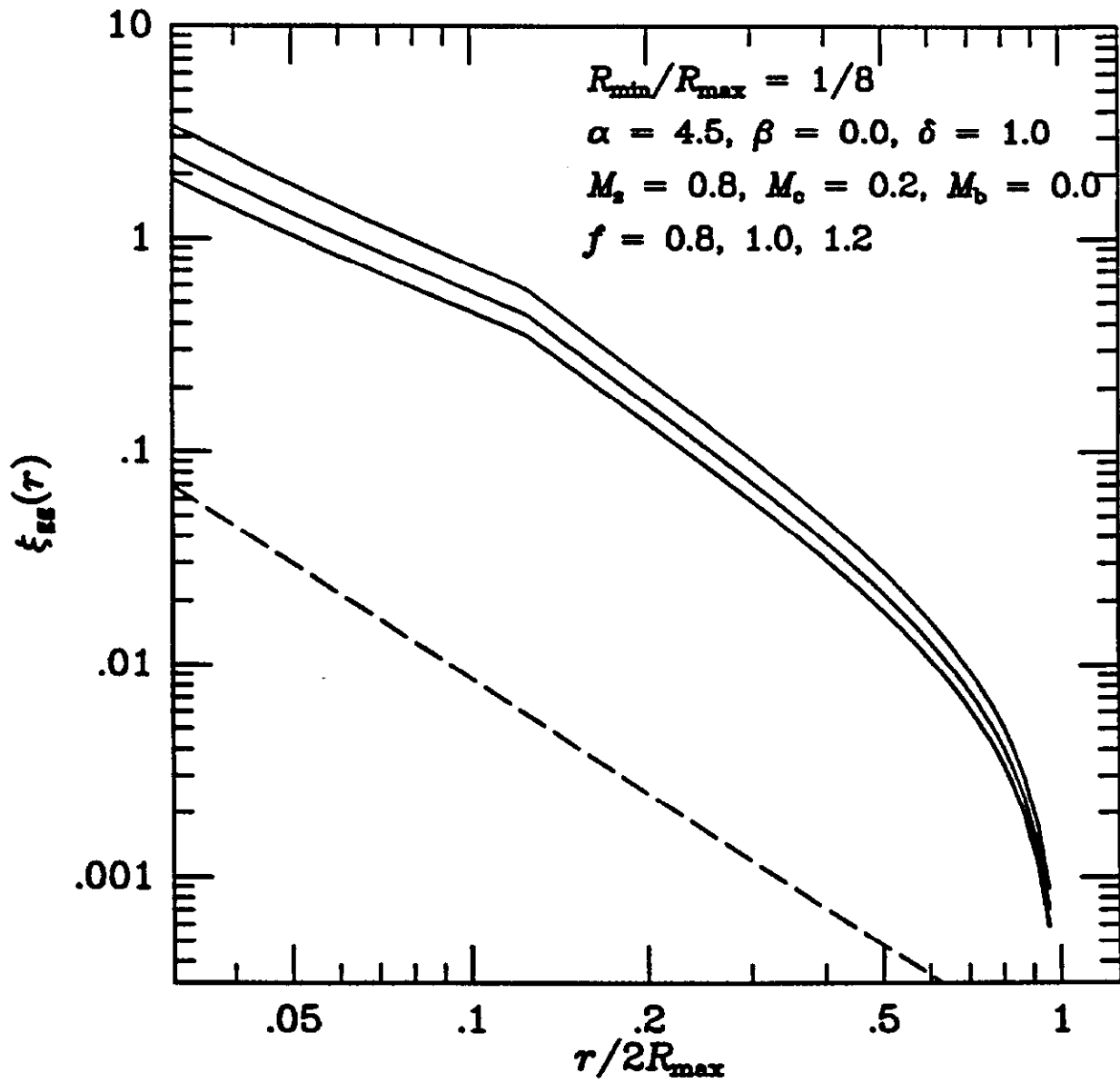


Fig 9b

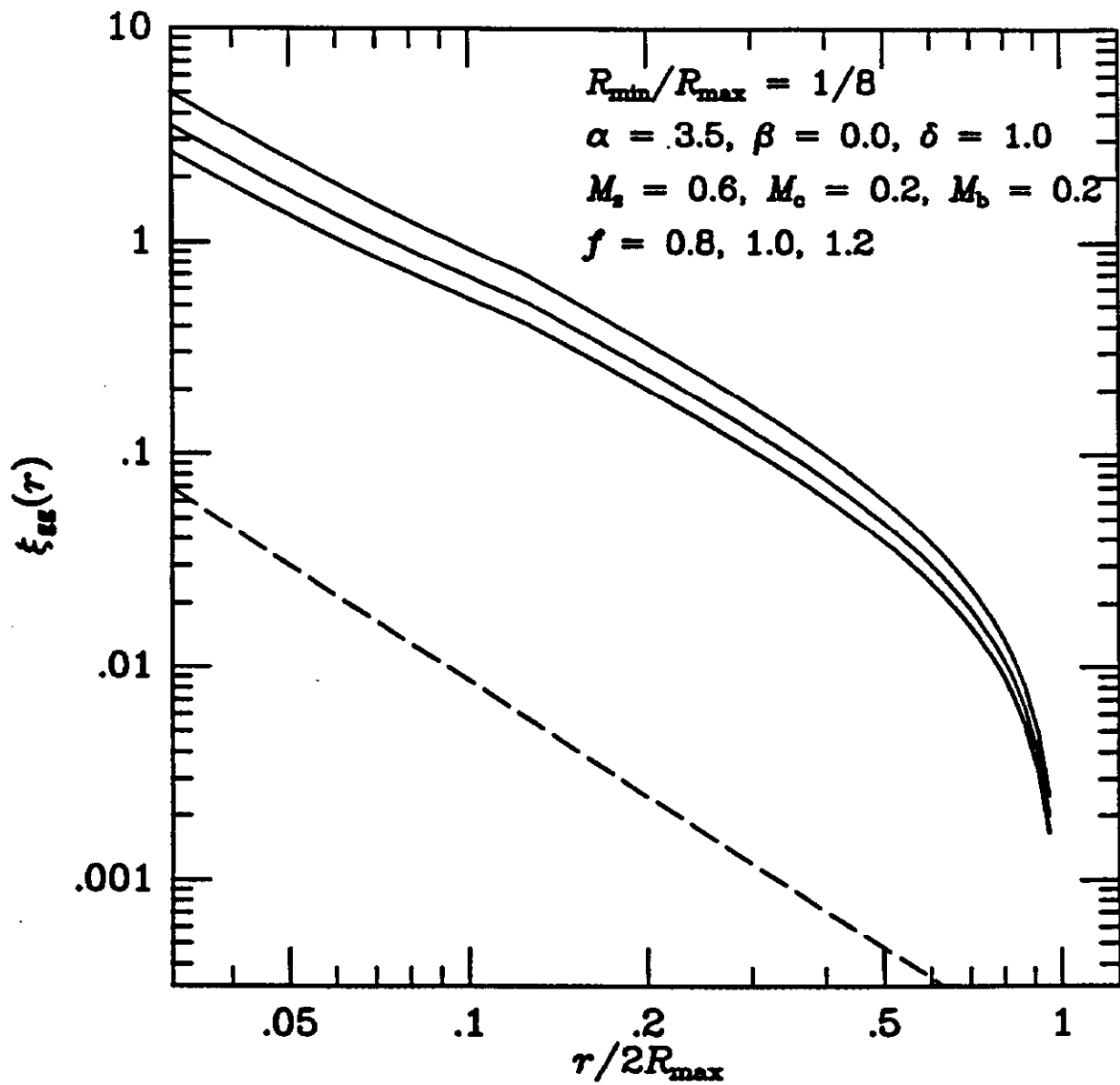


Fig 9c

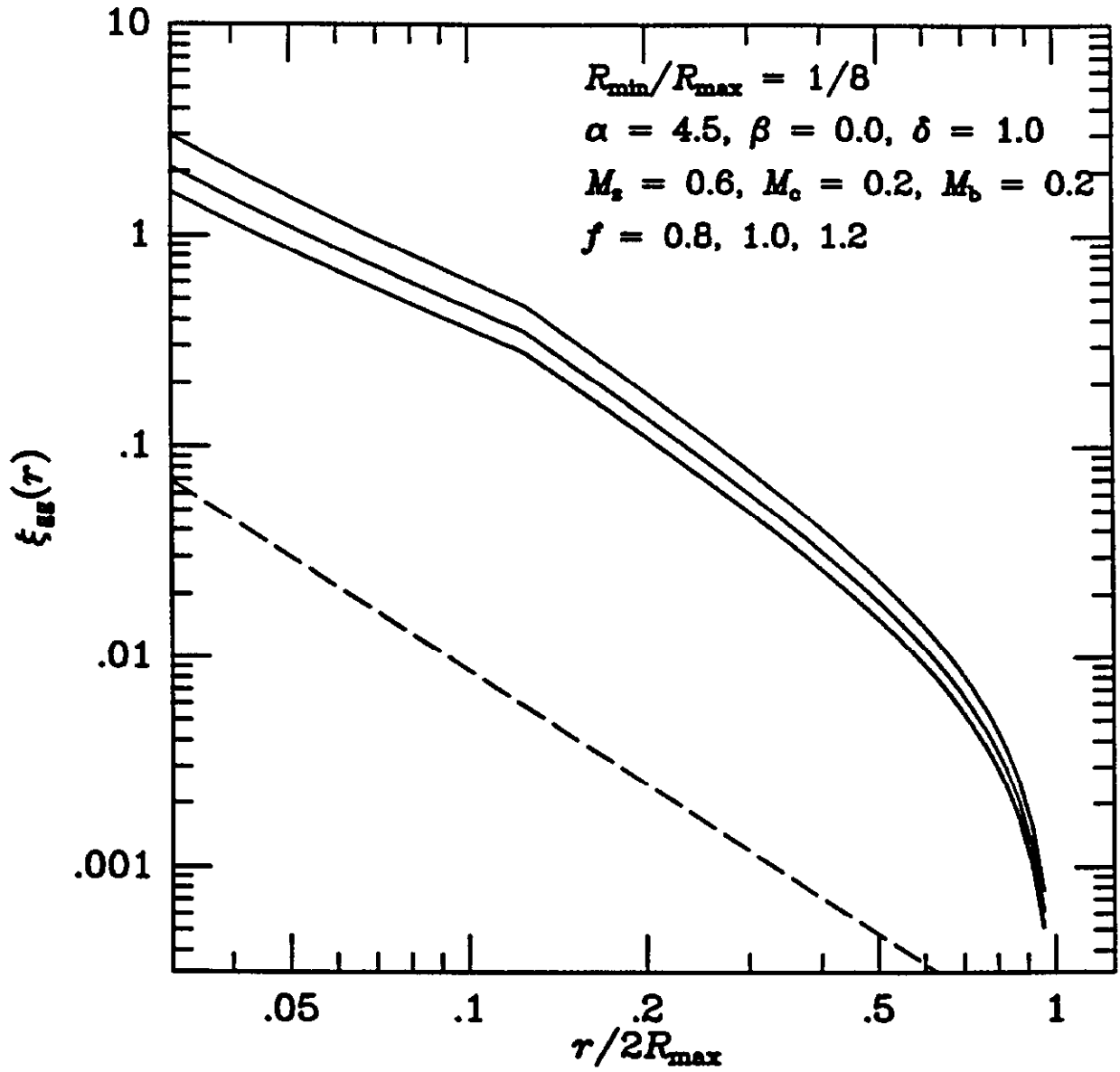


Fig 9d

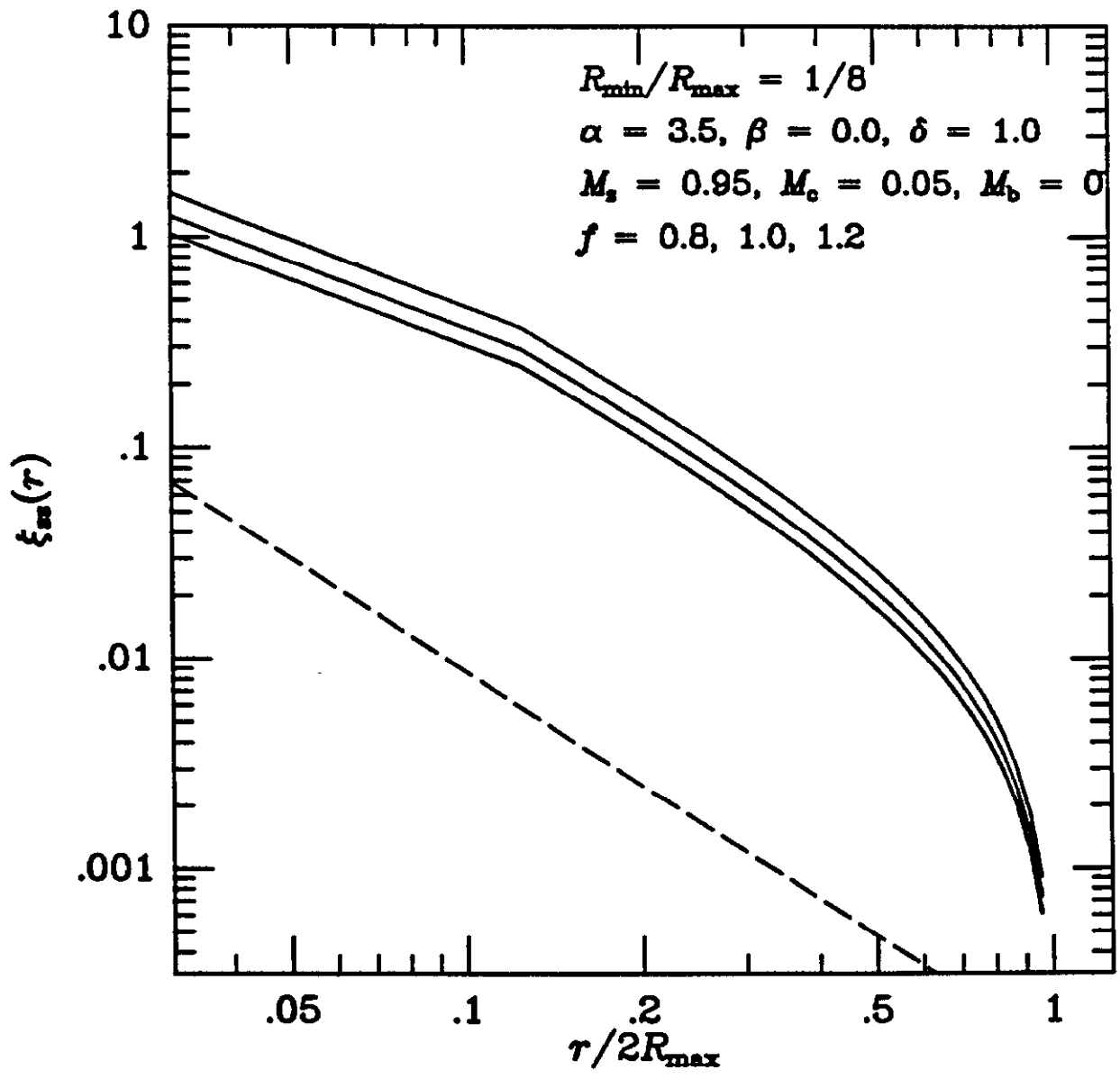


Fig 10a

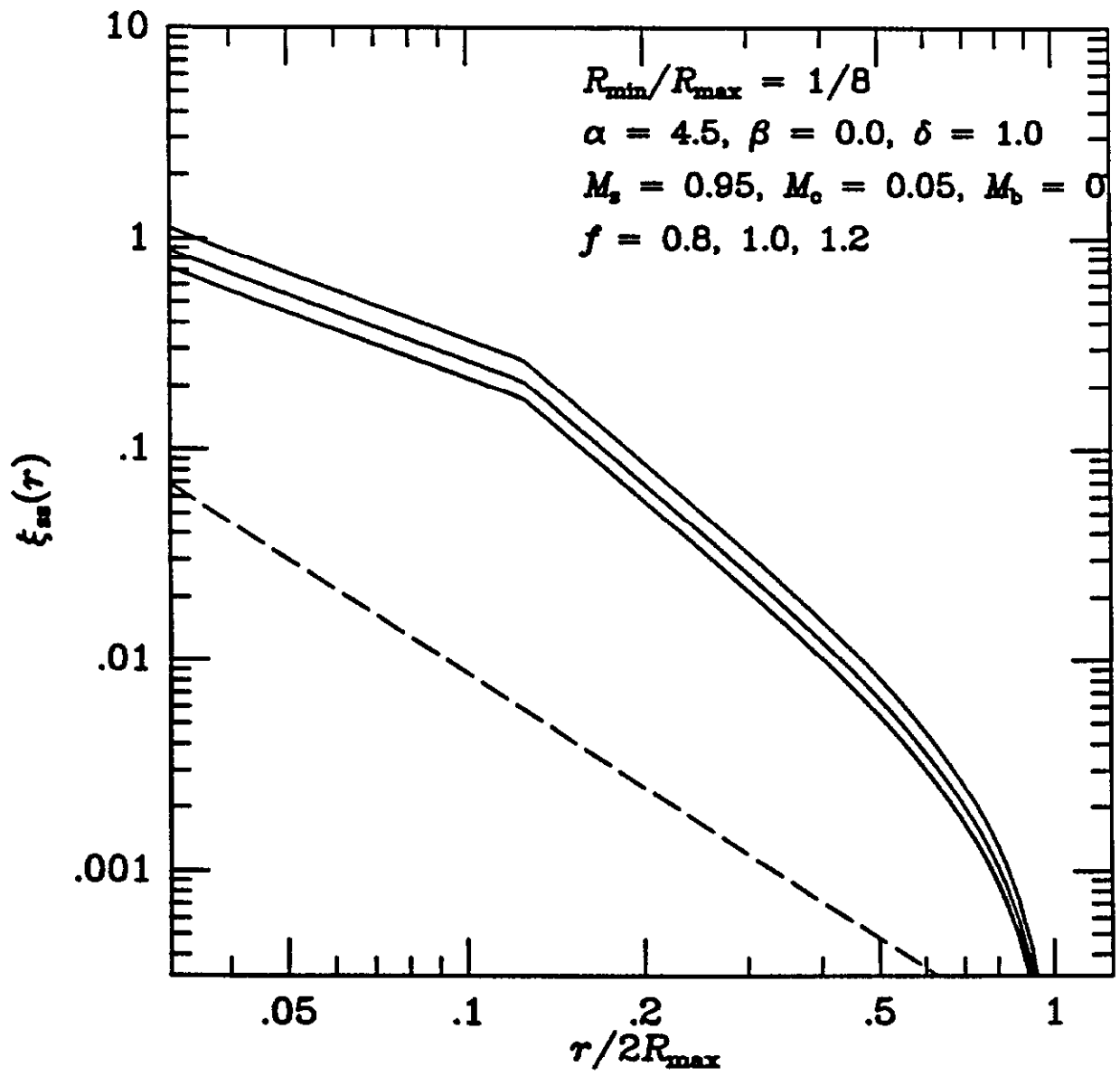


Fig 10b

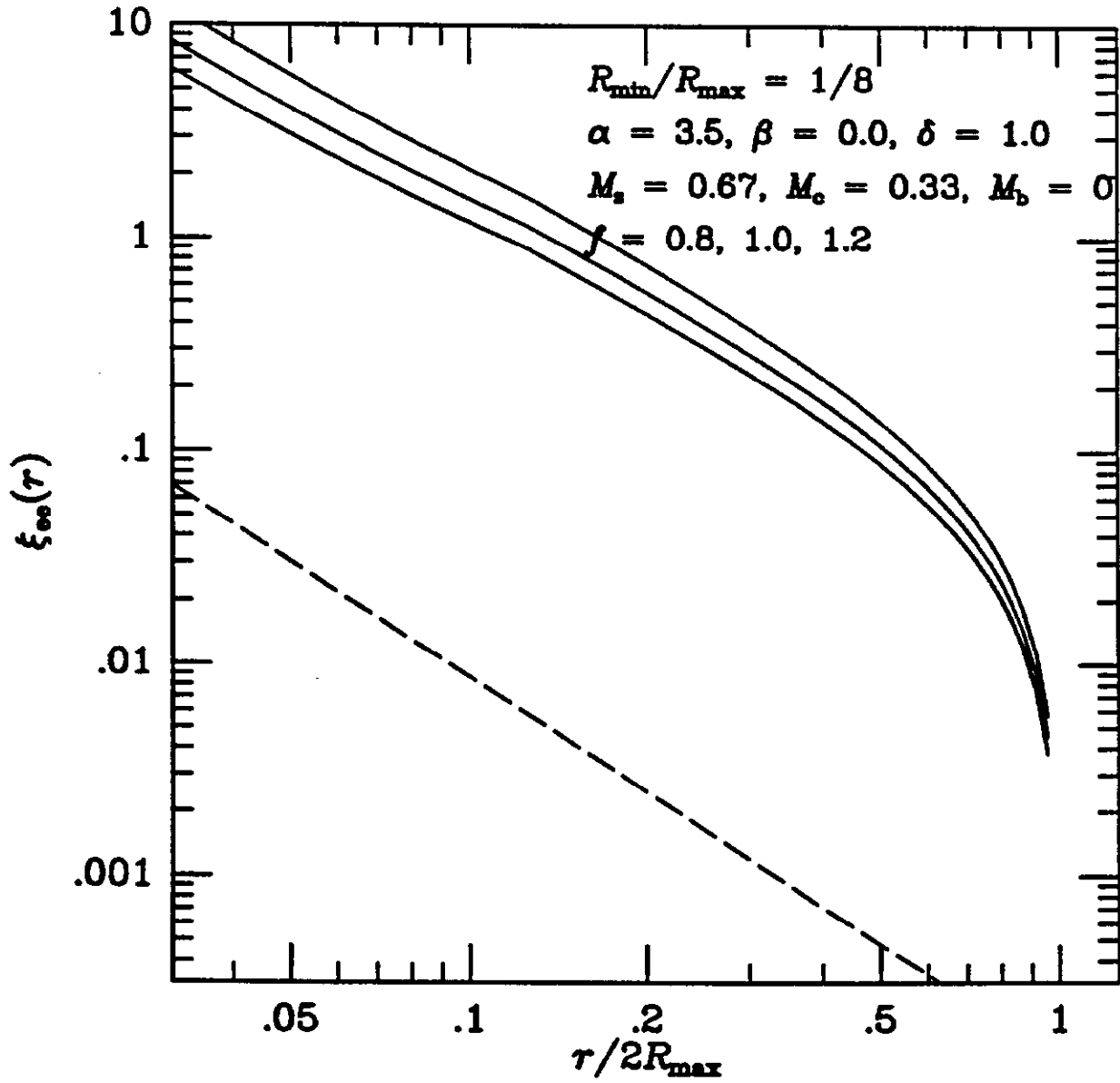


Fig 11a

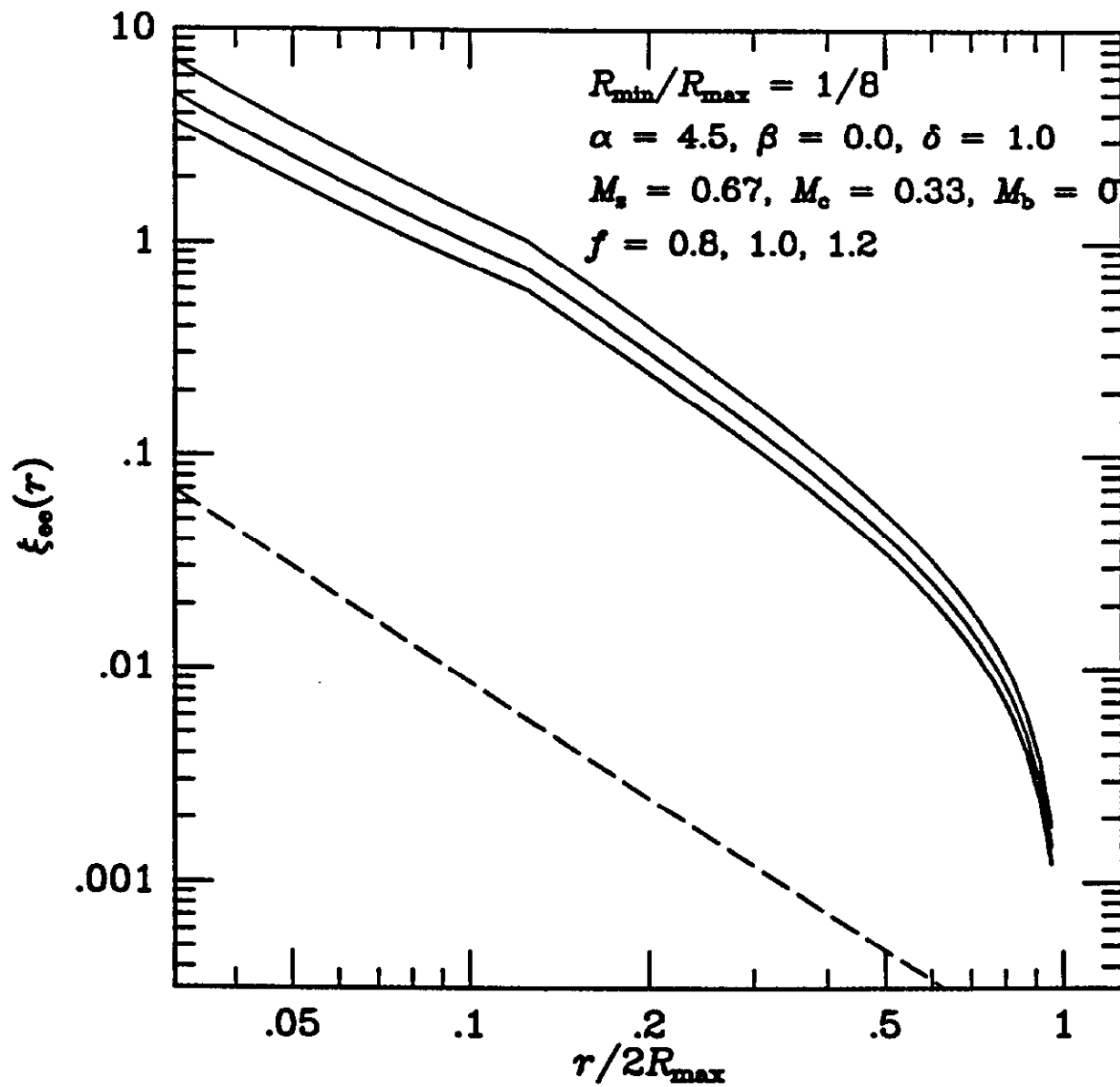


Fig 11b

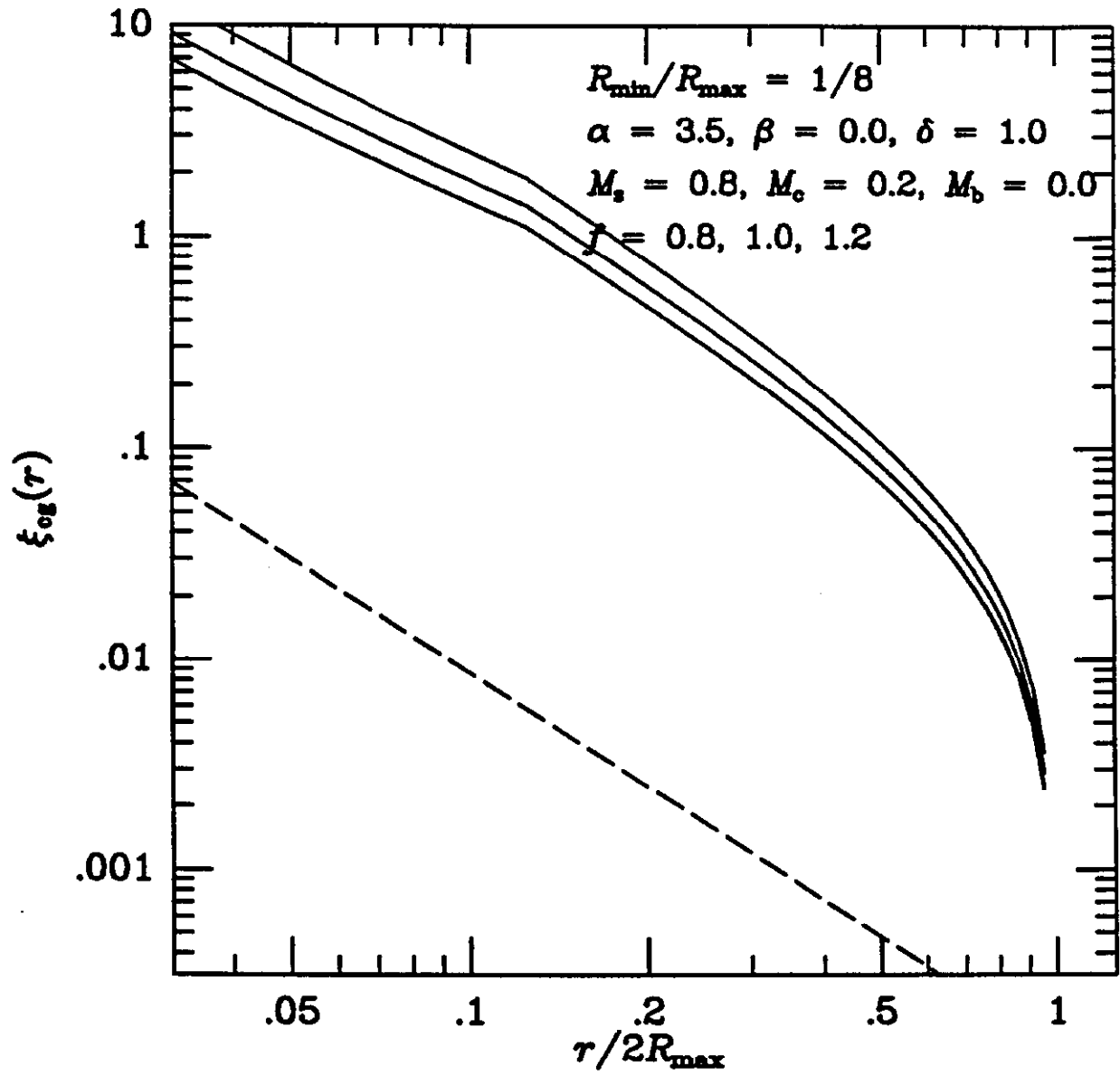


Fig12a

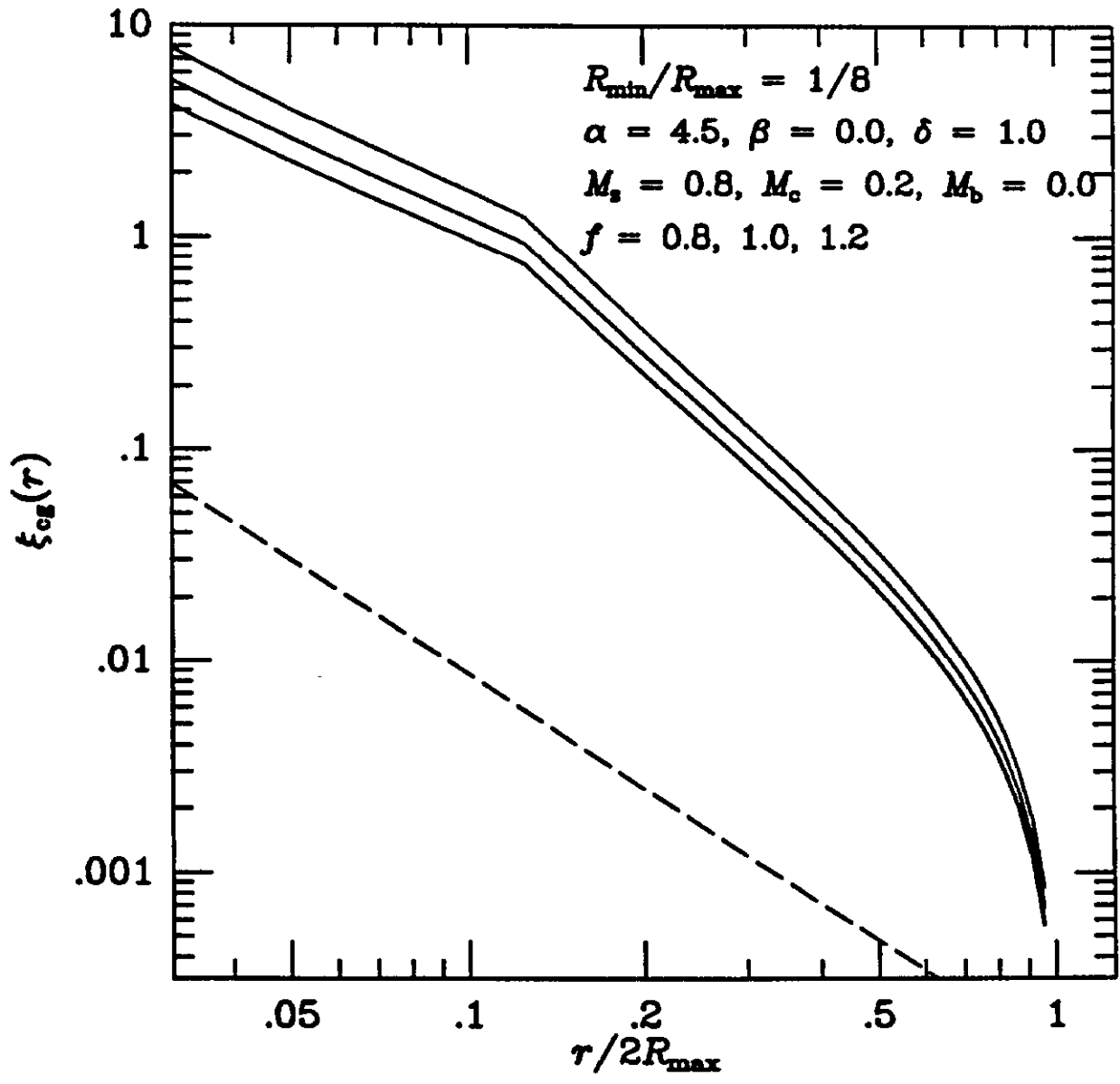


Fig12b

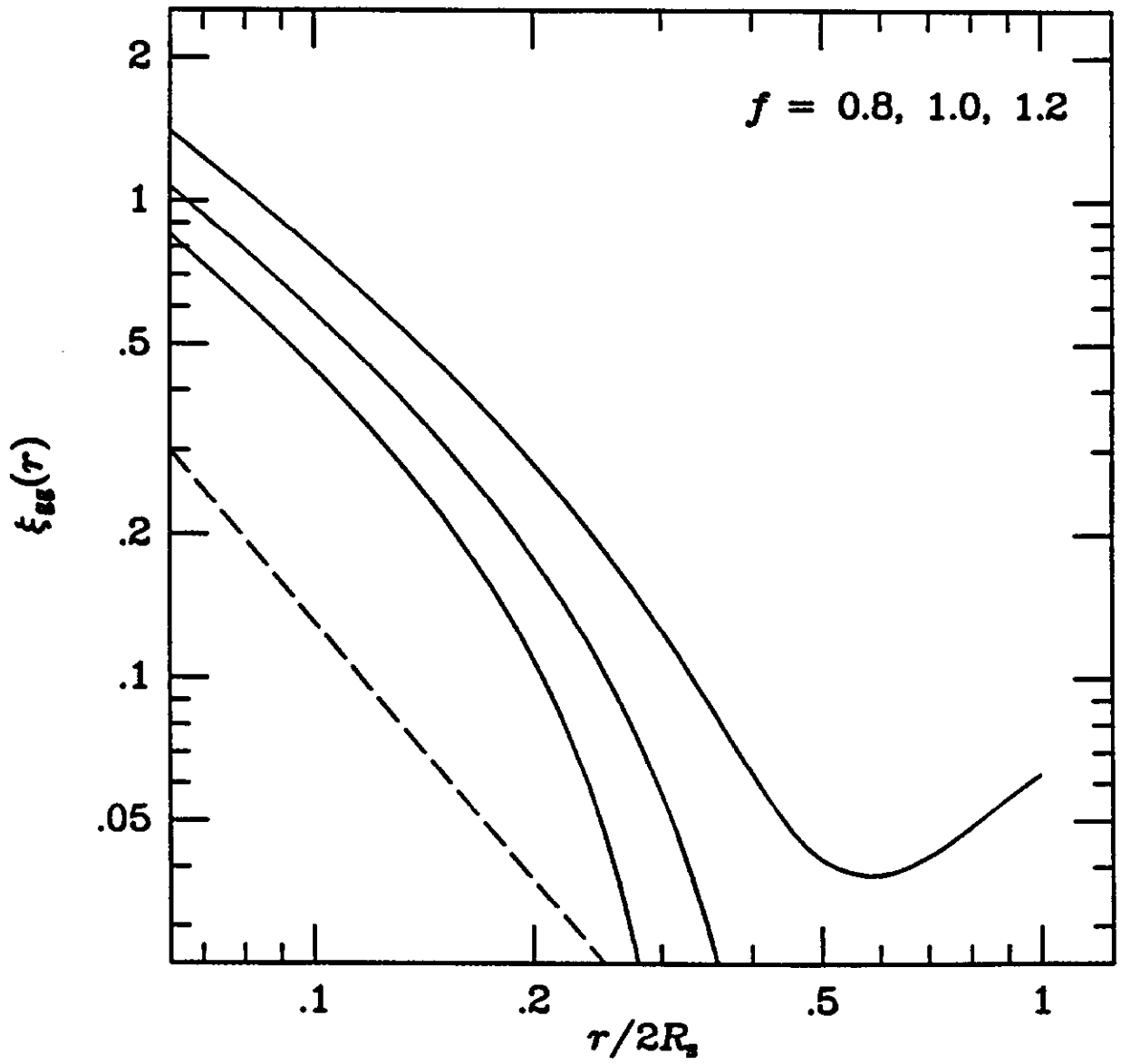


Fig 13

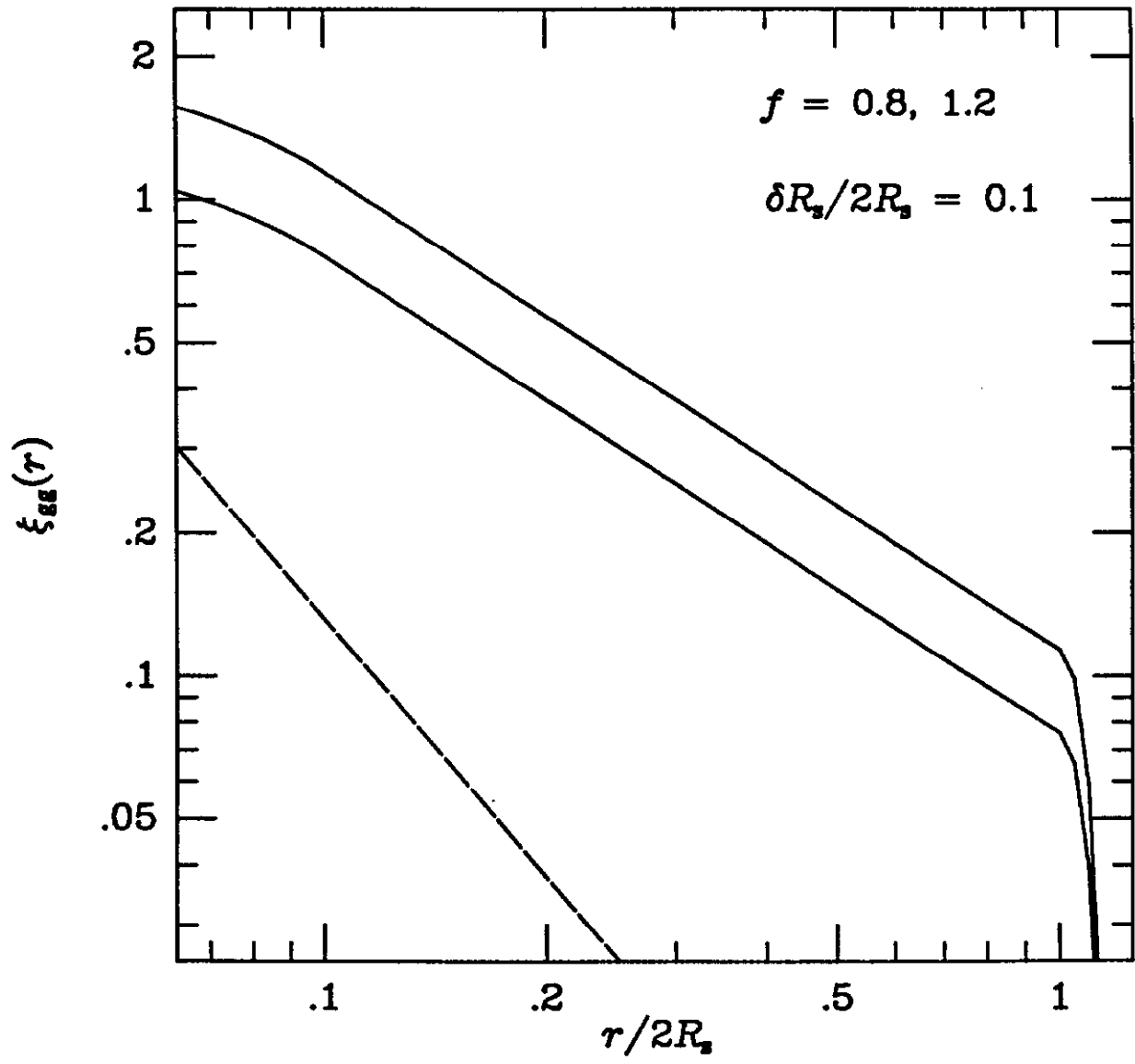


Fig A1

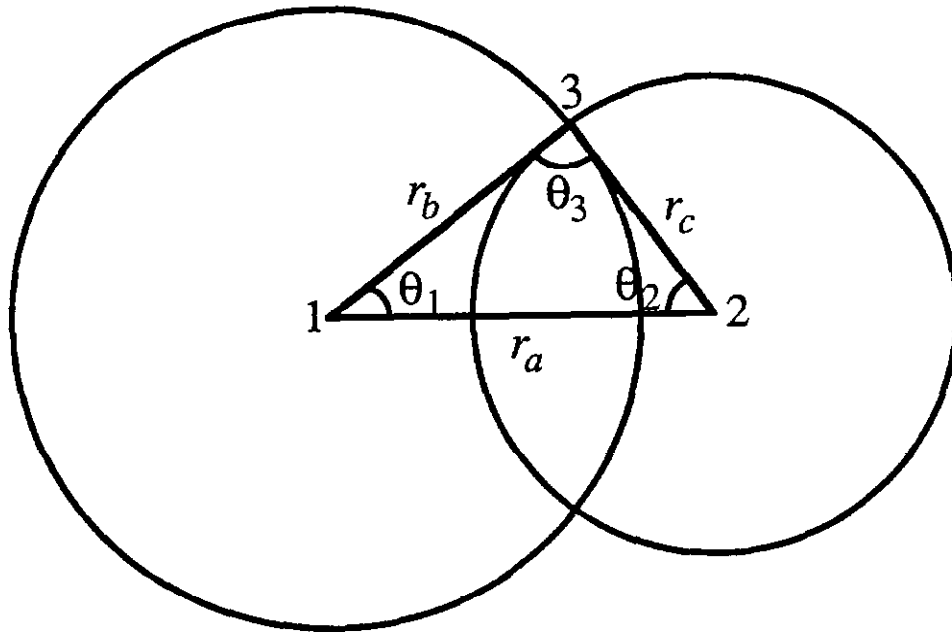


Fig. B1

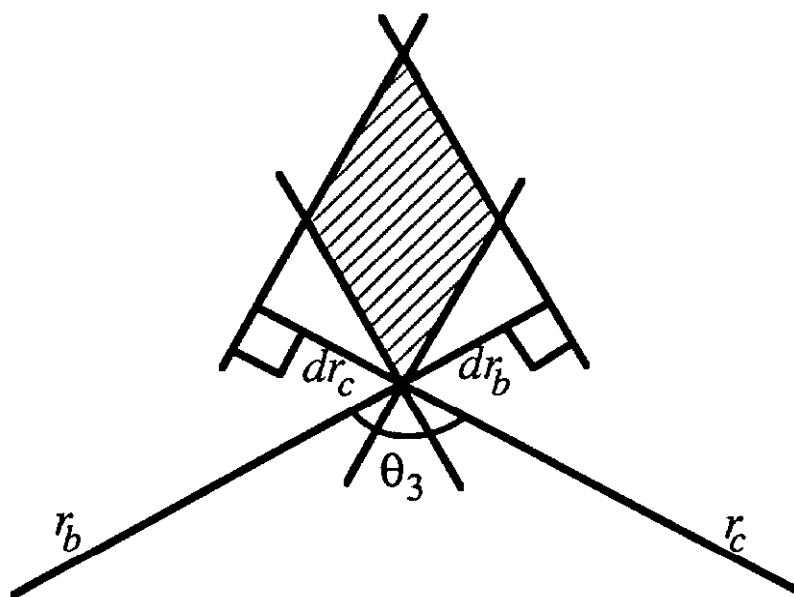


Fig. B2

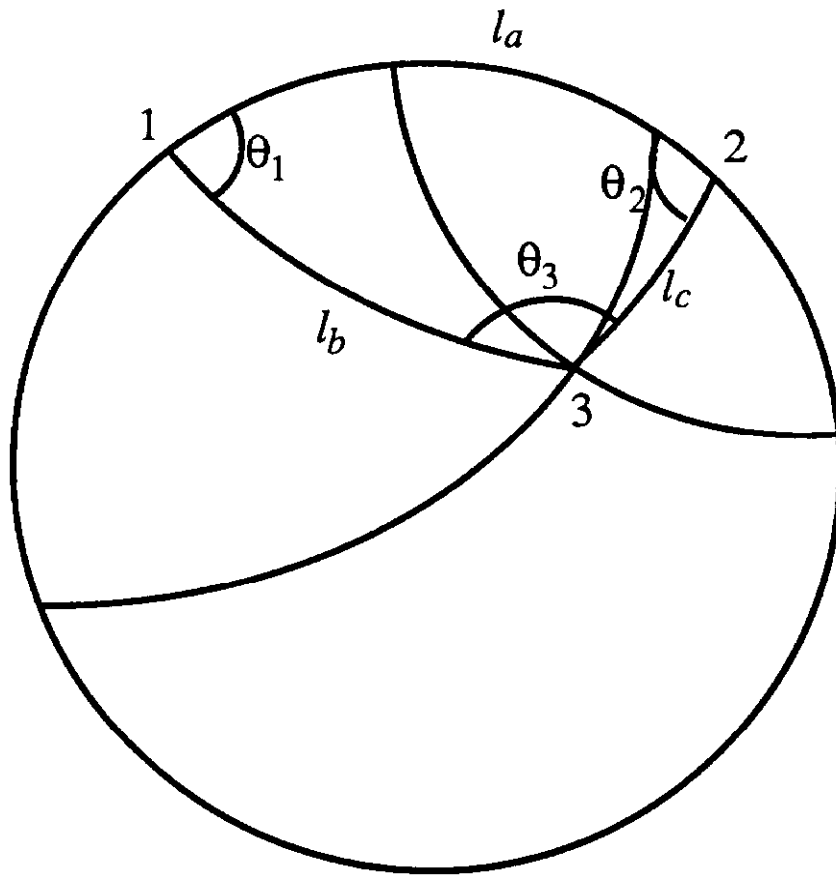


Fig C1